

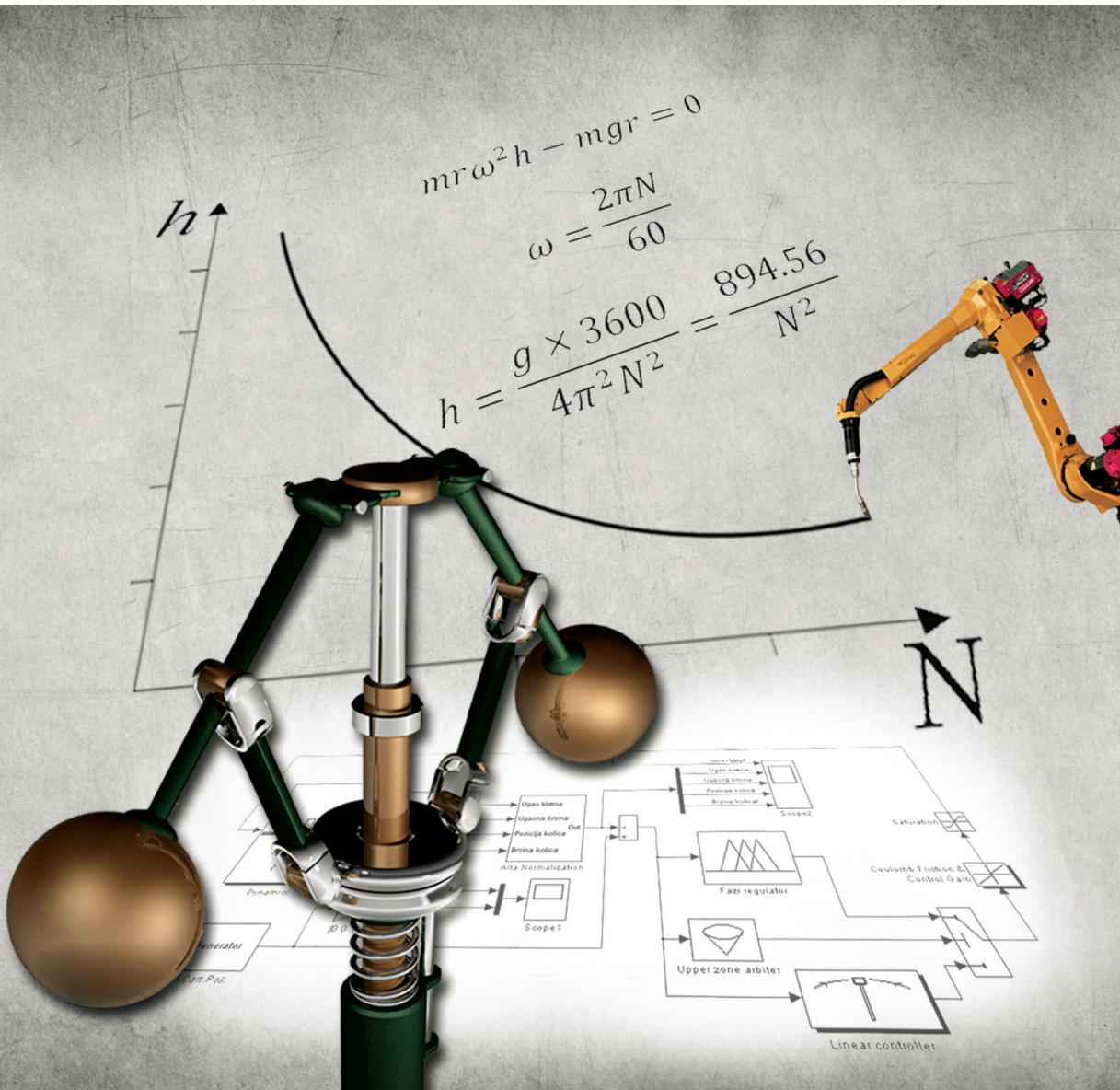


FACTA UNIVERSITATIS

Series

AUTOMATIC CONTROL AND ROBOTICS

Vol. 23, № 2, 2024



Scientific Journal **FACTA UNIVERSITATIS**
UNIVERSITY OF NIŠ

Univerzitetski trg 2, 18000 Niš, Republic of Serbia
Phone: +381 18 257 095 Telefax: +381 18 257 950
e-mail: facta@ni.ac.rs <http://casopisi.junis.ni.ac.rs/>

Scientific Journal FACTA UNIVERSITATIS publishes original high scientific level works in the fields classified accordingly into the following periodical and independent series:

<i>Architecture and Civil Engineering</i>	<i>Linguistics and Literature</i>	<i>Physical Education and Sport</i>
<i>Automatic Control and Robotics</i>	<i>Mathematics and Informatics</i>	<i>Physics, Chemistry and Technology</i>
<i>Economics and Organization</i>	<i>Mechanical Engineering</i>	<i>Teaching, Learning and Teacher Education</i>
<i>Electronics and Energetics</i>	<i>Medicine and Biology</i>	<i>Visual Arts and Music</i>
<i>Law and Politics</i>	<i>Philosophy, Sociology, Psychology and History</i>	<i>Working and Living Environmental Protection</i>

SERIES: AUTOMATIC CONTROL AND ROBOTICS

Editor-in-Chief: **Staniša Lj. Perić**, e-mail: fuacred@junis.ni.ac.rs
University of Niš, Faculty of Electronic Engineering
Republic of Serbia, 18000 Niš, Aleksandra Medvedeva 4
Phone: +381 18 529 363, Fax: +381 18 588 399

Technical Assistance: **Marko Milojković**, University of Niš, Faculty of Electronic Engineering,
Department of Control Systems, Niš, Republic of Serbia, e-mail: fuacrts@junis.ni.ac.rs

EDITORIAL BOARD:

Dragan Antić,

Faculty of Electronic Engineering,
University of Niš, Republic of Serbia

Branko Kovačević,

Faculty of Electrical Engineering,
University of Belgrade, Republic of Serbia

Emil Nikolov,

Faculty of Automatics,
Technical University of Sofia, Bulgaria

Stevan Stankovski,

Faculty of Technical Sciences,
University of Novi Sad, Republic of Serbia

Žarko Čučej,

Faculty of Electrical Engineering and Computer
Science, University of Maribor, Slovenia

Viacheslav Khasanovich Pshikhopov,

Head of the Electrical Engineering and
Mechatronics, Department Taganrog Technological
Institute Southern Federal University, Russia

Milić Stojić,

School of Electrical Engineering,
University of Belgrade, Republic of Serbia

Radu-Emil Precup,

Faculty of Automation and Computers,
"Politehnica" University of Timisoara, Romania

Branislav Borovac,

Faculty of Technical Sciences,
University of Novi Sad, Republic of Serbia

Mile Stankovski,

Faculty of Electrical Engineering and Information Technology,
Skopje, Macedonia

Georgi Dimirovski,

School of Engineering,
Dogus University, Istanbul, Republic of Turkey

Morten Hovd,

Norwegian University of Science and Technology, Trondheim,
Norway

Vlastimir Nikolić,

Faculty of Mechanical Engineering,
University of Niš, Republic of Serbia

Željko Đurović,

School of Electrical Engineering,
University of Belgrade, Republic of Serbia

Zoran Bučevac,

Faculty of Mechanical Engineering,
University of Belgrade, Republic of Serbia

Novak Nedić,

Faculty of Mechanical Engineering Kraljevo,
University of Kragujevac, Republic of Serbia

UDC Classification Associate: **Branka Stanković**, Library of Faculty of Electronic Engineering, Niš

English Proofreader: **Goran Stevanović**, University of Niš, Faculty of Civil Engineering and Architecture, e-mail: fuacrpr@junis.ni.ac.rs

The authors themselves are responsible for the correctness of the English language in the body of papers.

Computer support: **Mile Ž. Randelović**, Head of Publishing Department, University of Niš, e-mail: mile@ni.ac.rs

Secretary: **Aleksandra Golubović**, University of Niš, e-mail: saska@ni.ac.rs

Publication frequency – one volume, two issues per year.

Published by the University of Niš, Republic of Serbia

© 2024 by University of Niš, Republic of Serbia

Printed by ATLANTIS DOO, Niš, Republic of Serbia

Circulation 50

Previous title: Scientific Journal FACTA UNIVERSITATIS, Series Mechanics, Automatic Control and Robotics. – Vol. 1, No 1 (1991) – Vol. 6, No 1(2007). – ISSN 0354 – 2009

Since 2007 divided in two Series:

Scientific Journal FACTA UNIVERSITATIS, Series Mechanics. – Vol. 7, No 1(2008) – . – ISSN

Scientific Journal FACTA UNIVERSITATIS, Series Automatic Control and Robotics. – Vol. 7, No 1(2008) – . – ISSN 1820 – 6417

ISSN 1820 – 6417 (Print)
ISSN 1820 – 6425 (Online)
COBISS.SR-ID 158108940
UDC 62

FACTA UNIVERSITATIS

SERIES AUTOMATIC CONTROL AND ROBOTICS
Vol. 23, № 2, 2024



UNIVERSITY OF NIŠ

INSTRUCTION FOR AUTHORS

As an author, you are kindly advised to use the paper template available for downloading on journal web site (section Download documents). This way you have nothing to change in terms of paper and text format. Simply applying the styles defined in the document will be sufficient.

Paper submitted for publication may be written in English, French or German (preferably in English) and submitted in the final camera-ready form. It is mandatory to submit your original work in Microsoft Word format (.doc not .docx) by using our online manuscript submission system. You have to make "New Submission" and upload your paper by using the online interface. All subsequent versions should be uploaded by using the same paper ID and your defined password. We are unable to process files sent by E-mail. We will do the final formatting and all necessary format conversions of your paper.

Articles are usually 10 to 25 type-written pages long. However, in special cases, shorter or longer articles may be accepted with appropriate reasoning. Author name, affiliation and complete address are to be placed underneath the title. Each paper should be preceded by a brief summary (50-150 words) in the same language. The text should be concise.

Letters, figures, and symbols should be clearly denoted so that no doubts about their meaning can arise. Symbols which may lead to confusion (e.g. letter I and figure 1, figure 0 and letter O) should be distinguished by marks which are explained in "Remarks for the typesetter".

Equations should be typewritten using MathType add-on (<http://www.mathtype.com>). For equations in your paper (Insert | Object | Create New | or MathType Equation), and, with the number, placed in parentheses at the right margin. Reference to equations should use the form "Eq. (2)" or simply (2). Each formula should occupy one line.

All figures should be numbered with consecutive Arabic numbers, have descriptive captions, and be mentioned in the text. Figures submitted must be of a standard high enough for direct reproduction. Line drawings should be prepared in electronic form. Figures should be planned in advance, so as to allow reduction to 12.75 cm in column width.

References should be quoted in the text by the corresponding number in square brackets and listed at the end of the manuscript in the order as they shown in the paper, in the same way as the following examples (for a journal, book, unpublished paper, proceeding, thesis, user manual, internet document):

- [1] B. M. Danković, "A class of almost orthogonal filters," *Journal of Circuits, Systems, and Computers*, vol. 18, no. 5, pp. 923–931, 2009. [Online]. Available: <http://dx.doi.org/10.1142/S0218126609005447>
- [2] J. H. Holland, *Adaptation in Natural and Artificial Systems*. University of Michigan Press, Ann Arbor, 1975.
- [3] M. T. Milojković, D. S. Antić, S. S. Nikolić, Z. D. Jovanović, S. Lj. Perić, "On a new class of quasi-orthogonal filters," *International Journal of Electronics*, [Online]. Available: <http://dx.doi.org/10.1080/00207217.2012.743087>, to be published.
- [4] M.-B. Radac, R.-A. Achimescu, R.-E. Precup, S. Preitl, C.-A. Dragos, A.-I. Stinean, "Design and experiments for model-free PI control of DC drives," in *Proceedings of 8th IEEE International Symposium on Applied Computational Intelligence and Informatics*, Timisoara, Romania, pp. 103–108, 2013. [Online]. Available: <http://dx.doi.org/10.1225/sc.2013.018>
- [5] D. Mitić, Digital variable structure systems based on input-output model. PhD thesis, University of Niš, Faculty of Electronic Engineering, 2006.
- [6] Inteco, "The laboratory anti-lock braking system controlled from PC," User's manual, 2008. [Online]. Available: www.inteco.com.pl
- [7] MATLAB, The Language of Technical Computing, 2013. [Online]. Available: <http://www.mathworks.com/products/matlab> [Accessed on December 2013].

Electronic submission. Papers for consideration should be submitted to the Series Editor in electronic form via the Journal's home page: <http://casopisi.junis.ni.ac.rs/index.php/FUAutContRob/index>.

FACTA UNIVERSITATIS

Series

Automatic Control and Robotics

Vol. 23, N° 2, 2024

Contents

Regular Papers

- Filip Filipović, Milutin Petronijević, Nebojša Mitrović,
Bojan Banković, Vojkan Kostić**
REPETITIVE RIPPLE ESTIMATOR FILTER BASED PHASE-LOCKED LOOP 95-109
- Aleksandar Pantić, Adriana Petković, Sanja Aleksić**
DESIGN AND OPTIMIZATION OF SOLAR PARKING CANOPY
AS A PART OF ENERGY EFFICIENT URBAN PLANNING 111-121
- Milan Nikolić, Milan Banić, Milan Pavlović, Vukašin Pavlović,
Aleksandar Miltenović, Miloš Simonović**
PREDICTION OF THE FRICTION COEFFICIENT
BASED ON THE HYSTERESIS VALUE OF SHOE SOLE RUBBER..... 123-132
- Stevica Cvetković, Dušan Stojiljković, Ivan Ćirić, Rajko Turudija, Matija Špeletić**
INTEGRATED DATA ACQUISITION PLATFORM
FOR EXPLAINABLE CONTROL IN DISTRICT HEATING SYSTEMS 133-143
- Vesna Jovanović, Dragoslav Janošević, Jovan Pavlović,
Nikola Petrović, Đorđe Lazarević**
ANALYSIS OF VOLUMETRIC REGULATION OF HYDRAULIC PUMPS
IN HYDROSTATIC SYSTEMS 145-155

Survey Papers

- Nora Benmir**
A REVIEW OF DRILL STRING DYNAMICS
AND MODELING TECHNIQUES..... 157-177
- Nikola Danković, Saša S. Nikolić, Dragan Antić, Miodrag Spasić, Petar Đekić**
A COMPREHENSIVE REVIEW OF ORTHOGONAL POLYNOMIALS
AND FUNCTIONS WITH APPLICATION IN FILTER DESIGN 179-195

REPETITIVE RIPPLE ESTIMATOR FILTER BASED PHASE-LOCKED LOOP

UDC ((621.311+621.317.37):621.372.834.1)

**Filip Filipović, Milutin Petronijević, Nebojša Mitrović,
Bojan Banković, Vojkan Kostić**

University of Niš, Faculty of Electronic Engineering, Department of Power Engineering,
Republic of Serbia

ORCID iDs: Filip Filipović
Milutin Petronijević
Nebojša Mitrović
Bojan Banković
Vojkan Kostić

 <https://orcid.org/0000-0002-1930-9273>
 <https://orcid.org/0000-0003-2396-0891>
 <https://orcid.org/0000-0003-3767-3244>
 <https://orcid.org/0000-0002-5504-599X>
 <https://orcid.org/0000-0002-7714-469X>

Abstract. *In this paper, a novel phase-locked loop is presented based on a repetitive ripple estimator filter. The primary application of the presented phase-locked loop is in the monitoring of three-phase grid voltages and synchronization of grid connected power converters for renewable energy sources with the grid. The filter is inserted inside the loop filter of the phase-locked loop to reject oscillations that can be expected from common grid voltage disturbances. Details of the filter and phase-locked loop are presented, along with the influence of all freely adjustable parameters on overall system behaviour. In the end, the behaviour of the novel phase-locked loop is tested, validated and compared to the base phase-locked loop.*

Key words: *Renewable energy sources, phase-locked loop, synchronization.*

1. INTRODUCTION

As renewable energy sources increase their share in total electricity production, so does their role in the stability of electrical power systems [1]. It is up to the interface elements between renewable energy sources and power systems to positively contribute to the overall stability of power systems. In the case of hydropower plants, the conversion of the kinetic energy of water into electrical energy is done through power turbines and synchronous

Received September 24, 2024 / Accepted December 18, 2024

Corresponding author: Filip Filipović

University of Niš, Faculty of Electronic Engineering, Department of Power Engineering, Aleksandra Medvedeva 4,
18104 Niš, Republic of Serbia

E-mail: filip.filipovic@elfak.ni.ac.rs

machines. This process is well-researched and guidelines are established for safe and reliable operation [2]. In the case of modern renewable energy sources, like photovoltaic and wind power plants, electrical energy obtained after prime conversion is not suitable for exchange without additional modification. This modification is done using a grid connected inverter – power electronic-based device that serves as an interface element between renewable energy sources and an electrical power system [3].

Traditional synchronous machines require harmonization of generated voltages with the power system at the point of coupling with the power system before connection. This process is referred to as machine synchronization and includes matching of the machine's output voltage amplitude, frequency, phase angle and direction of rotation with the power system in the point of coupling. Synchronization is done before connection with the power system, and after a successful connection, the physical phenomena of generator-grid interaction maintains once achieved synchronization. On the opposite side, synchronization of grid-tie inverters has to be constantly performing during operation [4].

Over time, a broad spectrum of synchronization algorithms for grid-tie inverters was developed and adopted from similar applications. Along with the basic grouping of synchronization algorithms according to the number of phases (single phase and three phase), the largest classification is done according to the control method (open loop and closed loop). Open loop methods directly estimate grid voltage parameters necessary for synchronization. Closed loop methods incorporate feedback mechanisms for voltage parameter estimation. The majority of research papers today related to grid-tie inverters incorporates closed-loop methods due to their accuracy and performance, while the most popular methods in this group incorporate Phase-Locked Loop (PLL) [5].

Synchronous Reference Frame PLL (SRF-PLL) is ubiquitously exploited for the synchronization of grid-tie inverters, an algorithm that was thoroughly examined in scientific literature and easily implemented. But SRF-PLL can provide adequate performances when voltage unbalance is low, and there is no presence of voltage harmonics. If this is the case, undamped oscillations in the estimated grid voltage angle are present and the performance of all other algorithms that incorporate grid voltage angle deteriorates [6]. Coping with the voltage unbalance is usually done using Second Order Generalized Integrator (SOGI) [7] or Decoupled Double Synchronous Reference Frame (DDSRF) [8] modifications of basic SRF-PLL. These algorithms can be expanded to deal with oscillations resulting from voltage harmonics, but the practicality of that implementation is in question, due to a high number of elements and feedback loops. A more elegant method for dealing with disturbances due to voltage unbalance and/or harmonics incorporates a Moving Average Filter (MAF). It enables complete suppression of oscillations that are multiples of selected basic frequency, but with a cost on the dynamic performance of phase-locked loop [9].

In this paper, a novel method is proposed, based on repetitive control that provides the benefits of MAF without impacting the dynamic performance of the phase-locked loop. In subsequent chapters, theoretical analysis of oscillations in phase-locked loops, along with details of the proposed phase-locked loop is presented. The second chapter is dedicated to a detailed analysis of three-phase grid voltages, and the transfer of common grid disturbances in synchronous reference frame. In the third chapter basics of SRF-PLL are provided with a method for the calculation of freely selectable parameters. Forth chapter is dedicated to the proposed modification of SRF-PLL based on a repetitive filter. A detailed description of the filter is provided, its implementation, and the influence of all parameters on the overall system behavior. In the next section, validation of performance is done using MATLAB/Simulink on

a set of tests that include voltage sags and voltage harmonics. In the end, a conclusion is made according to the presented results.

2. THREE-PHASE GRID VOLTAGES

Time dependent form of phase values of three-phase grid voltages is presented using the following set of equations:

$$\begin{aligned}
 v_a(t) &= \sum_{h=0}^{\infty} V_{am,h} \cos(h\omega t + \varphi_{a,h}) \\
 v_b(t) &= \sum_{h=0}^{\infty} V_{bm,h} \cos(h\omega t + \varphi_{b,h} - h \frac{2\pi}{3}) \\
 v_c(t) &= \sum_{h=0}^{\infty} V_{cm,h} \cos(h\omega t + \varphi_{c,h} + h \frac{2\pi}{3})
 \end{aligned} \tag{1}$$

where, $v_a(t)$, $v_b(t)$ and $v_c(t)$ presents a time dependant resulting voltage in phases a , b and c , h is a harmonic number ($h = 1$ is a fundamental voltage harmonic), $V_{am,h}$, $V_{bm,h}$ and $V_{cm,h}$ represents the amplitude of h -th voltage harmonic, ω is the angular frequency of fundamental harmonic, $\varphi_{a,h}$, $\varphi_{b,h}$ and $\varphi_{c,h}$ are the phase angle of h -th voltage harmonic in phase a , b and c .

Using the method of symmetrical components [10], and under the assumption that only fundamental voltage harmonic can have unbalance, voltages (1) can be grouped according to the sequence they belong to like:

$$\begin{aligned}
 v_a(t) &= \sum_{h=1,7,13\dots} V_{m,h+} \cos(h\omega t + \varphi_{h+}) + \sum_{h=-1,-5,-11\dots} V_{m,h-} \cos(h\omega t + \varphi_{h-}) \\
 v_b(t) &= \sum_{h=1,7,13\dots} V_{m,h+} \cos(h\omega t + \varphi_{h+} - h \frac{2\pi}{3}) + \sum_{h=-1,-5,-11\dots} V_{m,h-} \cos(h\omega t + \varphi_{h-} - h \frac{2\pi}{3}) \\
 v_c(t) &= \underbrace{\sum_{h=1,7,13\dots} V_{m,h+} \cos(h\omega t + \varphi_{h+} + h \frac{2\pi}{3})}_{\text{Positive sequence}} + \underbrace{\sum_{h=-1,-5,-11\dots} V_{m,h-} \cos(h\omega t + \varphi_{h-} + h \frac{2\pi}{3})}_{\text{Negative sequence}}
 \end{aligned} \tag{2}$$

In the previous equation, $V_{m,h+}$ ($V_{m,h-}$) are amplitudes of h -th positive (negative) sequence voltage harmonics. In (2) zero order sequence components are omitted from consideration. Voltages (2) can be transferred in the synchronous reference frame (dq) using Park transformation. After transformation three-phase system of voltages can be written in the form:

$$\begin{aligned}
 v_d(t) &= \sum_{h=1,7,13\dots} V_{m,h+} \cos(h\omega t + \varphi_{h+} - \omega t) + \sum_{h=-1,-5,-11\dots} V_{m,h-} \cos(h\omega t + \varphi_{h-} - \omega t) \\
 v_q(t) &= \sum_{h=1,7,13\dots} V_{m,h+} \sin(h\omega t + \varphi_{h+} - \omega t) + \sum_{h=-1,-5,-11\dots} V_{m,h-} \sin(h\omega t + \varphi_{h-} - \omega t)
 \end{aligned} \tag{3}$$

Where $v_d(t)$ and $v_q(t)$ are direct and quadrature voltage components after Park transformation, and $\hat{\theta} = \hat{\omega}t$ presents an angle of Park transformation ($\hat{\omega}$ presents the angular frequency of Park transformation). If the fundamental positive voltage is separated from the sum in (3), and under the assumption of $\varphi_{1+} = 0$, the following expression can be obtained:

$$\begin{aligned}
 v_d(t) &= V_{m,1+} \cos(\omega t - \omega t) + \sum_{h=7,13,\dots} V_{m,h+} \cos(h\omega t + \varphi_{h+} - \omega t) + \\
 &\quad \sum_{h=-1,-5,-11,\dots} V_{m,h-} \cos(h\omega t + \varphi_{h-} - \omega t) \\
 v_q(t) &= V_{m,1+} \sin(\omega t - \omega t) + \sum_{h=7,13,\dots} V_{m,h+} \sin(h\omega t + \varphi_{h+} - \omega t) + \\
 &\quad \sum_{h=-1,-5,-11,\dots} V_{m,h-} \sin(h\omega t + \varphi_{h-} - \omega t)
 \end{aligned} \tag{4}$$

From (4) can be concluded that when the angular frequency of the fundamental harmonic matches the angular frequency of Park transformation ($\omega = \hat{\omega}$), the fundamental frequency in the synchronous reference frame is observed as a DC component. Other components can be grouped, and the following expression can be obtained

$$\begin{aligned}
 v_d(t) &= V_{m,1+} \cos(\omega t - \omega t) + f(2h, 6h, 12h\dots) \\
 v_q(t) &= V_{m,1+} \sin(\omega t - \omega t) + f(2h, 6h, 12h\dots)
 \end{aligned} \tag{5}$$

where $f(2h, 6h, 12h\dots)$ is a function that consists of the oscillation on $2h$, $6h$, $12h$ and a result of fundamental voltage unbalance, fifth and seventh harmonic, eleventh and thirteenth harmonic, respectively.

3. SYNCHRONOUS REFERENCE FRAME PHASE-LOCKED LOOP

Substituting $\hat{\theta} = \hat{\omega}t$ and $\theta_{1+} = \omega t$ in (5), and under previous assumption $\omega = \hat{\omega}$, the following equation can be obtained:

$$\begin{aligned}
 v_d(t) &= V_{m,1+} \cos(\theta_{1+} - \theta) + f(2h, 6h, 12h\dots) \\
 v_q(t) &= V_{m,1+} \sin(\theta_{1+} - \theta) + f(2h, 6h, 12h\dots)
 \end{aligned} \tag{6}$$

If the oscillatory term is neglected, when $\theta_{1+} \approx \hat{\theta}$, direct and quadrature components can be written in the form:

$$\begin{aligned}
 v_d(t) &= V_{m,1+} \cos(\theta_{1+} - \theta) \approx V_{m,1+} \\
 v_q(t) &= V_{m,1+} \sin(\theta_{1+} - \theta) \approx V_{m,1+} (\theta_{1+} - \theta)
 \end{aligned} \tag{7}$$

According to (7), when the fundamental grid voltage vector angle matches the Park transformation angle, the quadrature component in the synchronous reference frame is equal to zero. This is the basic mechanism behind the fundamental phase-locked loop – SRF-PLL.

The block structure of SRF-PLL is presented in Fig. 1. It consists of a Phase Detector (PD), Loop Filter (LF) and Voltage Controlled Oscillator (VCO). The role of PD is to provide an output proportional to the difference between the grid voltage angle and the estimated angle. LF determines the output dynamics and VCO generates a phase angle proportional to input frequency. PD in its basic variant consists of Park transformation, and the voltage v_q is used as a measure of phase difference (as shown in (7)). LF consists of a PI controller, and VCO consists of an integrator and feedforward angular frequency ω_{ff} (fixed to nominal grid frequency) to speed up the process of initial synchronization [11]. Laplace complex variable is denoted as p .

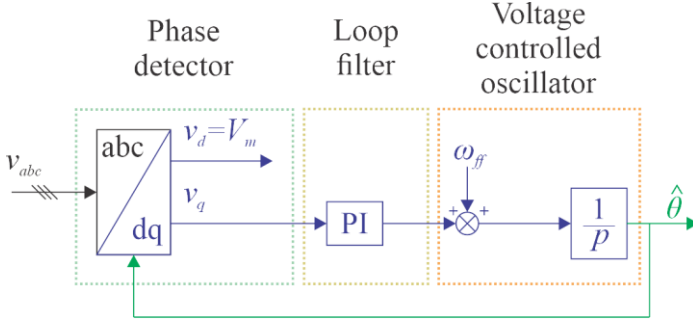


Fig. 1 Block structure of Synchronous Reference Frame Phase-Locked Loop (SRF-PLL)

A small signal model of SRF-PLL is shown in Fig. 2 [12], with $D(p)$ Laplace representation of oscillations shown in (6) is denoted $D(p) = L(f(2h, 6h, 12h...))$. As can be observed, oscillations have the same control path as the difference between the fundamental positive grid voltage angle and the estimated angle at the output of SRF-PLL θ . k_p and T_i are proportional gain and integral time constant of the PI controller.

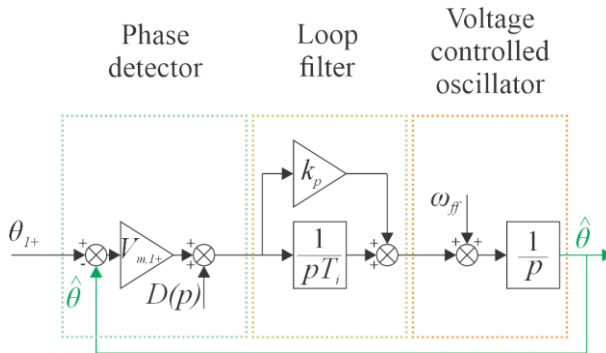


Fig. 2 Small signal model of SRF-PLL

The open loop transfer function of SRF-PLL can be presented in the form:

$$G_{ol}(p) = \frac{\theta(p)}{\theta_{i+}(p)} = V_{m,1+} \frac{pk_p T_i + 1}{p^2 T_i} \quad (8)$$

And closed-loop transfer function of SRF-PLL can be presented in the form:

$$G_{cl}(p) = \frac{G_{ol}(p)}{1 + G_{ol}(p)} = V_{m,1+} \frac{pk_p V_{m,1+} + \frac{V_{m,1+}}{T_i}}{p^2 + pk_p V_{m,1+} + \frac{V_{m,1+}}{T_i}} \quad (9)$$

Parameters of PI controller of SRF-PLL can be chosen by a comparison of closed loop transfer function of SRF-PLL and canonical form of the second order transfer function:

$$\frac{pk_p V_{m,1+} + \frac{V_{m,1+}}{T_i}}{p^2 + pk_p V_{m,1+} + \frac{V_{m,1+}}{T_i}} = \frac{p2\zeta\omega_n + \omega_n^2}{p^2 + p2\zeta\omega_n + \omega_n^2} \quad (10)$$

where ω_n is the natural frequency of the system, and ζ is the damping coefficient of the system. Based on the comparison between the left and right side of (10), PI controller parameters can be calculated using the following equation:

$$k_p = \frac{2\zeta\omega_n}{V_{m,1+}} \quad \wedge \quad T_i = \frac{V_{m,1+}}{\omega_n^2} \quad (11)$$

It is usual in scientific literature to tune SRF-PLL using the following parameters: $\zeta = \sqrt{2}/2$ and $\omega_n = 2\pi 20$ [13].

4. REPETITIVE RIPPLE ESTIMATOR FILTER BASED PHASE-LOCKED LOOP

The initial repetitive ripple estimator in a phase-locked loop was introduced in [14]. Although the presented estimator was able to suppress oscillations in the control loop due to voltage imbalance or harmonics, the dynamic of the phase-locked loop was related to the parameters of the filter. In this paper the modification of the filter was done to have a minimal effect on the dynamics of PLL. The proposed repetitive ripple estimator filter is shown in Fig. 3. It consists of two gain blocks with gain k_r , one delay block and one Moving Average Filter (MAF). The transfer function of the proposed filter is:

$$\frac{v_q}{v_q} = (1 + k_r) \frac{1 - e^{-pT_\omega} + \frac{1 - e^{-pT_\omega}}{pT_\omega}}{1 - e^{-pT_\omega} + \frac{1 - e^{-pT_\omega}}{pT_\omega} + k_r} \quad (12)$$

In Fig. 5 three models are presented for examination of the control structure:

- Large signal model that incorporates all nonlinearities in the control structure;
- Small signal model that incorporates a linearized version of all elements;
- Small signal model that omits dynamic of the proposed filter (for small values of k_r). This small signal model is identical to the small signal model of SRF-PLL.

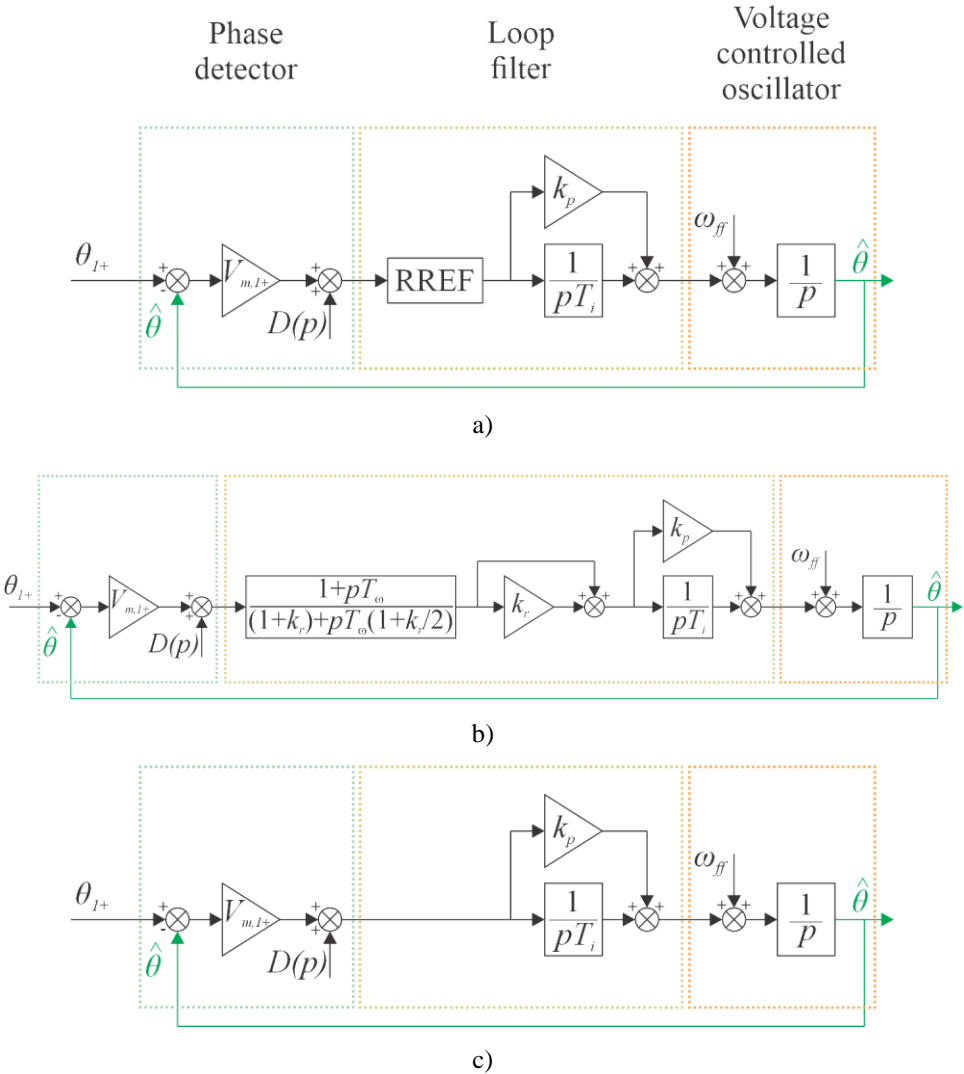


Fig. 5 Proposed RREF-PLL: a) large signal model; b) small signal model; c) small signal model for small k_r

Time delay in delay block and window of MAF T_ω is used for the suppression of the undesired oscillation in the control loop. It is well documented that MAF can suppress all

frequencies that are multiples of the window frequency ($f_\omega = 1/T_\omega$) [9]. With an appropriate T_ω a fundamental frequency for suppression can be selected, and all its multiples will also be suppressed.

The effect of k_r on filtering characteristics of the phase-locked loop can be observed in Fig 6. In the time period between 0.1 s and 0.2 s an unbalanced voltage sag without phase jump occurs that generates an oscillation in the PLL control structure. The proposed filter manages to suppress the induced oscillation. Lower values of k_r enable a more gradual suppression of disturbances in a signal. On the opposite side, higher values of k_r provide a more aggressive suppression of disturbances, but that can also result in abrupt jumps of the filtered signal. When $k_r = 0$ the filter has no effect (system behaves as SRF-PLL). The other characteristic of a filter is that it can inject disturbances once they are no longer available in the signal – the time it takes the filter to suppress oscillations is the time it needs to recover once oscillations are no longer present.

From Fig. 7 can be observed the dynamic response of the proposed RREF-PLL, along with its proposed large signal model and small signal model for different values of k_r . For the comparison test of the dynamic response, the following simulation experiment is conducted:

- In 0.1 s from the start, phase jump of 30 degrees occurs;
- In 0.2 s from the start, phase jump of 30 degrees in opposite direction occurs;
- In 0.3 s from the start, fundamental frequency jumps from 50 Hz to 55 Hz;
- In 0.4 s from the start, fundamental frequency jumps from 55 Hz to 50 Hz.

Based on the response from Fig. 7 it can be concluded that the large signal model is a good representation of RREF-PLL. Also, the response of the small signal model resembles SRF-PLL more for smaller values of k_r .

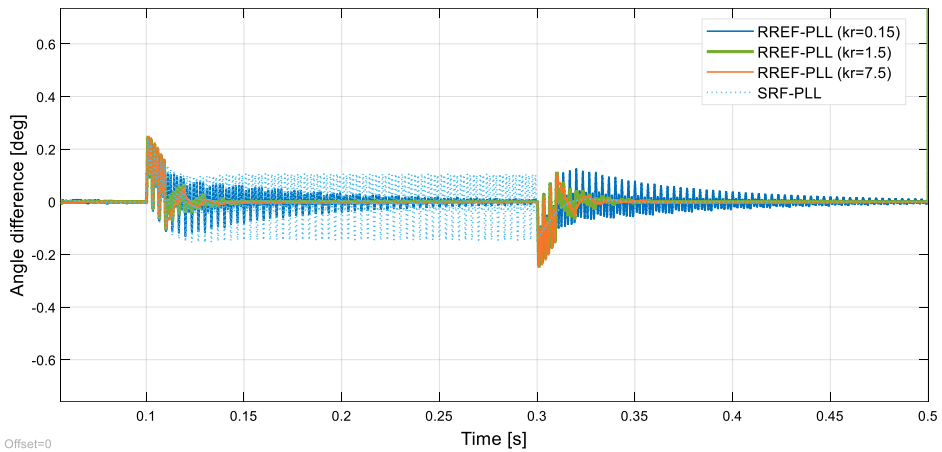
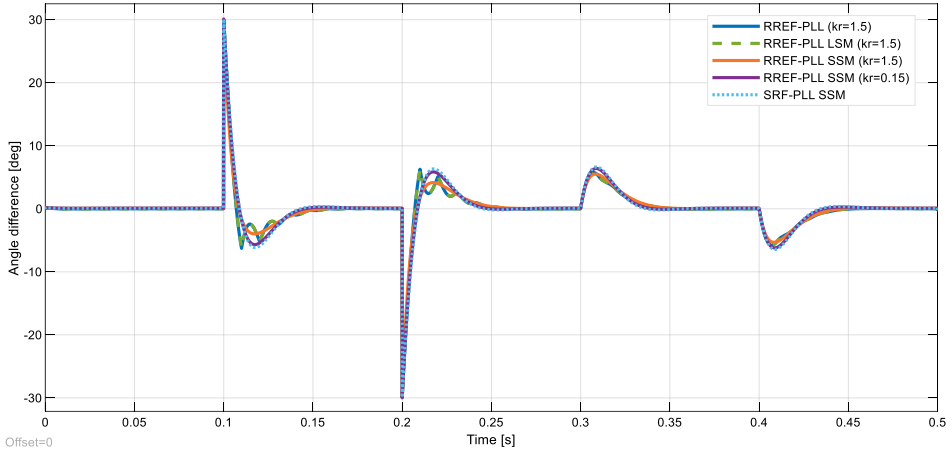
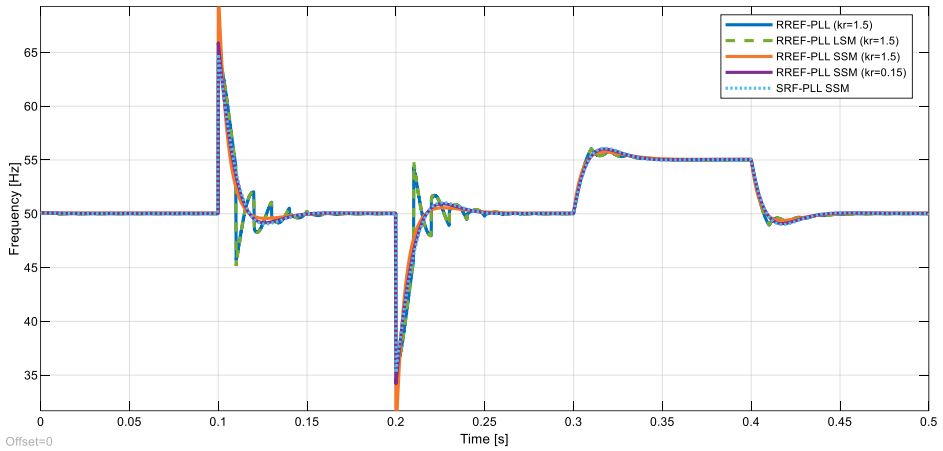


Fig. 6 Influence of parameter k_r on filtering characteristics of phase-locked loop



a)



b)

Fig. 7 Comparison of dynamic response of RREF-PLL, its proposed large signal model and small signal model with various values of k_r a) estimation of phase angle; b) estimation of frequency

The tuning procedure of all freely adjustable parameters of RREF-PLL can be deduced to the following steps:

- The parameters of PI controller can be calculated according to (11);
- The parameter T_ω is selected to suppress expected oscillations in the control loop;
- The parameter k_r is selected by trial and error according to the desired speed of oscillation suppression.

6. PERFORMANCE VALIDATION

Performance validation of the proposed RREF-PLL is done in simulation using MATLAB/Simulink R2024a. Proposed RREF-PLL is compared to SRF-PLL in the following set of tests:

- Unsymmetrical voltage sag – in the specific case Voltage sag type B [15], with a sag dip of 30%;
- Voltage harmonics – upper limits of 5-th, 7-th and 11-th harmonic continuously permissible by EN 50160:2023.

The grid voltage amplitude and all freely adjustable parameters of PLLs are listed in Table 1.

Table 1 Parameters of phase-locked loops

Algorithm\Parameter	$V_{m,1+}$	ζ	ω_n	k_p	T_i	T_ω	k_r
RREF-PLL	$230\sqrt{2}$	$\sqrt{2}/2$	$2\pi 20$	0.546	0.021	0.01	1.5
SRF-PLL	$230\sqrt{2}$	$\sqrt{2}/2$	$2\pi 20$	0.546	0.021	/	/

Details of PLL implementation in MATLAB/Simulink R2024a are shown in Fig. 8.

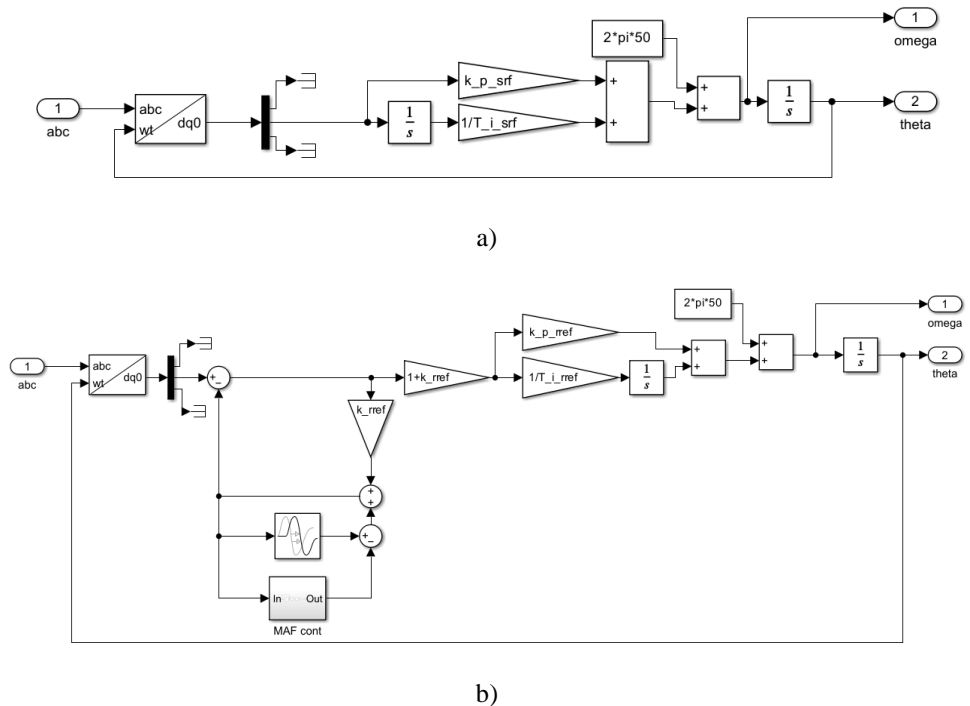


Fig. 8 Details of PLL implementation in MATLAB/Simulink R2024a: a) SRF-PLL; b) RREF-PLL

The voltage sag test is shown in Fig. 9. The sag transition was rectangular, and 30 degrees phase jump accompanied the sag. SRF-PLL exhibited undamped oscillations during sag on twice the fundamental frequency, while RREF-PLL successfully suppressed the oscillations and was able to provide the exact fundamental positive sequence voltage phase angle estimation.

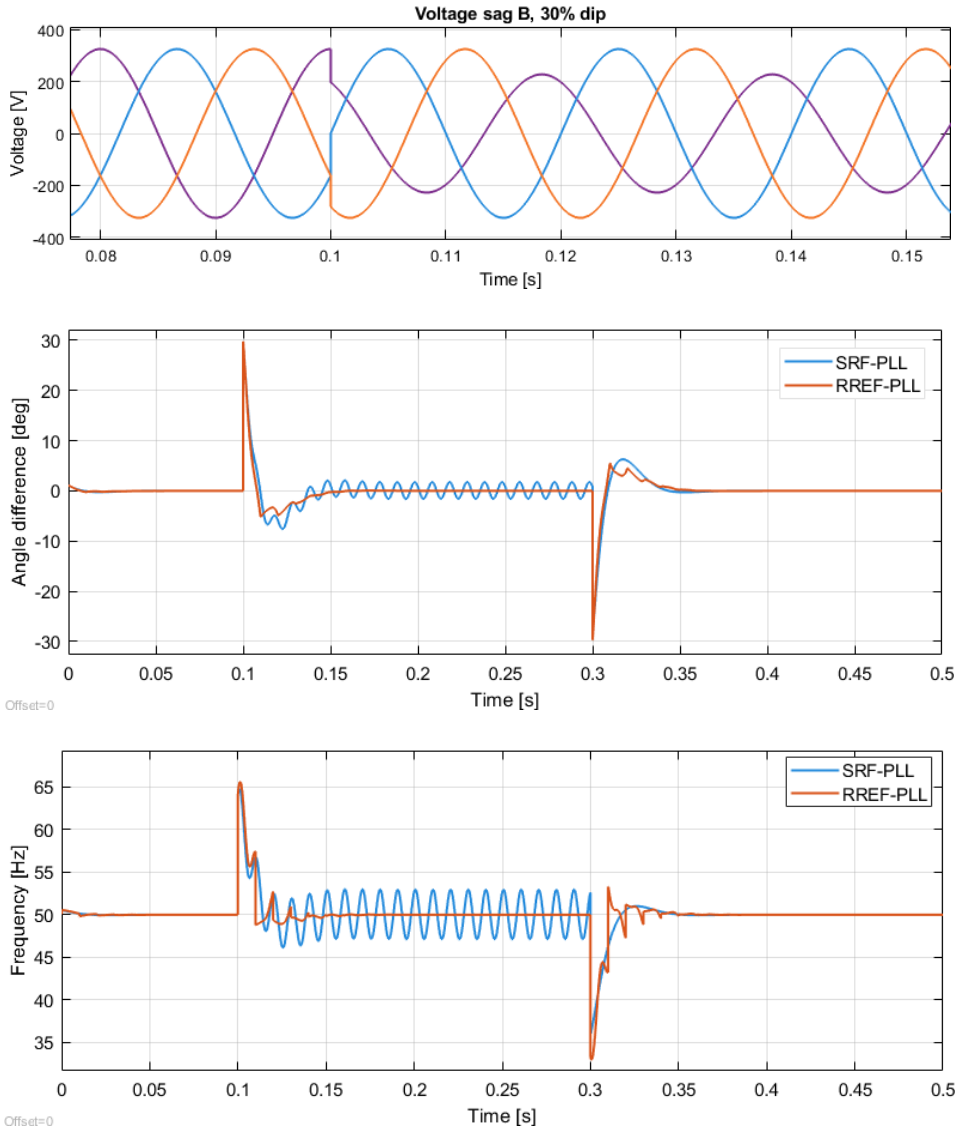


Fig. 9 Dynamic response of proposed RREF-PLL compared to SRF-PLL in the event of voltage sag

The voltage harmonics test is shown in Fig 10. As in the voltage sag test, SRF-PLL exhibits undamped oscillations during the period with harmonics. RREF-PLL iteratively suppressed harmonics within the time of about 50 milliseconds. About 50 milliseconds after the harmonics were terminated, RREF-PLL generated oscillations until it was able to provide an accurate prediction of the phase angle.

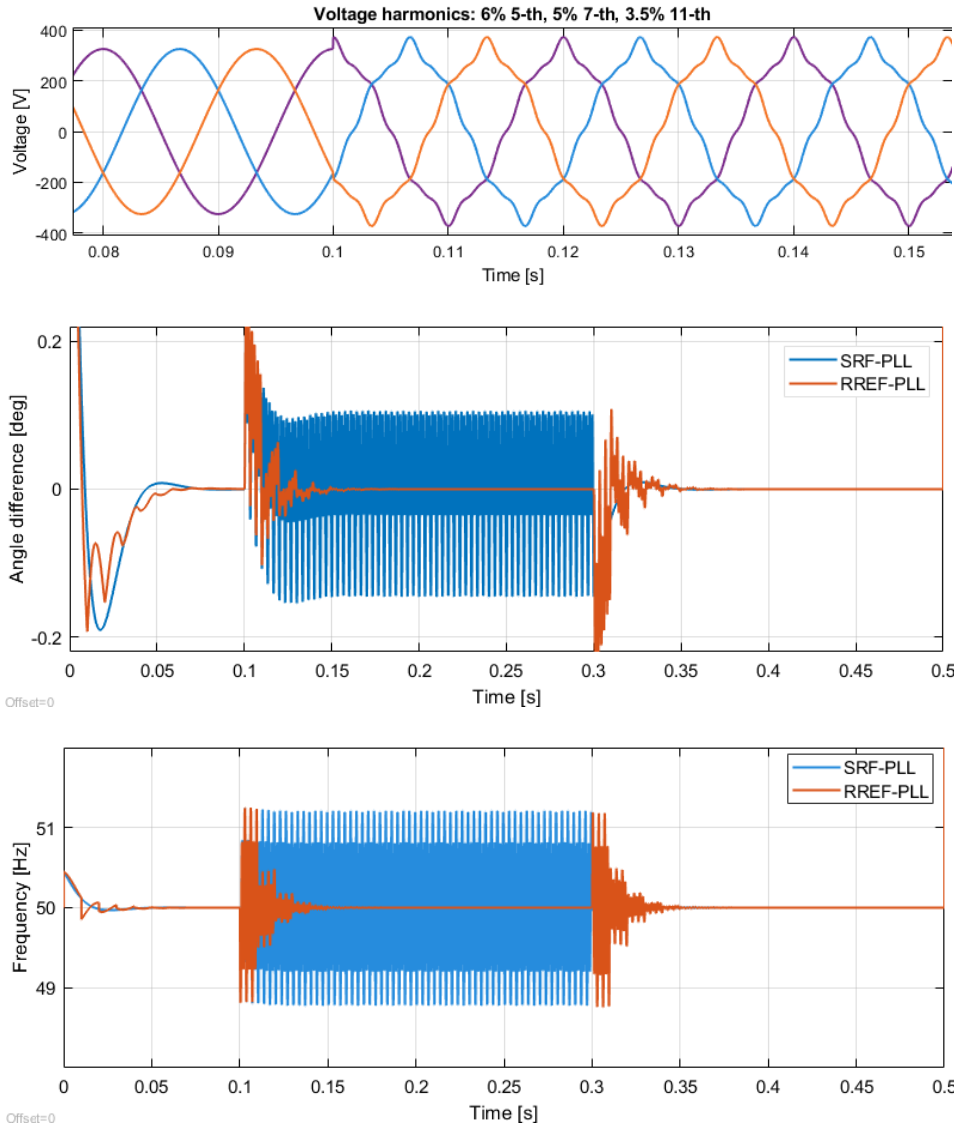


Fig. 10 Dynamic response of proposed RREF-PLL compared to SRF-PLL in the event of voltage harmonics

Abrupt variations of the phase angle estimation for large values of k_r does not make RREF-PLL suitable for coordinate transformations of vector-controlled grid-tie inverters, but rather for acquisition and monitoring algorithms. Smaller values of k_r make RREF-PLL suitable for coordinate transformations of vector-controlled grid-tie inverters, at the cost of disturbances in the estimated phase angle for a longer period than in the case of larger k_r . Also, smaller values of k_r can induce oscillations after their cause is eliminated in the measured voltages, that can lead to an unexpected behaviour of the device where the proposed RREF-PLL is implemented.

7. CONCLUSION

In this paper a novel phase-locked loop is presented based on the SRF-PLL and repetitive ripple estimator filter. A detailed design procedure was provided, accompanied by a proposed large signal model and a small signal model. The proposed repetitive ripple estimator filter provides unity gain for the DC component. For small values of k_r , parameters of the proposed RREF-PLL can be calculated as for the SRF-PLL. The parameter T_ω is selected to suppress expected oscillations in the control loop as for MAF-PLL. The effectiveness of the repetitive ripple estimator was shown in suppressing undesired oscillations originating from the voltage unbalance or voltage harmonics in the simulation.

Acknowledgement: *This work was supported by the Ministry of Science, Technological Development and Innovation of the Republic of Serbia [grant number 451-03-65/2024-03/200102].*

REFERENCES

- [1] B. Qin, M. Wang, G. Zhang, and Z. Zhang, "Impact of renewable energy penetration rate on power system frequency stability," *Energy Reports*, vol. 8, pp. 997–1003, Nov. 2022. doi:10.1016/j.egy.2022.05.261.
- [2] B. Xu et al., "Stability Analysis of a hydro-turbine governing system considering inner energy losses," *Renewable Energy*, vol. 134, pp. 258–266, Apr. 2019. doi:10.1016/j.renene.2018.11.026.
- [3] V. Boscaino et al., "Grid-connected photovoltaic inverters: GRID codes, topologies and control techniques," *Renewable and Sustainable Energy Reviews*, vol. 189, p. 113903, Jan. 2024. doi:10.1016/j.rser.2023.113903.
- [4] W. Jarzyna, "A survey of the synchronization process of synchronous generators and Power Electronic Converters," *Bulletin of the Polish Academy of Sciences Technical Sciences*, pp. 1069–1083, Dec. 2019. doi:10.24425/bpasts.2019.131565.
- [5] P. Gawhade and A. Ojha, "Recent advances in synchronization techniques for grid-tied PV system: A Review," *Energy Reports*, vol. 7, pp. 6581–6599, Nov. 2021. doi:10.1016/j.egy.2021.09.006.
- [6] N. Jaalam, N. A. Rahim, A. H. A. Bakar, C. Tan, and A. M. A. Haidar, "A comprehensive review of synchronization methods for grid-connected converters of renewable energy source," *Renewable and Sustainable Energy Reviews*, vol. 59, pp. 1471–1481, Jun. 2016. doi:10.1016/j.rser.2016.01.066.
- [7] M. Ciobotaru, R. Teodorescu, and F. Blaabjerg, "A new single-phase PLL structure based on second order Generalized Integrator," 2006 37th IEEE Power Electronics Specialists Conference, Jun. 2006. doi:10.1109/pesc.2006.1711988
- [8] P. Rodriguez et al., "Double synchronous reference frame PLL for power converters control," 2005 IEEE 36th Power Electronics Specialists Conference, vol. 4, pp. 1415–1421, 2005. doi:10.1109/pesc.2005.1581815
- [9] S. Golestan, M. Ramezani, J. M. Guerrero, F. D. Freijedo, and M. Monfared, "Moving average filter based phase-locked loops: Performance Analysis and Design Guidelines," *IEEE Transactions on Power Electronics*, vol. 29, no. 6, pp. 2750–2763, Jun. 2014. doi:10.1109/tpe.2013.2273461

- [10] C. L. Fortescue, "Method of symmetrical co-ordinates applied to the solution of Polyphase Networks," *Transactions of the American Institute of Electrical Engineers*, vol. XXXVII, no. 2, pp. 1027–1140, Jul. 1918. doi:10.1109/t-aiee.1918.4765570
- [11] "Synchronous reference frame PLL," *Enhanced Phase-Locked Loop Structures for Power and Energy Applications*, pp. 133–145, Mar. 2014. doi:10.1002/9781118795187.ch6
- [12] Z. Dai et al., "Global Stability Analysis for synchronous reference frame phase-locked loops," *IEEE Transactions on Industrial Electronics*, vol. 69, no. 10, pp. 10182–10191, Oct. 2022. doi:10.1109/tie.2021.3125655
- [13] Y. F. Wang and Y. Wei Li, "Analysis and digital implementation of cascaded delayed-signal-cancellation PLL," *IEEE Transactions on Power Electronics*, vol. 26, no. 4, pp. 1067–1080, Apr. 2011. doi:10.1109/tpe.2010.2091150
- [14] F. Filipovic, M. Petronijevic, N. Mitrovic, B. Bankovic, and V. Kostic, "Application of repetitive ripple estimator in synchronization of three phase grid tie inverters," *2019 20th International Symposium on Power Electronics (Ee)*, pp. 1–6, Oct. 2019. doi:10.1109/pee.2019.8923405
- [15] M. H. Bollen, *Understanding Power Quality Problems*, 1999. doi:10.1109/9780470546840

DESIGN AND OPTIMIZATION OF SOLAR PARKING CANOPY AS A PART OF ENERGY EFFICIENT URBAN PLANNING

UDC (621.383.51:622.7.012)


Aleksandar Pantić, Adriana Petković, Sanja Aleksić

University of Niš, Faculty of Electronic Engineering,
Department of Microelectronics, Republic of Serbia

ORCID iDs: Aleksandar Pantić
Adriana Petković
Sanja Aleksić

 <https://orcid.org/0000-0003-2351-498X>

 <https://orcid.org/0009-0007-0453-8704>

 <https://orcid.org/0000-0003-4414-6442>

Abstract. *This paper proposes the optimal use of available space on canopies of parking spaces in urban areas for the installation of low and medium power photovoltaic systems and electricity production. Simulations show that a PV1 system offers a return on investment of 187% with a payback period of 5.6 years, while a PV2 system achieves an ROI of 91.9% with an 8.4-year payback. These findings emphasize the cost-effectiveness and environmental benefits of solar parking canopies in urban planning. The obtained electricity could be used to power nearby residential and business premises or electric car chargers. Also, there is a possibility of direct injection of produced electricity into the distribution network. Two configurations of the photovoltaic system at a specific location were analyzed in order to find the optimal solution in terms of the relationship between the price of the system, the electricity produced and the time required to return the investment. The program PVsyst was used for the design and optimization of photovoltaic systems. The obtained simulation results for both proposed photovoltaic systems are presented and compared.*

Key words: *Solar energy, PV system, parking, canopy, urban planning.*

1. INTRODUCTION

Population growth projections indicate that by 2050. over 70% of the global population will live and work in cities since metropolitan development will continue progressing in the upcoming decades [1]. The continuous temperature increases in the urban areas, affected by rapid urbanization and undeniable climatic change, are escalating the energy problem of cities and intensifying the pollution problems. The main impact of cities on the local

Received October 28, 2024 / Accepted December 19, 2024

Corresponding author: Aleksandar Pantić

University of Niš, Faculty of Electronic Engineering, Department of Microelectronics, Aleksandra Medvedeva 4,
18104 Niš, Republic of Serbia

E-mail: aleksandar.pantic@elfak.ni.ac.rs

weather is the Urban Heat Island (UHI). Parking lots are large pavement surfaces that absorb the sun's energy and retain heat, therefore contributing to the UHI effect. The number of spaces per vehicle is rising as the adult population has become more dependent on cars; thus, a large portion of the urban environment is dedicated to parking lots. Installing a solar canopy over an existing parking lot is a more efficient use of the duplicate square footage and could turn an open pavement surface into a significant electricity generator. Solar energy, as renewable energy, is seen as a necessary step toward sustainable energy development, reduction of fossil fuel usage, and mitigation of climate change.

Public spaces are the structural elements of any architectural environment, areas of social cohesion, spaces of coexistence and outbreaks of urbanity programmatically designed to attract all types of publics, reunite the citizens of the city, and improve the dynamics of the urban space; in one word, the city's front window. The quality of urban space is primarily determined by the quality of the public areas belonging to the city, the areas that the city offers for common use to its inhabitants. Architecture and reason usually go together: we build for a specific purpose, for specific functions; we use materials and methods that are directly related to the situations in which we need to interfere; we calculate, anticipate, and ensure as much as possible that our interventions in the public space will be used in the way that we have imagined. But what would happen if we did not have these motivations? If we would only build to change the image of the city, to renew the relationship between man and architecture. Can we rebuild so that we sublimate our present experience? This paper proposes an incursion that provides an answer to these actions: to build, beautify, regain, experience, plan, perceive, criticize, program, and transform our relationship with architecture and the city. These actions, with their possible variations and associated ramifications, are the main directions or, rather, the effects of small landscape designs in the lost or forgotten spaces of the city. This paper also, in addition to all the above, offers a solution on how to optimally and efficiently use the existing space on the canopies of the parking lot to install photovoltaic systems and obtain electricity.

Solar radiation reaching the Earth's surface is estimated at about 190 million TWh annually. This energy is about 170 times greater than the total reserves of coal worldwide and, compared to the energy needs of humankind, which amount to 130 thousand TWh annually [2]. Serbia has an average of 272 sunny days and about 2300 sunny hours. The average daily energy of global radiation, in the territory of the Republic of Serbia ranges from 1,1 kWh/m² in the north to 1,7 kWh/m² in the south during the winter period, while for the summer period, it ranges from 5,9 kWh/m² in the north to 6,6 kWh/m² in the south. Annually, the average value of the overall sun radiation for the territory of the Republic of Serbia ranges from 1200 kWh/m² in northwest Serbia to 1550 kWh/m² in southeast Serbia, while in the middle part, it is about 1400 kWh/m² (Fig. 1 (left)). Therefore, our Nisava region has very great potential when it comes to the use of solar energy for electricity production. It is estimated that the value of specific photovoltaic power output (PVOUT), which represents yearly average values of photovoltaic electricity delivered by a PV system and normalized to 1kWp of installed capacity, ranges from 3,22kWh/kWp to 3,77kWh/kWp (Fig. 1 (right)) [3].

It is obvious that solar radiation in Serbia and our region is about 40% higher than in the countries in European Union, but we are still significantly behind in terms of installed photovoltaic capacities. This gives us great opportunities to replace fossil fuels in the coming period and start getting significant amounts of electricity from medium and small photovoltaic power plants.

2. BENEFITS OF UTILIZATION OF SOLAR ENERGY

Renewable energy is seen as the solution for managing both increasing electricity demand and environmental sustainability. Solar canopies are an innovative way to maximize an existing space for multiple purposes and benefits. Photovoltaics are seen to be generally of benign environmental impact, generating no noise or chemical pollutants during use. It is one of the most viable renewable energy technologies used in an urban environment, replacing existing building cladding materials [4]. The University of Kansas predicted electricity production with close to zero emissions [5], meaning no CO₂, NH₄, or N₂O was produced. In their research, the most significant effect of PV parking spots was reducing carbon dioxide (CO₂) emitted by the University. It was estimated that the University would save 2.5 metric tons of CO₂ emissions per year for each covered parking space. The CO₂ emission reductions in methane (NH₄) and nitrous oxide (N₂O) of metric tons and 0.03 metric tons would also occur, chemicals known to cause acid rain and increase global warming.

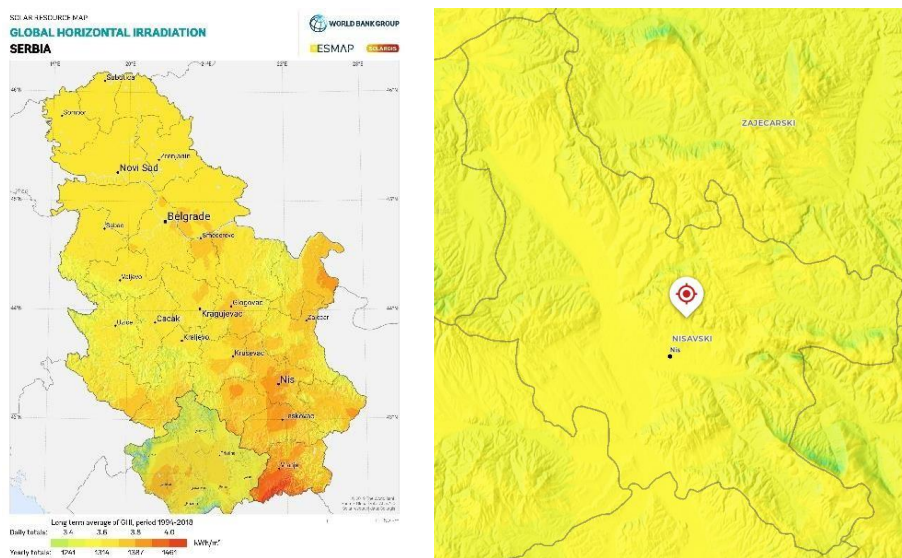


Fig. 1 Global horizontal irradiation (GHI) for the Republic of Serbia (left), and specific photovoltaic power output (PVOUT) for Nisava region (right) [3,4]

Furthermore, UHI leads to greenhouse gas emissions and increased summer peak energy demands and that could be mitigated by installing solar parking canopies. Solar panels absorb solar energy to produce energy used in buildings. During this process, they modify the energy balance of the urban surface in contact with the atmosphere and thus influence the urban microclimate. A scenario of large but realistic deployment of solar panels in the Serbia urban area was simulated in the research [6], and the results showed a reduction in the UHI of 0.2 K by day and up to 0.3 K at night. Also, in the same study, it was calculated that for the summer period, the solar panels reduced the energy needed for air-conditioning by 12%. Since the UHI effect is most pronounced during summer peak power demands, the applied PV panels to mitigate is beneficial for the amount of power produced by the PV panels.

One of the apparent benefits considering the solar parking canopy is the shade provided by the solar panels covering the vehicles. Shade considerably reduces the vehicle temperature during the day, protecting it from sun damage, such as paintwork damaged or cracked and warped interiors during the hot summer period. In a typical parking lot, a car is subjected to direct sunlight exposure in the spring and summer months. According to the Centers for Disease Control and Prevention, if the temperature reaches 27°C or more, the temperature inside a vehicle can quickly climb between 37°C to 54°C degrees. The research [7] shows that at 35°C , the energy consumption would increase from 2% to 70% and that these increases were due to the extra energy required to run the air-conditioning system to maintain 22°C cabin temperatures. These increases in energy consumption depended on the air-conditioning system type, powertrain architecture, powertrain capabilities, and drive patterns. The more efficient the powertrain, the more significant climate control (heating or cooling) impact on energy consumption.

Additionally, lower internal temperature provides more comfort for drivers entering the car after sun exposure and reduces their heatstroke risk. As the survey shows [8], drivers perceive shade as a valuable parking lot asset. Furthermore, the solar parking canopy could protect from both rain and snow.

3. SIMULATION RESULTS

In this paper, we consider the possibilities of realizing a photovoltaic power plant in the electrical engineering school “Nikola Tesla” parking lot (Fig. 2 (left)), whereby solar panels would be placed on the canopy of the parking lot. The cross section of the canopy structure is shown in the fig. 2 (right). City of Niš is situated in the southern and eastern Serbia region at the $43^{\circ}19'$ latitude north and $21^{\circ}54'$ longitude east, at about 200 meters above sea level, in the Nišava region.

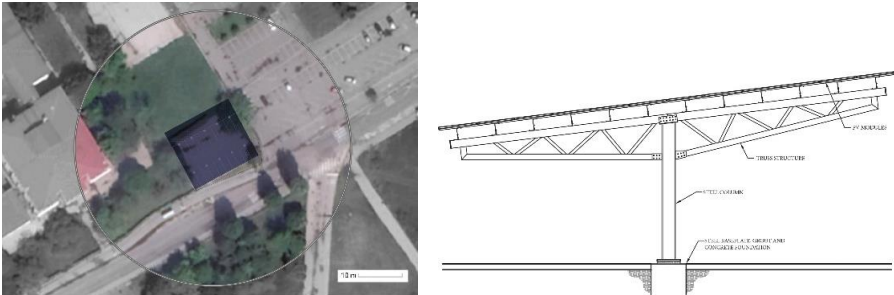


Fig. 2 Location of high school “Nikola Tesla” Niš parking lot and proposed solar canopy (left), and potential truss canopy construction (right)

There are no visible markings for parking places, and the concrete suffered mechanical damage over time. Groundwork, reconstruction of the car access is suggested, and the formation of 20 parking spaces. The 90° parking angle would provide the most parking spaces for a given area, two rows with ten parking spaces each, divided by two-way traffic flow. The pedestrian zone is designed in the north part of the lot, making the straight line to the High School entrance plane. A truss canopy is proposed for a solar mounting canopy structure. Two, five columns, solar canopies are designed with a length of 24m and a width of 9m for ten cars in a row. A total of 432 m^2 of space is at the solar canopy shade.

By analyzing the situation on the ground, we can see that the orientation of the parking lot and the canopy on it deviates from the ideal, which would allow maximum use of available solar radiation. Provided that the construction of the parking canopy is monitored, the solar panels would be placed at an angle of -23° azimuth angle facing south, while the elevation slope would be 10° slope, which corresponds to the slope of the canopy structure.

3.1. Case studies configuration and simulation

As already indicated, we will design two variants of the photovoltaic system, where in the first case study, PV1, cheaper solar panels of lower power are used, while in the second case study, PV2, more expensive solar panels of higher power are installed. The goal is to determine which configuration will be more favorable, both in terms of the total required investment, and in terms of the amount of electricity produced and the time of return on investment. The characteristics of the used solar panels are given in Table 1.

Table 1 Solar panel characteristics

Solar panel	PV1	PV2
Model	GCL-M3/60GDF	GCL-M3/72GD
Manufacturer	GLC	GLC
Technology	Si-mono	Si-mono
Nominal power	300 Wp	400 Wp
Short-circuit current	9.48A	10.28A
Open-circuit voltage	39.80V	49.20V
Efficiency	20.07%	22.25%
Dimension	1706×1006mm	2030×1000mm
Weight	25,90kg	28,20kg
Price	195€	250€

Solar panels based on the technology of the monocrystalline Si renowned manufacturer GCL System Integration Technology Co. Ltd were used. Both used solar panels are newer generation products, have very good characteristics and are available on our market. Photovoltaic system (PV) configuration and preliminary simulations were done in PVsyst software tool. This software tool offers a large database with meteorological data for our location, as well as a large selection of PV system elements. Perspective of the PV-field and surrounding shading scene are defined using the PVsyst program which is shown in fig. 3. The

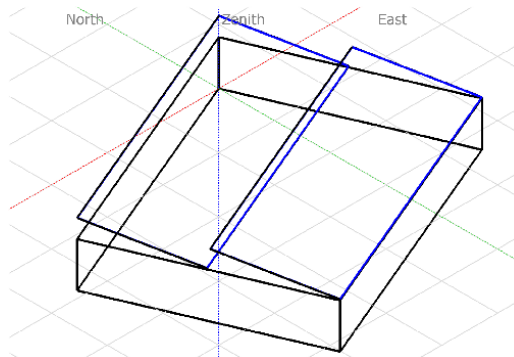


Fig. 3 Perspective of the PV-field and surrounding shading scene

deviation of the constructed PV field from the optimal orientation to the south can be clearly seen.

Fig. 4 shows an iso-shadings diagram for our location that shows the trajectory of the Sun for characteristic dates during the year, as well as losses due to shading, which are, as can be seen, most present during the winter months.

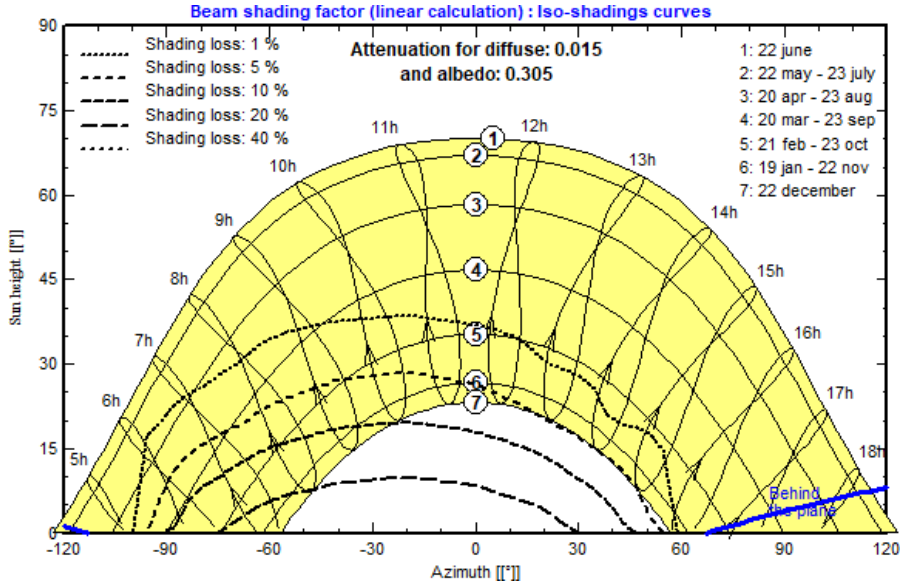
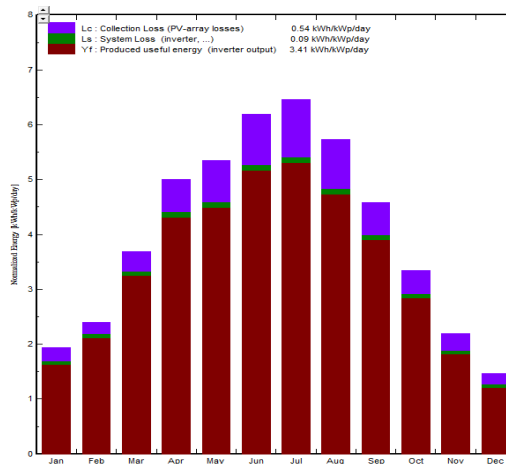


Fig. 4 Iso-shadings diagram

The first designed and optimized photovoltaic system PV1 used mono-Si solar panels GCL-M3/60GDF-300. PV1 system consists of 247 PV modules (string with 13 modules in series and 19 strings in parallel) with total area of 424 m² where the effective area of solar cells is 370 m². Global nominal power (STC) of PV1 system is 74,1 kWp, whereby under normal operating conditions at 50°C the power of PV1 is 67,2 kWp. In this system we use 6 inverters, Sunny Boy 10000TLUS-12-240 produced by SMA Energy System, with the nominal power of 10 kW and operating voltage between 345 and 480 V. Balances and main results (GlobHor - horizontal global irradiation, DiffHor - horizontal diffuse irradiation, T_Amb - average temperature, EArray - effective energy at the output of the array, E_User - energy supplied to the user, E_Solar - energy from the sun, E_Grid - energy injected into grid), by months, obtained by the simulation are given in the table 2. The designed photovoltaic system PV1 would produce about 92 MWh of electricity per year, and as can be noticed, photovoltaic system provides the school with a significant amount of electricity, and in addition, a good part of the produced energy is delivered to the electricity distribution network. Monthly normalized production (per installed kWp) of PV1 is shown in the fig. 5. As can be expected, the system provides the most energy in the period from March to October, while in the winter months the production of electricity is somewhat lower.

Table 2 Balances and main results for PV1 system

	GlobHor	DiffHor	T_Amb	GlobInc	GlobEff	EArray	E_User	E_Solar	E_Grid	EfrGrid
	kWh/m ²	kWh/m ²	°C	kWh/m ²	kWh/m ²	kWh	kWh	kWh	kWh	kWh
January	49.8	25.60	0.61	60.0	55.3	3892	9150	2284	1465	6865
February	59.0	32.53	2.37	67.0	63.3	4548	9150	2657	1745	6493
March	104.9	57.05	7.71	114.2	108.8	7662	9139	3429	4045	5710
April	142.5	64.31	12.21	150.0	144.2	9805	9150	3959	5631	5191
May	162.2	79.92	17.58	165.8	159.1	10567	9150	4178	6148	4971
June	184.3	84.04	20.16	185.8	178.4	11728	9150	4598	6880	4552
July	197.0	79.05	22.77	200.4	193.0	12439	9150	4460	7726	4690
August	169.6	67.78	22.65	177.5	171.0	11115	9150	4180	6706	4970
September	126.6	50.72	16.69	137.6	132.0	8878	9150	3750	4934	5400
October	90.7	40.77	12.66	103.6	98.4	6697	9150	3070	3453	6079
November	54.6	27.43	6.85	65.6	60.6	4186	9150	2459	1585	6691
December	37.8	22.76	2.31	45.5	41.6	2918	9150	1970	814	7180
Year	1379.3	631.94	12.11	1473.0	1405.7	94435	109787	40994	51131	68792


Fig. 5 Monthly normalized production (per installed kWp) of PV1.

The second designed and optimized photovoltaic system PV2 used mono-Si solar panels GCL-M3/72GD-400. PV2 system consists of 210 PV modules (string with 15 modules in series and 14 strings in parallel) with total area of 426 m² where the effective area of solar cells is 378m². Global nominal power (STC) of PV2 system is 84,0 kWp, whereby under normal operating conditions at 50°C the power of PV1 is 76,0 kWp. In this system we use 3 inverters, Sunny Tripower 25000TL-JP-30 produced by SMAEnergy System, with nominal power of 25 kW and operating voltage between 390 and 800 V. Balances and main results, by months, obtained by simulation are given in the table 3, while the monthly normalized production (per installed kWp) of PV2 is shown in the fig. 6.

The designed photovoltaic system PV2 would produce about 107 MWh of electricity per year, which is about 15 MWh more than the photovoltaic system PV1. Monthly normalized production (per installed kWp) of PV2 is shown in the fig. 6.

Table 3 Balances and main results for PV2 system

	GlobHor	DiffHor	T_Amb	GlobInc	GlobEff	EArray	E_User	E_Solar	E_Grid	EFrGrid
	kWh/m ²	kWh/m ²	°C	kWh/m ²	kWh/m ²	kWh	kWh	kWh	kWh	kWh
January	49.8	25.60	0.61	60.0	54.3	4372	9150	2425	1873	6725
February	59.0	32.53	2.37	67.0	62.6	5001	9150	2770	2148	6380
March	104.9	57.05	7.71	114.2	108.2	8604	9150	3556	4909	5594
April	142.5	64.31	12.21	150.0	143.9	11199	9150	4082	6922	5068
May	162.2	79.92	17.58	165.8	159.0	12094	9150	4324	7553	4826
June	184.3	84.04	20.16	185.8	178.2	13404	9150	4735	8430	4415
July	197.0	79.05	22.77	200.4	192.8	14247	9150	4584	9397	4566
August	169.6	67.78	22.65	177.5	170.8	12675	9150	4288	8159	4862
September	126.6	50.72	16.69	137.6	131.4	10027	9150	3852	6002	5298
October	90.7	40.77	12.66	103.6	97.3	7464	9150	3190	4147	5960
November	54.6	27.43	6.85	65.6	59.6	4636	9150	2580	1978	6569
December	37.8	22.76	2.31	45.5	40.9	3199	9150	2109	1030	7041
Year	1379.3	631.94	12.11	1473.0	1399.1	106923	109797	42495	62548	67302

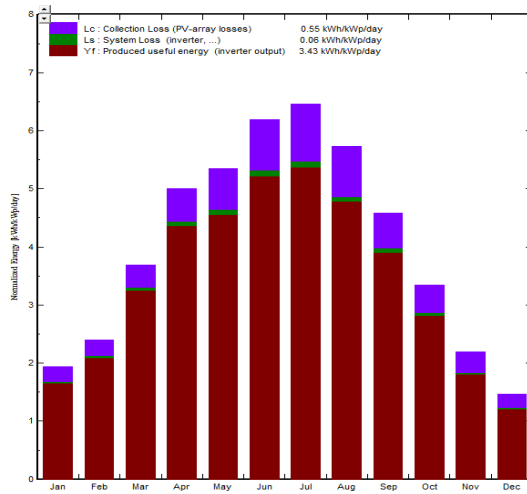


Fig. 6 Monthly normalized production (per installed kWp) of PV2

3.2. PV canopies comparison and techno-economic analysis

The obtained simulation results of both photovoltaic systems show the justification of the investment. Of course, it is necessary to make a choice between these two systems, depending on the given conditions and circumstances. Therefore, we will first compare their characteristics. A comparison of the obtained simulation results for photovoltaic systems PV1 and PV2 is given in Table 4. We compared the effective energy that photovoltaic systems provide E Array, the amount of electricity we supply to distribution network E Grid, as well as their performance ratio PR, which in fact represent a measure of the quality of a PV system that is independent of location and it therefore often described as a quality factor. It is clear that these are PV systems with similar characteristics. Thereby photovoltaic system PV2 produces slightly more electricity and has a better performance ratio.

Table 4 Comparison of the simulation results for case studies PV1 and PV2

	PV1			PV2		
	E_Array	E_Grid	PR	E_Array	E_Grid	PR
	[MWh]	[MWh]	[ratio]	[MWh]	[MWh]	[ratio]
January	3.89	1.465	0.877	4.37	1.873	0.929
February	4.55	1.745	0.870	5.00	2.148	0.920
March	7.66	4.045	0.851	8.60	4.909	0.901
April	9.80	5.631	0.830	11.20	6.922	0.881
May	10.57	6.148	0.792	12.09	7.553	0.847
June	11.73	6.880	0.785	13.40	8.430	0.841
July	12.44	7.726	0.765	14.25	9.397	0.823
August	11.11	6.706	0.775	12.67	8.159	0.833
September	8.88	4.934	0.800	10.03	6.002	0.854
October	6.70	3.453	0.838	7.46	4.147	0.890
November	4.19	1.585	0.852	4.64	1.978	0.905
December	2.02	0.814	0.892	3.20	1.030	0.941
Year	94.44	51.131	0.812	106.92	62.548	0.866

A detailed overview of the prices of photovoltaic system components, design, studies and maintenance, as well as techno-economic evaluation is shown in Table 5. From the attached data, it is obvious that it is more profitable to invest in the first photovoltaic system PV1, despite the fact that it has less installed power. Namely, the price of produced electricity obtained from this system is lower, the return on investment (payback time) is shorter and the net profit is higher, which shows us the ROI (return of investment) index it represents the ratio of realized benefits and total investments. The cumulative cashflow for PV1 and PV2 for the total lifetime of the project is shown in the Fig. 7.

Table 5 Economic evaluation

	PV1			PV2		
Investment						
PV modules	247 units	195€	48,165€	210 units	250€	52,500€
Inverters	6 units	2,000€	12,000€	3 units	3,500€	10,500€
Studies and analyses			6,000€			6,500€
Taxes and subsidies			12,270€			15,030€
Net investment			50,435€			68,530€
Operating cost per year			3,750€			5,305€
Cost of produced energy		€/kWh	0.068		€/kWh	0.087€
Return of investment						
PV lifetime	years		20			20
Payback	years		5.6			8.4
Net profit			94,318€			62,962€
ROI			187%			91.9%

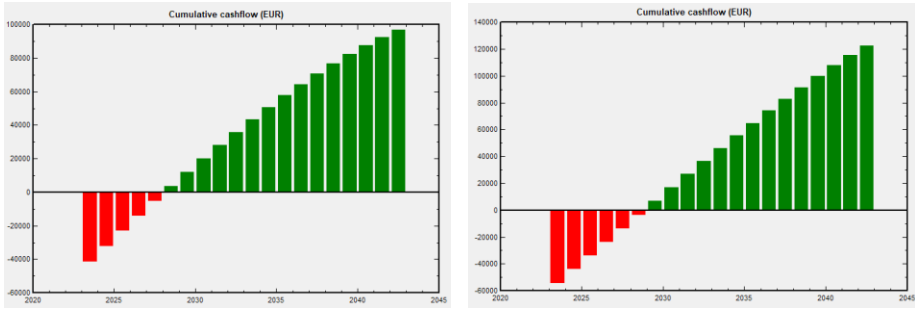


Fig. 7 Cumulative cashflow for PV1 (left) and PV2 (right)

4. CONCLUSION

This research successfully demonstrates the feasibility and advantages of implementing solar parking canopies as a sustainable solution to urban energy challenges. The analysis of the photovoltaic systems PV1 and PV2 at the parking lot of the Electrical Engineering High School "Nikola Tesla" in Niš highlights their potential to transform an underutilized space into a productive energy source. By leveraging available solar radiation, these systems can generate significant electricity, reduce greenhouse gas emissions, and contribute to mitigating urban heat island effects.

The techno-economic analysis reveals that while both systems are viable, PV1 offers a more attractive return on investment due to its lower initial costs and shorter payback period, despite PV2 producing slightly more electricity. These findings underscore the importance of balancing cost-efficiency with energy production in renewable energy projects.

Beyond economic benefits, the adoption of solar parking canopies aligns with global efforts to transition towards renewable energy and sustainable urban planning. By integrating energy production with urban infrastructure, cities can address growing energy demands, reduce environmental impact, and improve the quality of public spaces.

Furthermore, integrating Internet of Things (IoT) technologies with solar parking systems could amplify their effectiveness. As demonstrated in studies like [9], IoT-enabled parking solutions can improve space utilization, enhance energy efficiency, and provide real-time monitoring and management of parking and energy systems. This integration would enable smarter urban infrastructure, creating opportunities for automated energy management, dynamic charging for electric vehicles, and predictive maintenance for photovoltaic installations.

Future research should explore the long-term performance of such systems under varying climatic conditions, the integration of battery storage for enhanced energy management, and the potential scalability of the approach in different urban settings. Collaboration with policymakers and urban planners is crucial to maximize the adoption and impact of solar parking canopies in creating resilient and energy-efficient cities.

Acknowledgement: *This work was supported by the Ministry of Science, Technological Development and Innovation of the Republic of Serbia [grant number 451-03-65/2024-03/200102].*

REFERENCES

- [1] A. Mermoud, Figut: Software for the Study and Simulation of Photovoltaic Systems, PVsyst SA (formerly ISE, University of Geneva) - www.pvsyst.com
- [2] H. Bybee, J. Durrant, A. McNeel, R. Millsap, R. Vasquez, E. Wiley, Feasibility Study to Install Photovoltaic Structures at the University of Utah; University of Utah: Salt Lake City, UT, USA, 2010.
- [3] Global Solar Atlas, available at <https://globalsolaratlas.info/>
- [4] H. Lohse-Busch, M. Duoba, E. Rask, K. Stutenberg, V. Gowri, L. Slezak, and D. Anderson, Ambient Temperature (20°F, 72°F and 95°F) Impact on Fuel and Energy Consumption for Several Conventional Vehicles, Hybrid and Plug-In Hybrid Electric Vehicles and Battery Electric Vehicle. *SAE Technical Paper 2013-01-1462*, 2013.
- [5] L. Erickson, Third report on the installation of shaded parking lot structures with integrated photovoltaic power system at Kansas State University, USA, 2011.
- [6] Lj. Stamenić, Solar photovoltaic power in Serbia, Jefferson Institute, Washington, USA, 2009.
- [7] T. Tsoutsos, N. Frantzeskaki, V. Gekas, Environmental impacts from the solar energy technologies.
- [8] *Energy Policy*, 33(3), 2005, pp 289–96.
- [9] V. Masson, M. Bonhomme, J.-L. Salagnac, X. Briottet and A. Lemosu, Solar panels reduce both global warming and urban heat island. *Frontiers in Environmental Science*, 2(14), 2014, pp 1-10.
- [10] B. Bogicević, I. Petović, D. Brkić and J. Pavlović, “Improving Internet of Things Parking Systems,” *Facta universitatis, Series: Automatic Control and Robotics* vol. 19, no. 3, pp. 163-174, 2020, doi 10.22190/FUACR2003163B.

PREDICTION OF THE FRICTION COEFFICIENT BASED ON THE HYSTERESIS VALUE OF SHOE SOLE RUBBER

UDC ((537.226.3+004.032.26):665.941)

Milan Nikolić¹, Milan Banić², Milan Pavlović¹, Vukašin Pavlović²,
Aleksandar Miltenović², Miloš Simonović²

¹Academy of Technical-Educational Vocational Studies Niš, Serbia

²University of Niš, Faculty of Mechanical Engineering, Serbia

ORCID iDs: Milan Nikolić

Milan Banić

Milan Pavlović


Vukašin Pavlović


Aleksandar Miltenović


Miloš Simonović


 N/A

 <https://orcid.org/0000-0001-8684-042X>

 <https://orcid.org/0000-0001-5024-3252>

 <https://orcid.org/0000-0002-5090-9277>

 <https://orcid.org/0000-0002-1453-2548>

 <https://orcid.org/0000-0003-1364-7746>

Abstract. *This paper present research focused on the prediction of the friction coefficient of shoe sole rubber by utilizing its measured hysteresis values, along with other influencing factors such as hardness, tile surface roughness, sliding speed, and surface conditions. Previous authors research determined that rubber hysteresis is an important property of rubber (among other mechanical and physical properties) to consider when performing tribological research of contact between rubber soles and a hard substrate (tiles, laminate, vinyl, concrete). Data required for design and training of a neural network were gathered by friction coefficient testing conducted on a specially designed test apparatus. Additionally, rubber hysteresis data were obtained using a uniaxial tensile testing machine. Given the role of rubber hysteresis in determining its properties, this study identifies it as a parameter that influences the friction coefficient and aids friction coefficient prediction through artificial neural networks (ANN). The research results showed a high correlation between the friction coefficient values predicted by ANN and actual experimental results, confirming that designed ANN can be used to predict the values of friction coefficient when the rubber hysteresis value is known.*

Key words: *Friction coefficient prediction, hysteresis, neural network, shoe sole rubber.*

Received November 29, 2024 / Accepted December 19, 2024

Corresponding author: Milan Nikolić

Academy of Technical-Educational Vocational Studies Niš, Aleksandra Medvedeva 20, 18000 Niš, Republic of Serbia

E-mail: milan.nikolic.ni@akademijanis.edu.rs

I. INTRODUCTION

Neural networks, inspired by biological neural systems, represent one of the most significant approaches in the field of artificial intelligence (AI). These networks have become a fundamental tool for solving complex problems in various domains, such as pattern recognition, natural language processing, and predictive analytics [1, 2]. Among other things, they are also used for predicting the friction coefficient based on various parameters. Chen et al [3] uses GA-BP neural network for friction prediction in bearing surface friction coefficient in bolted joints. They collect data for the friction coefficient and then use it for training the neural network. Zhang et al work [4] is interesting as it discusses the prediction of the friction coefficient between a car tire and asphalt. They use Mind Evolutionary Algorithm optimized Back-Propagation (MEA-BP) neural network model for the prediction of the tire-road friction coefficient and compare with the extreme learning machine (ELM) and BP neural network algorithms. Another work with similar research uses the Elman neural network for identification of the road friction coefficient [5]. In that paper, an identification method of road friction coefficient based on the Elman neural network was proposed.

Another study that deals with Artificial Neural Networks (ANN) to optimize time and cost in developing new friction brake systems, is a study which employed a Gate Recurrent Unit (GRU) algorithm enhanced by an improved Particle Swarm Optimization (PSO) method for predicting the coefficient of friction (COF) in braking applications [6].

In article [7], a genetic-algorithm-improved neural network (GAI-NN) was developed. Tree-dimensional (3D) point-cloud data of an asphalt pavement surface was obtained using a smart sensor (Gocator 3110). The friction coefficient of the pavement was then obtained using a pendulum friction tester.

Authors [8] make prediction models of the friction coefficient of asphalt pavement considering traffic volume and road surface characteristics. They use different pavement and tire parameters to make a model for friction coefficient prediction.

Also, authors [9] explore the prediction of the friction coefficient using 3D texture parameters of pavement surfaces by ANN.

Paper [10] presents a trained novel predictive model developed for the measurement of road surface friction considering a big dataset of 18 months with daily records through novel intelligent road-based passive sensor measurement, on a Spanish highway section. The trained predictive model is developed on the machine learning (ML) approaches, namely support vector machine (SVM), and validated with the K-Fold cross-validation (CV) algorithm considering various kernels.

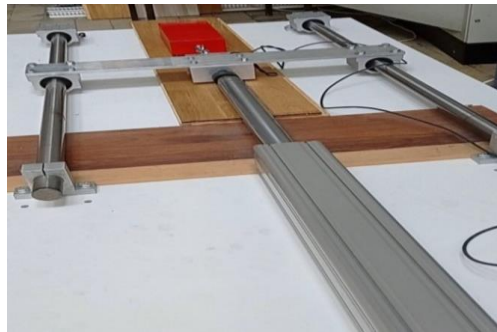
Authors [11] develop a model that classifies footwear outsoles based on how slip resistant they are on icy surfaces. They applied a transfer learning technique where the best classification model used the DenseNet169 pre-trained model and obtained an accuracy and F1-score of 0.93 ± 0.01 and 0.73 ± 0.03 , respectively.

In previous research, most authors have focused on the influence of rubber hardness on its tribological characteristics, neglecting its hysteresis properties, even though the hysteresis component is part of the friction mechanism in viscoelastic bodies. Authors who have studied the influence of hysteresis have concentrated on determining the contribution of the hysteresis component under different tribological conditions, without determining the actual hysteresis value as a property of rubber or its impact on the coefficient of friction. For the reasons noted above, the subject of scientific research in this paper is the predicting the friction coefficient of shoe sole rubber by utilizing its measured hysteresis values along with other factors such as

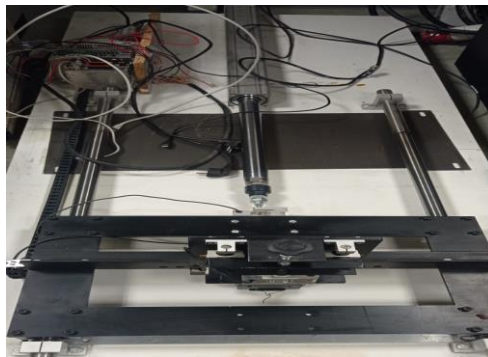
hardness, tile surface roughness, sliding speed, and surface conditions. The study employs an artificial neural network (ANN) to analyze data gathered from friction coefficient testing and rubber hysteresis measurements. The new approach in this research is the use of hysteresis as a parameter for predicting the friction coefficient of shoe sole rubber, which has not been previously utilized for this purpose.

2. EXPERIMENTS

Gathering data and performing experiments for this study took two months. A total of 240 data points for the friction coefficient were obtained. The dataset used for the artificial neural network to predict the friction coefficient based on rubber hysteresis included the following parameters: static and kinetic friction coefficients, rubber hysteresis, rubber hardness, substrate roughness, sliding speed, and surface condition (categorized as dry, wet, or soap-lubricated). Friction coefficient was measured on the testing device developed on Mechanical Faculty in Niš.



(a)



(b)

Fig. 1 Tribometer (a) and (b)

Figure 1(a) illustrates the friction coefficient testing device. This device was designed to support a wide range of speeds, accommodate various surface conditions (dry, wet, or lubricated), test different materials (rubber, tiles, metals...), and perform tests at a constant

speed. Figure 1(b) shows a modified version of the testing device, equipped with the capability to adjust the normal force.

The device includes a holder for rubber sliders, which acts as a weight to define the normal force, a force sensor, an electric linear actuator with a servo drive, and a base for placing different floor samples. The testing setup and some parameters (speed, stroke, normal force, slider dimension and arrangement) are based on the EN 13893:2011 [12] standard method for measuring the coefficient of friction. Also, the tests are conducted on high-hardness granite tiles to eliminate the influence of the substrate hardness on the value of the coefficient of friction at the footwear-floor contact. Surface condition (dry, wet, soap) were selected from previous similar researches.

The electric actuator (SMC) uses a ball screw mechanism and features a linearly integrated AC servo motor (Mitsubishi). For testing, the normal force was set to 100 N, resulting in a contact pressure of 83 kPa. The sliding speeds were 50 mm/s and 300 mm/s for kinetic friction and 1 mm/s for static friction tests, with a total travel distance of 600 mm for measuring the friction coefficient. Friction force measurements were taken using an HBM S2 sensor, capable of handling forces up to 200 N.

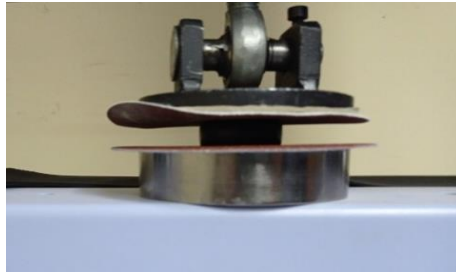


Fig. 2 Hysteresis testing

The samples for determining the hysteresis of the rubber are cylindrical shape, with a diameter of $\Phi 35.7$ mm and a height of 18 mm (shown on Fig. 3)



Fig. 3 Hysteresis rubber samples

The hysteresis testing of the rubber samples, shown in Figure 2, was conducted at the Faculty of Mechanical Engineering in Niš using a Shimadzu AGS-X uniaxial testing machine with a maximum load of 10 kN.

Hysteresis refers to the property of a material to expand and contract in the same manner, following an identical path during expansion and contraction on a force-displacement graph. This behavior is commonly observed in rubber and similar polymers. For instance, car tires heat up not due to friction but because of hysteresis in the rubber, as the tires deform momentarily upon contact with the road surface. This energy loss, which converts kinetic energy into heat, is described as the rolling resistance [13].

Rubber hysteresis plays a crucial role in determining the friction and energy absorption of shoe soles. It can be classified into the static hysteresis (examined in this study) and the dynamic hysteresis, such as Yearsley Hysteresis. The results obtained through this method closely align with those from the Yearsley method, showing a minimal result variance. This simpler method does not require specialized equipment and uses a uniaxial testing machine.

For the experiment, rubber compounds with hardness levels of 65 ShA (Method A) and 60 ShA were tested. Samples were cylindrical with a diameter of 35.7 mm and a height of 18 mm, produced by a local shoe sole manufacturer (Figure 3). The internal labels for these samples included OB202, OB290, OB2280, and OB221, among others.

Before testing, the rubber samples were conditioned at the testing temperature for at least 24 hours to stabilize the polymer chains. Once conditioned, their dimensions were verified. To increase the friction coefficient between the machine plates and the rubber sample, the samples were placed between two sheets of sandpaper. The applied axial pressure caused the cylindrical rubber samples to deform, pushing outward into a barrel-like shape.

For accurate rubber hysteresis testing, the samples underwent a conditioning process, which aimed to break weak bonds formed during vulcanization, stabilizing the rubber. The conditioning involved five cycles of applying vertical pressure at 0.25 mm/s until 9 mm of deformation (half the sample's height), followed by a 20-second hold and then a release at the same speed. This process was repeated for all samples, with three test samples per rubber mixture.

After conditioning, the samples rested for 30 minutes. The hysteresis test itself applied a vertical pressure force at 5 mm/min until 9 mm of deformation was reached and then released at the same speed. Force and deformation data were collected during the test to analyze the mechanical response of the samples.

3. ARTIFICIAL NEURAL NETWORK FOR PREDICTION OF COEFFICIENT OF FRICTION

For predicting the friction coefficient, a standard artificial neural network with backpropagation was used. The ANN was designed to have four layers: an input layer, two hidden layers, and an output layer. The variables used in the input layer of the network are the kinetic friction coefficient, hysteresis, hardness, substrate roughness, sliding speed, and surface condition. The variable in the output layer of the network is the kinetic friction coefficient.

The ANN was created using the MATLAB software tool. The input layer of the artificial neural network consists of 5 neurons because there are 5 input parameters, while the output layer has 1 neuron, output is 1 dependent variable (friction coefficient). The hidden layer consists of 10 neurons. The scheme of ANN is shown on figure 4.

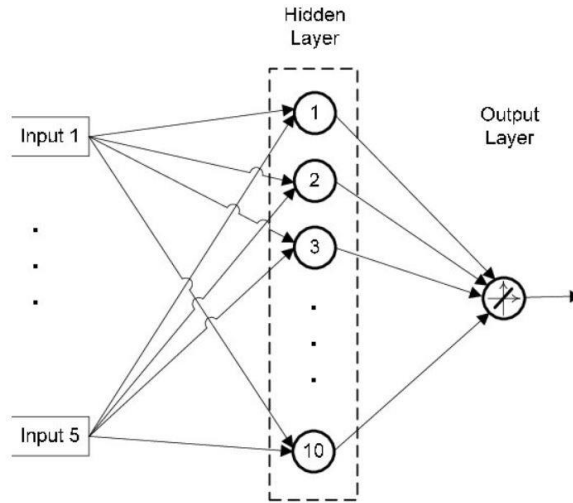


Fig. 4 Scheme of ANN

An artificial neural network was trained using the Levenberg-Marquardt backpropagation algorithm. The mean squared error was used to measure performance. The dataset consisted of 5 variables. Trial-and-error approach was used for determining the number of hidden layers and hidden neurons in these layers.

Table 1 presents input parameters for ANN, there are 5 input parameters: rubber hysteresis, rubber hardness, tile roughness (R_a), sliding speed and surface condition.

Table 1 Experimental inputs

No	Rubber hysteresis	Rubber hardness (ShA)	Granite tile roughness (μm)	Speed (mm/s)	Surface condition	Normal load (N)	Measuring distance (mm)
1.	0,24	65	0.03	50	Dry	100	300
2.	0,35	65	4.70	300	Wet		
3.	0,39	65			Soap		
4.	0,46	60					

For measuring network generalization, a validation sample of 60 data was used. When generalization stopped improving, network training was halted. During the ANN training process, although a larger number of iterations were expected, it was observed that fewer iterations were sufficient to train ANN (Fig. 5).

To evaluate the network's performance, the coefficient correlation R was used, with the results presented in Fig. 6. This coefficient indicates how effectively the network was trained by comparing the predicted "outputs" to the actual "targets." A higher R value signifies a better network performance, with $R=1$ representing a perfect match between "targets" and "outputs." As shown in Fig. 6, the correlation coefficient during ANN training was $R=0.99877$, indicating excellent training. The trained network was then tested on a

separate testing dataset, achieving $R=0.99854$. The overall performance of the trained ANN was $R=0.99792$, which is considered a highly satisfactory result.

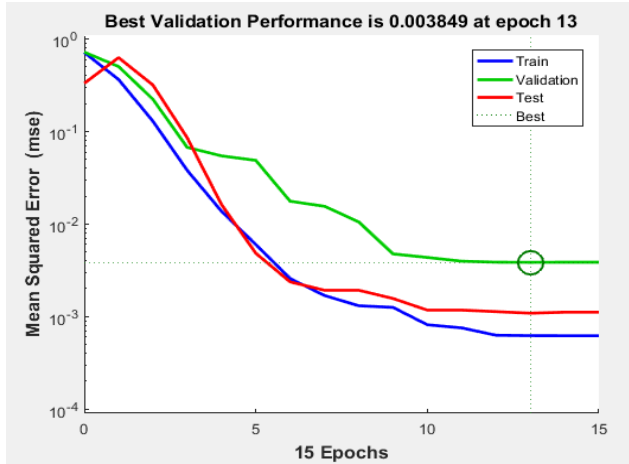


Fig. 5 Mean squared error during the ANN training process for kinetic friction coefficient prediction

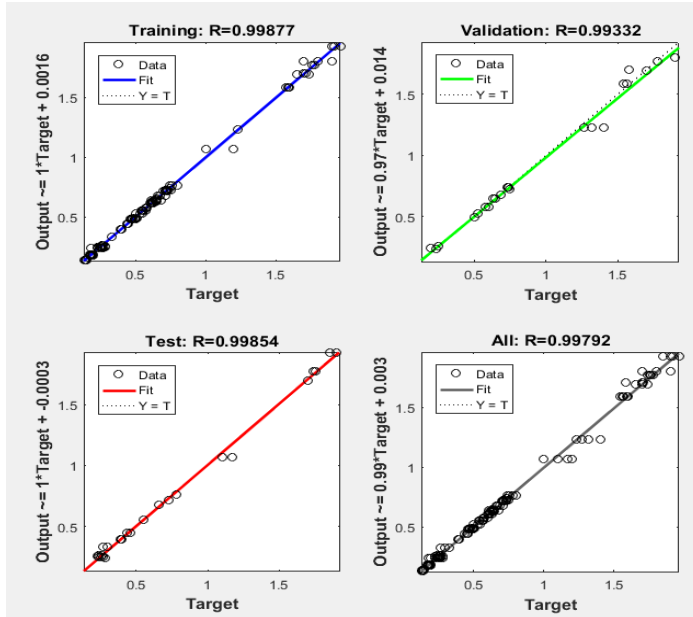


Fig. 6 The results of network performance for training, validation and test dataset (kinetic friction)

4. RESULTS AND DISCUSSION

It was determined by previous authors research [14] that the regression analysis cannot predict friction coefficient value well enough to agree with the experimental data. The difference between prediction of friction coefficient values and actual experimental results occurred because regression assumes a linear relationship, which obviously does not apply to rubber friction on ceramic tiles with different surface conditions. Additional methods, such as Taguchi method, yield better results [14], but again there is still discrepancy between the prediction values of friction coefficient and actual experimental data. As ANN have proven themselves as a valuable tool for prediction the friction coefficient values, this study focused on design and training of ANN to predict the friction coefficient value based on the following parameters: rubber hysteresis and hardness, surface roughness and condition (dry, wet, soapy) and sliding speed.

Table 2 shows the experimentally determined and predicted values of the kinetic coefficients of friction based on 5 input parameters and 3 sets of measurements used to train the network. The total number of measurements of kinetic friction coefficient used to train the network is 180 and 60 for confirmation.

Table 2 Predicted end measured kinetic friction coefficients

Hysteresis	Hardness (ShA)	Roughness ($Ra-\mu\text{m}$)	Speed (mm/s)	Surface condition		Measured μ_{kp}	Predicted μ_k	Deviation %
0.35	65	0.03	50	1	dry	1.72	1.73	0.75
0.35	65	0.03	300	1	dry	1.82	1.85	1.80
0.35	65	4.51	50	1	dry	0.57	0.84	47.96
0.35	65	4.51	300	1	dry	0.67	0.73	9.27
0.35	65	0.03	50	2	wet	0.33	0.33	0
0.35	65	0.03	300	2	wet	0.17	0.26	54.11
0.35	65	4.51	50	2	wet	0.66	0.82	23.94
0.35	65	4.51	300	2	wet	0.60	0.59	1.86
0.35	65	0.03	300	3	soap	0.16	0.23	43.83
0.35	65	4.51	50	3	soap	0.53	0.58	8.65
0.35	65	4.51	300	3	wet	0.46	0.60	31.82

Figure 7 shows a diagram with the predicted and measured kinetic COF. Some of the predicted values are almost identical with the measured ones, with a maximal error of 54%. The difference between prediction and actual experimental data is the largest for the higher sliding speed indicating that more experimental data are necessary at speeds between 50 and 300 mm/s to enable more accurate prediction at larger speeds.

Since the predicted results obtained by the neural network are satisfactory, it can be concluded that the neural network can be used to predict the friction coefficient. Comparing the values obtained by ANN and other statistic methods (regression and Taguchi) [14] it can be seen that ANN gives a better accuracy, as the correlation coefficient is much higher for ANN in comparison to regression and Taguchi method.

ANN should perform better with more experimental data used in a training set [15] and deviation from predicted and experimental results should be smaller. For further research and improvement of the neural network's prediction accuracy, a larger number of experiments should be conducted to increase the amount of input data for training the network.

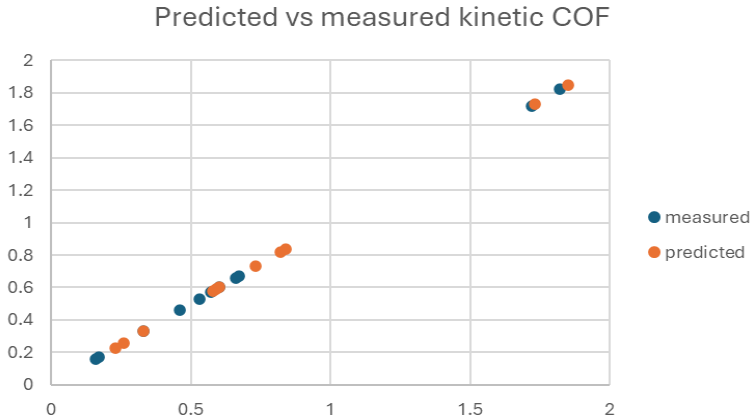


Fig. 7 Predicted vs measured friction coefficient diagram

Forecasting using neural networks essentially involves processing a specific dataset, training a model, and expecting the network to perform well in predicting the output. However, during the learning process, the network is typically trained on a limited dataset comprising both training and test data, which may not encompass the full diversity of inputs and scenarios encountered by the neural network in a real-world environment [9].

5. CONCLUSION

This paper describes an attempt to predict the friction coefficient using a neural network based on five input parameters, one of which is hysteresis, a factor not previously used for this purpose in the existing research. This research confirmed that rubber hysteresis is an important property of rubber (among other mechanical and physical properties) to consider when performing the tribological research of contact between rubber soles and a hard substrate (tiles, laminate, vinyl, concrete). Experimental research showed that different rubber mixtures with the same or similar hardness have different COF due to different hysteresis. The results obtained in this study show that the prediction of the friction coefficient can be accurate and with certain improvements and optimizations could be even better. It is necessary to collect more experimental data for better and precise ANN friction coefficient prediction. The created ANN showed a high correlation between the target data and the data gathered from the simulation of the artificial neural network. Further research should focus on increasing the training data through additional experimental measures and neural network optimizations.

REFERENCES

- [1] S. Perić, N. Vukić, D. Antić, M. Milojković, A. Đorđević, Application of Convolutional Neural Networks for road type classification, *Facta Universitatis, Automatic Control and Robotics* Vol. 22, No 1, 2023
- [2] Jianxun Cui, Huidong Gao, Miroslav Milovanović, Staniša Perić, Marko Milojković, A Review of Trajectory Prediction for Autonomous Vehicles Based on Generative Models, *XVII International Conference on Systems, Automatic Control and Measurements, SAUM 2024* (pp. 80-83)

- [3] W. Chen, Y. Li, Z. Liu, C. Zhang, Y. Zhao, Prediction model for bearing surface friction coefficient in bolted joints based on GA-BP neural network and experimental data, *Tribology International* Volume 201, January 2025
- [4] F. Zhang, W. Wu, Shuangyue Tian, M. Xu, A Mind Evolutionary Algorithm Optimized Back-Propagation Neural Network Model for Tire-Road Friction Coefficient Prediction, *Developments and Applications in SmartRail, Traffic, and Transportation Engineering* vol 1209. Springer, 2024
- [5] W. Wenguang, Z. Fanhao, X. Menglong, Identification of road friction coefficient based on Elman neural network, *Chongqing Daxue Xuebao/Journal of Chongqing University*, Volume 46, Issue 3, Pages 118 – 128, March 2023
- [6] S. Wang, Y. Yu, S. Liu, D. Barton, Braking Friction Coefficient Prediction Using PSO–GRU Algorithm Based on Braking Dynamometer Testing, *Lubricants* 2024, *Tribology in Vehicles*
- [7] Z. Sun, X. Hao, W. Li, J. Huyan, and H. Sun, Asphalt pavement friction coefficient prediction method based on genetic-algorithm-improved neural network (GAI-NN) model, *Canadian Journal of Civil Engineering*, 2022.
- [8] M. Yu, S. Liub, Z. You, Z. Yang, J. Li, L. Yang and G. Chen, A prediction model of the friction coefficient of asphalt pavement considering traffic volume and road surface characteristics, *International Journal of Pavement Engineering*, 2023., Vol 24, No1
- [9] M. Kováč, M. Brna, P. Pisca and M. Decký, Prediction of Friction Coefficient Based on 3D Texture Characteristics of Road Surfaces, *Applied sciences*, 2024.
- [10] M. Rasol, F. Schmidt, S. Ientile, FriC-PM: Machine Learning-based Road surface friction coefficient predictive model using intelligent sensor data, *Constr Build Mater*, 370 (2023)
- [11] L. Kaylie, Fernie G., Roshan Fekr, A., A novel method to predict slip resistance of winter footwear using a convolutional neural network, *Footwear Science*; Sep 2023, Vol. 15 Issue 3, p219-229
- [12] EN 13893:2011
- [13] <https://www.kvis.ac.th/userfiles/files/Hysteresis%20for%20rubber.pdf> (last access: 12.1.2024.)
- [14] M. Nikolić, M. Banić, D. Stamenković, M. Simonović, A. Stamenković, V. Pavlović, The Influence of Rubber Hysteresis on the Sliding Friction Coefficient During Contact Between Viscoelastic Bodies and a Hard Substrate, *Appl. Sci.* 2024, *14*(24), 11820; <https://doi.org/10.3390/app142411820>
- [15] H. Chen, J. Chen, J. Ding, "Data evaluation and enhancement for quality improvement of machine learning," *IEEE Transactions on Reliability*, vol. 70, no. 2, pp. 831-847, 2021, doi: 10.1109/TR.2021.3070863

INTEGRATED DATA ACQUISITION PLATFORM FOR EXPLAINABLE CONTROL IN DISTRICT HEATING SYSTEMS






UDC ((621.039.576:681.5.01)+332.155)

Stevica Cvetković¹, Dušan Stojiljković², Ivan Ćirić²,
Rajko Turudija², Matija Špeletić¹

¹University of Niš, Faculty of Electronic Engineering,
Department of Electronics, Republic of Serbia

²University of Niš, Faculty of Mechanical Engineering,
Department of Mechatronics and Control, Republic of Serbia

ORCID iDs: Stevica Cvetković
Dušan Stojiljković
Ivan Ćirić
Rajko Turudija
Matija Špeletić

 <https://orcid.org/0000-0001-5719-3761>
 <https://orcid.org/0000-0002-6787-4533>
 <https://orcid.org/0000-0003-0430-8937>
 <https://orcid.org/0000-0002-6324-5967>
 <https://orcid.org/0009-0002-9827-7691>

Abstract. *This paper presents a comprehensive data acquisition platform designed for the intelligent management of District Heating Systems (DHS), aiming to optimize energy efficiency, reduce environmental impact, and minimize heat loss. A DHS is a centralized network that transfers thermal energy to multiple buildings via an insulated pipeline infrastructure. Traditional DHS configurations rely on PLCs and SCADA for data collection and heating control, but integrating real-time monitoring and advanced decision-making capabilities can significantly enhance system efficiency. Our Data Acquisition Platform aggregates data from diverse sources, including IoT sensors, weather stations, and smart meters, into a unified database for time-series analysis. The platform supports automated data retrieval through cron job scheduling and integrates with SCADA systems for remote data collection and monitoring. It is integral part of an intelligent DHS control approach named XAI4HEAT. This approach leverages explainable artificial intelligence algorithms and model-based predictive control to dynamically adjust heat supply based on demand and weather forecasts. Key benefits of this approach include improved load balancing, optimized energy distribution, and the potential integration of alternative energy sources.*

Key words: District heating system, data acquisition, predictive control, energy efficiency.

Received November 29, 2024 / Accepted December 20, 2024

Corresponding author: Ivan Ćirić

University of Niš, Faculty of Mechanical Engineering, Department of Mechatronics and Control, Aleksandra Medvedeva 4, 18000 Niš, Republic of Serbia

E-mail: ivan.ciric@masfak.ni.ac.rs

1. INTRODUCTION

A District Heating System (DHS) generates and distributes thermal energy to multiple buildings via a network of insulated pipes. Heat is produced at a central heating plant, typically using fuel-burning boilers, and transported through supply lines to substations (Fig. 1). The primary heat distribution network consists of supply and return lines that carry hot and cool fluid, respectively, between the central plant and substations. At the substations, heat exchangers transfer energy from the primary to the secondary network while keeping fluids separate. The secondary network, which consists of smaller pipes, delivers thermal energy from the substations to end-users, such as residential apartments.

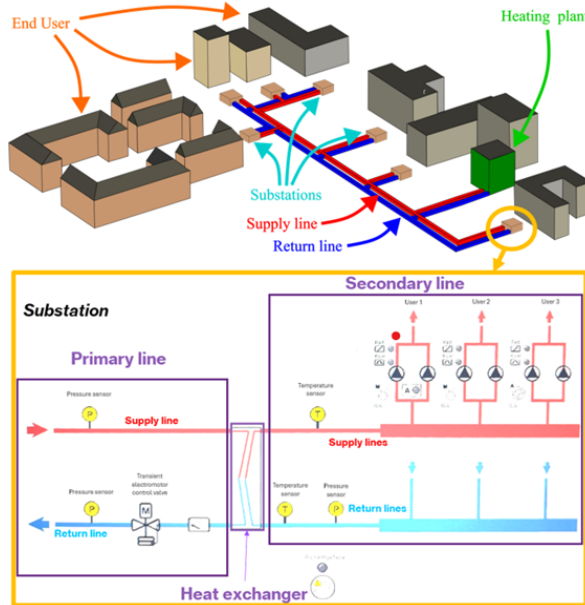


Fig. 1 Overall architecture of a DHS with multiple substations and a single heating plant

The Data Acquisition Platform presented in this work supports research in the intelligent control of district heating systems, with a focus on the heat demand response and load shifting to optimize the system performance through the improved heat demand forecasting [1]. Additionally, it could serve as a valuable resource of information for the development of explainable AI models and tools, enabling the generation of interpretable insights from data and offering explanations for variations in heat fluid supply [2]. The following sections of the paper provide a detailed description of the proposed platform. Section 2 provides a brief review of the related work relevant to the paper. Section 3 presents the architecture of the proposed data acquisition platform, while Section 4 discusses the design and functionality of the software components within the data acquisition platform.

2. RELATED WORK

In the paper [3] the optimization of the district heating and cooling operation plant using distributed and scalable optimization algorithms is proposed. This plant is subject to technical limitations and uncertainties in energy demand, which makes it a perfect subject for optimizing operations using forecasting tools. Paper [4] presents comprehensive surveys that explore how artificial intelligence could be applied to detect and diagnose faults in district heating systems, highlighting key research gaps and challenges. A case study on using the load forecasting and predictive models to sequence equipment to reduce energy use in a heating and cooling plant with four boilers and five chillers, was conducted in paper [5]. In paper [6] the application of artificial intelligence techniques to forecast short-term future heating demand in a district heating system, focusing on deep learning models is investigated. Study [7] compares predictive control strategies tested at two demonstration sites, focusing on energy demand forecasting and optimizing system performance in real-world conditions. Evaluation of the STORM controller is presented in paper [8]. It uses predictive algorithms to manage energy peaks and improve efficiency in district heating systems demonstrated into operational networks: in Heerlen (The Netherlands) and Rottne (Sweden). Paper [9] discusses AI-driven predictive control strategies used in commercial and institutional buildings for improving energy performance. It uses the Model Predictive Control algorithm for the reduction of natural gas consumption. Paper [10] focuses on minimizing primary energy consumption using the predictive control integrated with thermal energy storage in solar district heating systems. Study [11] develops data-driven control strategies for improving the efficiency of cooling systems within commercial and institutional buildings. Three control strategies were investigated: (a) chiller sequencing, (b) free cooling, and (c) air temperature reset supply. In paper [12] the development of a user-friendly weather forecast tool designed to support predictive control addressing the challenge of integrating accurate weather predictions is presented. Paper [13] presents the development and testing of a smart demand response control system for a real-time optimization of district heating network temperature levels, focusing on both return and supply pipe temperatures. Paper [14] explores a multi-model approach utilizing machine learning techniques to develop control-oriented models for optimizing the operation of electric and natural gas boilers in a Canadian institutional building, aiming to reduce greenhouse gas emissions while maintaining comfort. Reference [15] is a study that investigates the use of artificial intelligence in heating and cooling energy station control systems, emphasizing how it may improve energy management, lower consumption, and increase occupant thermal comfort. Study [16] looks at how to install an AI-based heating system in energy stations and shows how well it works to lower energy use, increase management effectiveness, and improve thermal comfort for occupants while encouraging wise energy conservation. By incorporating a specialist control expertise, paper [17] introduces an intelligent control system with a fuzzy logic-based control module for district heating plants, improving automated control, equipment longevity, and lowering manual interventions. Compared to existing reinforcement learning techniques, reference [18] explains an intelligent control strategy for district heating systems with use of a deep reinforcement learning-based algorithm, resulting in the improved precision, stable control, and greater rewards. In [19], authors presented an artificial neural network model trained to forecast the hourly electricity consumption of energy in industry for a day-ahead. Input vector impact on short-term heat load prediction of small district heating system was analyzed in [20]

In our previous work [21], we introduced the fundamental concepts of a data acquisition system, while this paper provides a detailed and comprehensive analysis of all components of the proposed Data Acquisition Platform.

3. ARCHITECTURE OF THE PROPOSED DATA ACQUISITION PLATFORM

Intelligent management of DHS involves the systematic acquisition, processing, and application of data to optimize the production, distribution, and consumption of thermal energy within a specified district. The primary objective of the proposed Data Acquisition Platform is to collect all relevant data that enhances the energy efficiency and minimizes heat losses by adjusting the heat supply in response to a real-time demand. This approach aids in balancing the heating load across various stakeholders, thereby improving the overall efficiency of the system.

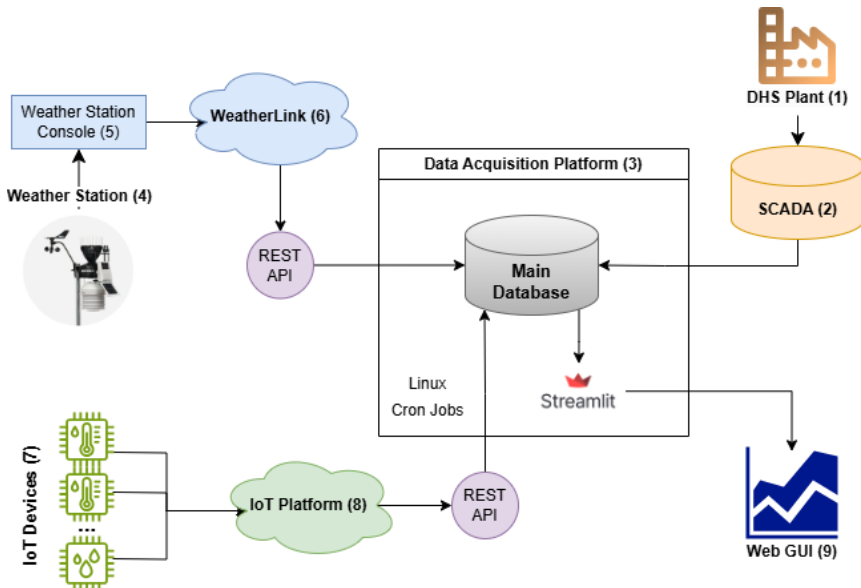


Fig. 2 The proposed architecture of Data Acquisition Platform of a DHS

The integration of heterogeneous data from diverse sources and external systems presents substantial technical challenges. A fundamental component of any advanced DHS is the Data Acquisition Platform, which consolidates data from multiple sources into a cohesive repository. This repository serves as the foundation for subsequent analytical, visualization, and alerting processes. To implement this integration, we have developed a real-time data ingestion and processing pipeline capable of efficiently assimilating data from external Internet of Things (IoT) devices and subsystems. The data is stored into a centralized PostgreSQL database, enabling explainable intelligent analyses and facilitating the effective handling and transformation of large data volumes.

In Fig. 2, the overall architecture of the proposed Data Acquisition Platform is illustrated. The flow of hot water or steam from the heating plant (1) is monitored to

regulate heat delivery. Key components include sensors that collect data on temperature, pressure, flow rates, energy consumption, and heat losses from various points within the District Heating System (DHS). Additionally, a SCADA system (2) manages and processes the data obtained from these sensors, providing a centralized platform for operators to continuously monitor the heating system's performance. The collected data is transferred to the main database which is an integral part of the central Data Acquisition Platform (3).

Simultaneously, the Davis Vantage Pro2 weather station (4) gathers environmental data through sensors, including an anemometer, temperature sensor, humidity sensor, and rain gauge. This data is displayed on the Vantage Pro2 weather station console (5). The station is connected to the internet via the WeatherLink Live base unit, which uploads real-time weather data to the WeatherLink platform (6). Data from both the weather station console and the WeatherLink platform is then transmitted to the central PostgreSQL database with the Timescale extension for time-series data analyses.

Furthermore, smart meters, specifically Air Quality Monitors (7), measure temperature, humidity, CO₂ levels, and emissions of HCHO and total volatile organic compounds (TVOCs) for individual users in residential settings. These measurements are transmitted to a public IoT cloud platform server (8) and the main database. Both the WeatherLink platform and the IoT platform serve as backups for storing data in the cloud. The platform's data visualization GUI is built with Streamlit web framework (9), that allows to visualize time-series data from the PostgreSQL database by plotting parameters like temperature and humidity against timestamps.

4. DESIGN AND FUNCTIONALITY OF SOFTWARE COMPONENTS IN THE DATA ACQUISITION PLATFORM

The core of the Data Acquisition Platform software is implemented as a robust central service that operates on a 15-minute schedule, managed through a cron job. This scheduling mechanism ensures the systematic and timely retrieval of data from multiple external sources, enabling the platform to maintain an up-to-date repository of critical information.

4.1. Data Sources

The primary service has been carefully designed to integrate with a variety of external data sources, each of which provides unique and essential inputs for the platform's operation:

- **Meteorological Data:** Real-time data from weather stations located in the proximity to the DHS is integrated using a REST API provided by Weatherlink (<https://api.weatherlink.com/v2>). This data includes temperature, humidity, wind speed, and other atmospheric variables essential for optimizing the DHS performance and forecasting energy demand.
- **SCADA Data:** Operational data from the DHS is accessed directly through a SQL database. A dedicated SQL view has been created to streamline data export and ensure efficient querying. This integration provides vital insights into the system performance, operational metrics, and real-time control parameters, forming the backbone of system analytics and decision-making.

- **Indoor Air Quality Data:** Temperature and humidity data from residential units is obtained through an IoT platform connected to sensors installed within the units. The platform leverages a REST API from two sources: <https://thermionyx.com/> and <https://openapi.tuya.eu.com/>, to provide valuable data for assessing indoor comfort levels and optimizing heating delivery to individual units.
- **Weather Forecast Data:** Additional weather forecasting data is retrieved from the <https://api.met.no/weatherapi/> using REST API calls. This data includes short-term and long-term weather predictions, which are critical for anticipating energy demand fluctuations and adjusting system operations proactively.

Data from SCADA system is retrieved through direct queries to an SQL database. This process allows for the efficient extraction of data, which is essential for the monitoring and optimization of system. An example SQL query for retrieving data from the SCADA system is given below:

```
SELECT rpIstorijatTagova.DatumVremePromene,
CASE WHEN kpTagovi.TipPodataka = 1 AND rpIstorijatTagova.Vrednost > 32768
THEN (rpIstorijatTagova.Vrednost - 65535)/POWER(10.0, kpTagovi.DecimalnaTacka)
ELSE rpIstorijatTagova.Vrednost/POWER(10.0, kpTagovi.DecimalnaTacka)
END AS Vrednost,
rpIstorijatTagova.Stanje,
kpTagovi.*,
kpUredjaji.Naziv AS Lokacija
FROM rpIstorijatTagova
JOIN kpTagovi ON rpIstorijatTagova.IdTaga = kpTagovi.IdTaga
JOIN kpUredjaji ON kpTagovi.IdUredjaja = kpUredjaji.IdUredjaja
WHERE kpUredjaji.Naziv IN ('TPS Lamela L4', 'TPS Lamela L8', 'TPS Lamela L12', 'TPS Lamela
L17', 'TPS Lamela L22') AND DATEDIFF(day, DatumVremePromene, GETDATE()) <= 3000
ORDER BY DatumVremePromene DESC
```

An example of an HTTP response in the JSON format, obtained from the WeatherLink REST API, is shown below. This response includes detailed meteorological data, with each field representing a specific weather parameter and its corresponding value, along with timestamps indicating when the data was recorded. By parsing this JSON response, the platform can integrate real-time weather information.

```
API Response: {
  "station_id": 194332,
  "station_id_uuid": "99608905-d0a6-4bbf-9ddb-8eab4b6c827e",
  "sensors": [
    {
      "lsid": 766119,
      "sensor_type": 51,
      "data_structure_type": 2,
      "data": [
        {
          "ts": 1725526822,
          "tz_offset": 7200,
          "bar_trend": -20,
          "bar": 29.881,
          "temp_in": 85.9,
          "hum_in": 37,
```

```

        "temp_out": 84.8,
        "wind_speed": 3,
        "wind_speed_10_min_avg": 2,
        "wind_dir": 15,
        "hum_out": 40,
        "rain_rate_mm": 0,
        "uv": null,
        "solar_rad": 610,
        "rain_storm_mm": 0,
        "rain_storm_start_date": null,
        "rain_day_mm": 0,
        "rain_month_mm": 0,
        "rain_year_mm": 192.8,
        "et_day": 0.034,
        "et_month": 0.004,
        "et_year": 2.801,
        "forecast_rule": 45,
        "forecast_desc": "Increasing clouds with little temp change.",
        "dew_point": 58,
        "heat_index": 84,
        "wind_chill": 85,
        "wind_gust_10_min": 6
    }
}
]
"generated_at": 1725527186
}

```

All the previously retrieved and parsed data is stored in a structured relational PostgreSQL database, which enhances the capacity for conducting comprehensive and explainable analyses. As a result, it delivers a significant value across diverse fields, spanning from research to industry.

The modular and API-driven architecture of the Data Collection Platform enables it to handle diverse data types and formats, ensuring compatibility with external systems while maintaining scalability and reliability. This design not only supports current integration needs but also facilitates future extensions, such as incorporating additional data sources or enhancing data processing capabilities.

4.2. Software Components Description

The accompanying class diagram illustrates the architecture of the data acquisition software. The *Main* class serves as the entry point of the application. It contains the *run_loaders()* method, which orchestrates the execution of different data loaders. The *Loader* interface defines a contract for all data loaders with the *run()* method. This design ensures that every loader implements the necessary functionality for data retrieval and processing. Subclasses of the *Loader* interface include:

- **SCADALoader**: Responsible for retrieving SCADA data via SQL database queries.
- **WeatherLinkLoader**: Handles the integration of meteorological data from the WeatherLink REST API.

- **ThermionyxLoader**: Focuses on the integration of Thermionyx sensor data via its API.
- **TuyaLoader**: Manages the retrieval of indoor climate data using the Tuya IoT platform.

Each *Loader* has a dependency on a *Database* instance (*destination*), enabling data storage after retrieval and processing. The *SCADALoader* subclass maintains another reference to a *Database* instance (*source*), that defines where the data is ingested from. The *Main* class maintains a collection of *Loader* instances (*loaders*) and sequentially executes them through the *run_loaders()* method.

The *Database* interface outlines a contract for database interaction. It includes methods for connecting (*connect()*), executing batch queries (*execute_many(query, values)*), and closing the connection (*close()*). Two implementations of the *Database* interface are provided:

- **SQLServerDatabase**: Supports integration with Microsoft SQL Server, facilitating SCADA data retrieval.
- **PostgresDatabase**: Represents the PostgreSQL database (with TimescaleDB extension) used for storing and analyzing collected data.

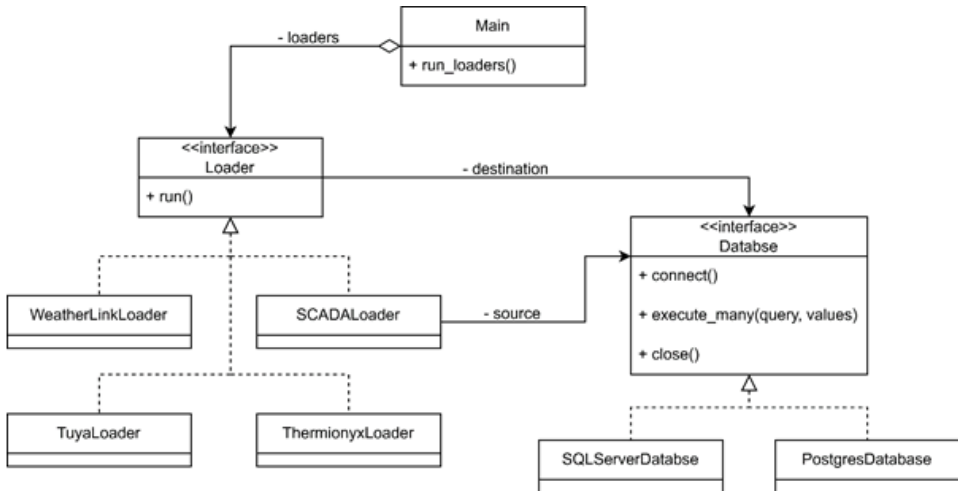


Fig. 3 Class diagram of the implemented software platform

This modular and interface-driven design ensures the high cohesion and loose coupling, making the platform extensible and maintainable. For instance, additional loaders or database implementations can be added with minimal changes to the existing system. The use of interfaces also promotes the use of dependency injection, enhancing testability and scalability of the system.

4.3. Data Visualization

The data visualization module of the platform includes a simple yet intuitive graphical user interface (GUI), developed using the Streamlit web framework [22]. The GUI allows users to visualize the time-series data stored in the PostgreSQL database with TimescaleDB, by plotting the data for different parameters (e.g., temperature, humidity) against their

corresponding timestamps. Each graph represents a single data type and can display multiple plot lines, distinguishing data from various locations. The GUI also displays system logs, enabling users to identify and diagnose errors or issues within the data gathering system. This GUI enhances the usability of the platform by providing clear and interactive data visualizations of the gathered data.



Fig. 4 Preview of the web-based GUI of the presented data acquisition platform

5. CONCLUSION

Intelligent control systems are integral to forecasting future heat demand by leveraging weather data, occupancy trends, and user behavior, utilizing both historical and real-time information. These systems employ modern artificial intelligence frameworks to predict demand and adjust heat production accordingly. Real-time system adaptation enables rapid responses to external factors, such as weather fluctuations or variations in demand, thereby optimizing the heating process. By forecasting periods of high demand, these systems can proactively adjust heat production, alleviating strain during peak times. AI and machine learning technologies are expected to further enhance the predictive and adaptive control by enabling the automated decision-making and improving the accuracy of demand forecasting. To fully realize the potential of an intelligent control in District Heating Systems, the collection and integration of data from diverse sources is paramount. A robust Data Acquisition Platform is crucial for gathering, consolidating, and analyzing large volumes of data from IoT sensors, weather stations, smart meters, and other external systems. This platform supports the real-time monitoring, processing, and visualization of data, facilitating dynamic system adjustments based on current conditions. Through predictive algorithms, the platform enables the optimization of heat supply and load distribution, reducing energy costs and enhancing overall system efficiency.

By enabling intelligent decision-making based on real-time and historical data, the Data Acquisition Platform enhances the adaptability and sustainability of DHS, ensuring that systems can respond to changing conditions, maintain reliable service, and reduce environmental impact. Ultimately, the incorporation of advanced technologies into the data collection process not only ensures the efficient operation of DHS but also contributes to a more sustainable and cost-effective approach to heat distribution.

Acknowledgement: *This research was supported by the Science Fund of the Republic of Serbia, Grant No. 23-SSF-PRISMA-206, Explainable AI-assisted operations in district heating systems - XAI4HEAT.*

REFERENCES

- [1] M. Zdravković, S. Cvetković, M. Ignjatović, I. Ćirić, D. Mitrović, M. Stojiljković, V. Nejković, D. Stojiljković, and R. Turudija. "XAI4HEAT: Towards Demand-Driven, AI Facilitated Management of District Heating Systems." In Conference on Information Technology and its Applications, pp. 23-34. Cham: Springer Nature Switzerland, 2024.
- [2] M. Zdravković, M., I. Ćirić, and M. Ignjatović, "Explainable heat demand forecasting for the novel control strategies of district heating systems," *Annual Reviews in Control*, 53, pp.405-413, 2022.
- [3] S. Moustakidis, I. Meintanis, G. Halikias, and N. Karcianas, "An innovative control framework for district heating systems: Conceptualisation and preliminary results," *Resources*, vol. 8, no. 1, p. 27, 2019. doi: 10.3390/resources8010027.
- [4] J. van Dreven, V. Boeva, S. Abghari, H. Grah, J. A. Koussa, and E. Motoasca, "Intelligent approaches to fault detection and diagnosis in district heating: Current trends, challenges, and opportunities," *Electronics*, vol. 12, no. 6, p. 1448, 2023. doi: 10.3390/electronics12061448.
- [5] H. B. Gunay, A. Ashouri, and W. Shen, "Load forecasting and equipment sequencing in a central heating and cooling plant: A case study," *ASHRAE Trans.*, vol. 125, pp. 513–523, 2019.
- [6] J. Runge and E. Saloux, "A comparison of prediction and forecasting artificial intelligence models to estimate the future energy demand in a district heating system," *Energy*, vol. 269, p. 126661, 2023. doi: 10.1016/j.energy.2023.126661.

- [7] E. Saloux, J. Runge, and K. Zhang, "Field implementation of a predictive control strategy in district heating systems: A tale of two demonstration sites," in *Energy Informatics*, B. N. Jørgensen, L. C. P. da Silva, and Z. Ma, Eds. Cham: Springer, 2024, vol. 14468, doi: 10.1007/978-3-031-48652-4_21.
- [8] T. Van Oevelen, D. Vanhoudt, C. Johansson, and E. Smulders, "Testing and performance evaluation of the STORM controller in two demonstration sites," *Energy*, vol. 197, p. 117177, 2020. doi: 10.1016/j.energy.2020.117177.
- [9] N. Cotrufo, E. Saloux, J. M. Hardy, and J. A. Candanedo, "A practical artificial intelligence-based approach for predictive control in commercial and institutional buildings," *Energy Build.*, vol. 206, p. 109563, 2019. doi: 10.1016/j.enbuild.2019.109563.
- [10] E. Saloux and J. A. Candanedo, "Model-based predictive control to minimize primary energy use in a solar district heating system with seasonal thermal energy storage," *Appl. Energy*, vol. 291, p. 116840, 2021. doi: 10.1016/j.apenergy.2021.116840.
- [11] E. Saloux, K. Zhang, and J. A. Candanedo, "Data-driven model-based control strategies to improve the cooling performance of commercial and institutional buildings," *Buildings*, vol. 13, no. 2, p. 474, 2023. doi: 10.3390/buildings13020474.
- [12] J. A. Candanedo, E. Saloux, J. M. Hardy, R. Platon, and V. Raissi-Dehkordi, "Preliminary assessment of a weather forecast tool for building operation," presented at the 5th Int. High Perform. Buildings Conf., Purdue, 2018.
- [13] T. Van Oevelen, T. Neven, A. Brès, R.-R. Schmidt, and D. Vanhoudt, "Testing and evaluation of a smart controller for reducing peak loads and return temperatures in district heating networks," *Smart Energy*, vol. 10, p. 100105, 2023. doi: 10.1016/j.segy.2023.100105.
- [14] E. Saloux, N. Cotrufo, and J. A. Candanedo, "A practical data-driven multi-model approach to model predictive control: Results from implementation in an institutional building," presented at the 6th Int. High Perform. Buildings Conf., Purdue, 2021.
- [15] H. Qi, Q. Ouyang, and L. Ma, "Application of artificial intelligence control in the control system of cooling and heating energy stations," *Thermal Science*, vol. 28, pp. 1321–1328, 2024. doi: 10.2298/TSCI2402321Q.
- [16] Y. Ding, T. Timoudas, Q. Wang, S. Chen, H. Brattebø, and N. Nord, "A study on data-driven hybrid heating load prediction methods in low-temperature district heating: An example for nursing homes in Nordic countries," *Energy Convers. Manage.*, vol. 269, p. 116163, 2022. doi: 10.1016/j.enconman.2022.116163.
- [17] V. Vansovits, A. Tepljakov, K. Vassiljeva, and E. Petlenkov, "Towards an intelligent control system for district heating plants: Design and implementation of a fuzzy logic based control loop," in *Proc. IEEE 14th Int. Conf. Ind. Informatics (INDIN)*, 2016, pp. 405–410. doi: 10.1109/INDIN.2016.7819193.
- [18] M. Gong, Y. Liu, J. Sun, W. Xu, W. Li, C. Yan, and W. Fu, "Intelligent control of district heating system based on RDPG," *Eng. Appl. Artif. Intell.*, vol. 129, p. 107672, 2024. doi: 10.1016/j.engappai.2023.107672.
- [19] M. A. Stošović, N. Radivojević, I. Jovanović, A. Petrušić, "Artificial neural networks application to prediction of electricity consumption," *Facta Universitatis Series: Automatic Control and Robotics Vol. 20, No 1*, pp. 33 – 42, 2021. <https://doi.org/10.22190/FUACR201231003A>
- [20] M. Simonović, V. Nikolić, E. Petrović, "Input vector impact on short-term heat load prediction of small district heating system," *Facta Universitatis Series: Automatic Control and Robotics Vol. 15, No 2*, pp. 95 – 103, 2016.
- [21] D. Stojiljković, I. Ćirić, S. Cvetković, R. Turudija, D. Srećković, "Data-Driven Approaches for Intelligent Control in District Heating Systems", *Proc. of XVII Int. Conf. SAUM 2024*, Niš, Serbia, November 14-15, 2024.
- [22] M. Khorasani, M. Abdou, and J. Hernández Fernández, "Web Application Development with Streamlit," *Software Development*, pp.498-507, 2022.

ANALYSIS OF VOLUMETRIC REGULATION OF HYDRAULIC PUMPS IN HYDROSTATIC SYSTEMS

UDC (621.82/.85:621.3.078)

**Vesna Jovanović¹, Dragoslav Janošević¹, Jovan Pavlović¹,
Nikola Petrović¹, Đorđe Lazarević²**

¹ University of Niš, Faculty of Mechanical Engineering, Republic of Serbia

² University of Niš, Faculty of Electronic Engineering, Republic of Serbia

ORCID iDs: Vesna Jovanović


Dragoslav Janošević

Jovan Pavlović

Nikola Petrović


Đorđe Lazarević

 <https://orcid.org/0000-0001-9252-7894>

 <https://orcid.org/0009-0001-1771-3985>

 <https://orcid.org/0000-0002-8825-7307>

 <https://orcid.org/0000-0002-9166-1263>

 <https://orcid.org/0000-0002-6391-9706>

Abstract. *The paper presents the results of the conducted researches related to the analysis of the parameters of the drive system, the crawler hydraulic excavator, with hydraulic pumps with collective regulation according to the criterion of constant hydraulic power and the regulator of ideal hyperbolic characteristics. A crawler excavator weighing 16,000 kg with a three-member manipulator with boom, arm and bucket with a volume of 0.6 m³ was tested. The paper discusses the principles of volumetric regulation of hydrostatic systems, which is achieved by changing the specific flow rate of the hydraulic pumps. For pumps with constant specific flow rates, regulation is performed by reducing the flow through the hydraulic motors, which increases the pressure in the pump's delivery line and is controlled by a safety valve. This method, however, can lead to oil heating and energy loss. In contrast, pumps with variable specific flow rates use modular regulators that adjust the pump's characteristics based on system parameters, ensuring efficient operation under varying load conditions. The study's findings indicate that the use of hydraulic pumps with combined power regulation and an ideal hyperbolic characteristic regulator allows for the maintenance of constant hydraulic power even with changing loads. This regulation method ensures efficient use of the engine's power and prevents motor overload, enhancing the overall performance and longevity of the excavator. The research underscores the significance of proper hydraulic pump regulation in achieving optimal machine efficiency and durability.*

Key words: *Drive system, regulation, hydraulic pumps.*

Received November 27, 2024 / Accepted December 20, 2024

Corresponding author: Vesna Jovanović

University of Niš, Faculty of Mechanical Engineering, Aleksandra Medvedeva 14, 18000 Niš, Republic of Serbia

E-mail: vesna.jovanovic@masfak.ni.ac.rs

1. INTRODUCTION

In construction, agriculture, and industry, mobile machines with regulated hydraulic drives have the widest application. The working conditions and the fulfillment of the basic functions of these machines require the ability to widely regulate movement and manipulation parameters [1,2]. The advantages of control and the agility of the regulation system's response to the load of the drive mechanisms have become the focus of research [4,5]. Compared to mechanical or electrical transmissions, the energy efficiency of hydraulic systems is relatively low, so much work has been invested in improving energy efficiency [6-8]. Adapting the supply flow to actual loads during movement and manipulation tasks of machines, such as flow matching systems [9,10], hydraulic transformers [11], load sensing systems [12-14], and pump-controlled cylinders [15,16], are some of the potentially useful solutions. Generally, the supply flow can be adjusted in two ways [17]. The first way is that a variable speed motor drives a fixed displacement pump, thus determining the delivered flow.

In that case, the speed regulation dynamics are basically determined by the motor inertia. Another solution is hydraulic systems with a variable displacement pump driven by either an internal combustion engine or an electric motor at constant speeds, where the supply flow can be changed by varying the displacement volume of the pump. In these systems, the regulation of hydraulic pumps is predominant. The most commonly used pumps with variable displacement are the swash plate and bent axis types.

Due to the lower inertia of the rotating mass in the swash plate design [18], a wider range of hydraulic system parameters is achieved, making it a good candidate for applications requiring fast dynamics. To achieve better performance, mathematical models and various feedback control methods for managing nonlinear systems have been developed.

In the paper [19], emphasis is on the performance robustness of an open circuit axial piston pump with respect to both variations in the internal physical parameters of the pump as well as the type of application-dependent load which the pump is expected to drive. The pressure control is established by means of cascade control utilizing four control loops, with the outer being the pump pressure and then, in succession, the swash plate rotation, the spool position, and the voice coil current.

The paper [20] utilizes robust control methods to design and analyze control systems for a variable-displacement hydraulic pump. The system studied features a variable-displacement swash-plate hydraulic pump with a constant drive speed model. The system's input is the current that actuates the control valve position, while the output is the pump's discharge pressure. Both a PD controller and an H-infinity two degrees-of-freedom controller were designed. The robustness of these two designs is compared using the frequency domain analysis. Time domain results indicate that the PD controlled system outperforms the two degrees-of-freedom controlled system. Additionally, time domain simulations demonstrate an improved robustness to parametric variations.

The paper [17] focuses on the supply pressure control problem for a self-supplied variable displacement axial piston pump subjected to unknown time-varying load flow disturbances. Due to the self-supply mechanism of the pump, the mathematical model exhibits a switching characteristic, and one of the two subsystems is non-minimum phase, complicating the controller design. A control strategy using the method of output redefinition combined with a switching control scheme is proposed. By defining a new output, the new system becomes minimum phase with respect to the revised output, facilitating a feedback controller design.

Based on the proposed load flow disturbance observer, a new desired output is proposed to reduce tracking errors in the presence of time-varying load flow disturbances. Two feedforward controllers along with a switching scheme are also proposed, and a common feedback controller is used to stabilize the system. The stability of the whole system is proved. Experimental results are provided to illustrate the effectiveness of the proposed controller.

This paper presents the results of the conducted researches related to the analysis of the parameters of the drive system, the crawler hydraulic excavator, with hydraulic pumps with collective regulation according to the criterion of constant hydraulic power and the regulator of ideal hyperbolic characteristics. The study's findings indicate that the use of hydraulic pumps with combined power regulation and an ideal hyperbolic characteristic regulator allows for the maintenance of constant hydraulic power even with changing loads. This regulation method ensures the efficient use of the engine's power and prevents the motor overload, enhancing the overall performance and longevity of the excavator. The research underscores the significance of proper hydraulic pump regulation in achieving optimal machine efficiency and durability.

In the mining and construction sectors, earthmoving equipment is essential. Hydraulic excavators are common examples [21]. With the classic five-member configuration of the kinematic chain, a crawler support movable member L_1 , a rotating platform L_2 , a manipulator with boom L_3 , arm L_4 , and bucket L_5 , hydraulic crawler excavators (Fig. 1a) carry out a typical digging function. An excavator's hydrostatic drive system with a crawler support movable mechanism is generally composed of the following components [22]: diesel engine 1 (Fig. 1b), hydraulic pump 3, main distributor 4, integral crawler drive c_1 with hydraulic motor 5, reducer 6, and sprocket 7.

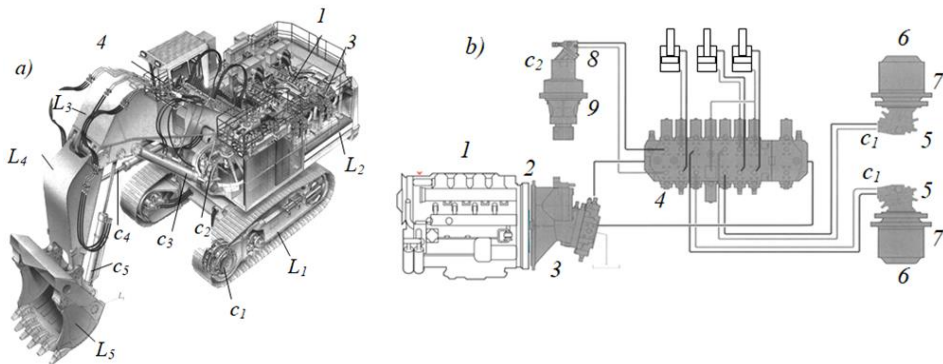


Fig. 1 Crawler excavator: a) physical model, b) drive system

Hydraulic cylinders of boom c_3 , arm c_4 , and bucket c_5 are actuators of the manipulator's drive system. The rotary platform drive mechanism's actuator is an integral transmission made up of a reducer 9 and a hydraulic motor 8. In hydrostatic systems, hydraulic pumps typically convert the mechanical power characteristics that are received into hydraulic power parameters, which are subsequently transferred to the oil as the carrier. The torque M_p at the hydraulic pump's input shaft and the rotational speed n_p are the input mechanical power parameters N_p . The flow rate Q_p and the oil pressure p in the pump's pressure line are the output hydraulic power parameters.

2. HYDRAULIC PUMP REGULATION

The specific flow rate q_p , volumetric efficiency η_{pv} , and mechanical efficiency η_{pm} of the hydraulic pump are the fundamental parameters of its transfer function. The working volume of the hydraulic pump's transformation mechanism, which may theoretically suction and discharge oil with no losses per revolution of the pump's input shaft, is known as the specific flow rate, or q_p . The specific flow rate determines the size of the hydraulic pump. The following equations provide the hydraulic pump transfer functions, which relate the input and output parameters [22]:

- the low in the pressure line of the hydraulic pump:

$$Q_p = \frac{q_p \cdot n_p}{1000} \eta_{pv} \quad [l/min] \quad (1)$$

- the rotational speed of the hydraulic pump's shaft:

$$n_p = \frac{1000 \cdot Q_p}{q_p \cdot \eta_{pv}} \quad [min^{-1}] \quad (2)$$

- the torque at the input shaft of the hydro pump:

$$M_p = \frac{q_p \cdot P}{2 \cdot \pi \cdot \eta_{pm}} \quad [Nm] \quad (3)$$

- the power required to drive the hydraulic pump:

$$N_p = \frac{Q_p \cdot P}{60 \cdot \eta_{pv} \cdot \eta_{pm}} = \frac{Q_p \cdot P}{60 \cdot \eta_{pu}} \quad [kW], \quad (4)$$

where: q_p - specific flow rate of the pump, η_{pv} - is the volumetric efficiency of the pump, η_{pm} - is the mechanical efficiency of the pump, Q_p - is the pump flow rate [l/min], p_p - is the pressure in the pump pressure line [MPa], and $\eta_{pu} = \eta_{pv} \cdot \eta_{pm}$ is the overall efficiency of the pump.

Excavators with hydrostatic systems can adjust their fundamental characteristics, such as the pressure and flow, based on criteria that match variations in the machine's operating parameters. In principle, there is the damping and volumetric regulation of hydrostatic systems.

3. VOLUMETRIC REGULATION OF HYDRAULIC PUMPS

Volumetric regulation of hydrostatic systems is achieved by altering the specific flow rate of hydraulic pumps. In fixed displacement hydraulic pumps, regulation is achieved by reducing the flow to the hydraulic motor, which is done by decreasing the flow cross-sections of the distributor. This results in an increase in pressure in the working line of the hydraulic pump, which is regulated by a safety valve, thereby reducing the supply flow to the hydraulic motor and consequently the number of revolutions of the output shaft [23]. However, the oil heats up during this process, which is called "throttling the

oil stream," which results in some of the hydrostatic system's power being lost and transformed into heat.

The regulation of variable displacement hydraulic pumps is performed using special modular devices – regulators that are integrally connected with the hydraulic pump [24].

The characteristics of the regulators are adapted to different operating conditions of the system. The signals on which the regulators base their characteristics are either predefined or depend on the system's functional parameters. They can be mechanical, hydraulic, electrical, or electronic in nature.

The following equation represents the hydraulic pump regulation based on the constant hydraulic power criterion:

$$N_h = \frac{p \cdot Q}{60 \cdot \eta_u} = k_n \cdot p \cdot Q = const, \quad (5)$$

where: p - pressure of the hydraulic pump, Q -flow of the hydraulic pump, k_n -constant. By changing the flow rate of the hydraulic pump given by the expression:

$$Q = \frac{q_p \cdot n_p}{1000} \eta_{vp} = k_q \cdot q_p \cdot n_p \quad (6)$$

in equation (5) it is obtained:

$$N_h = k_n \cdot p \cdot k_q \cdot q_p \cdot n_p = k_h \cdot p \cdot n_p \cdot q_p = const, \quad (7)$$

where: n_p - number of revolutions of the input shaft of the hydropump, q_p - specific flow of the hydropump, k_h - constant.

If for further analysis it is assumed that the number of revolutions of the hydropump n_p is equal to the number of revolutions of the engine n_{en} ($n_p = n_{en} = const$) at its maximum power, according to equation (7), the regulator of the hydropump according to the criteria the constant hydraulic power should enable a hyperbolic change in the specific flow q_p of the hydropump depending on the change in pressure p in the pressure line of the hydropump, expressed by the equation:

$$q_p = \frac{N_h}{k_h \cdot p \cdot n_p} = \frac{k}{p} = f_q(\alpha) \quad (8)$$

where: α - parameter on which the change in the specific flow of the hydraulic pump depends, k - constant.

Enabling the use of the maximum engine power, or the hydraulic power of the system, under various functional parameters (such as resistances and movement speeds) during the machine's work cycle is one of the main needs of the hydrostatic system. Drive system pumps with volumetric regulation and an optimal hyperbolic characteristic regulator based on the requirement of constant hydraulic power are standard on modern hydraulic excavators. With the help of an integrated power divider 3.12 (Fig. 2a, b) in the form of gears, an elastic connection 2, a diesel engine 1 powers these hydraulic pumps (Fig. 2), which are two identical pumps housed in the same housing.

In these hydraulic pumps, the regulator consists of: the cylinder 3.1 (fig. 2b) with a differential piston 3.2 supported by a spring 3.6 and a two-armed lever 3.4. The pivot block of the hydraulic pump 3 is connected by a linkage 3.7 to the differential piston 3.2.

A small piston 3.3 is transversely placed within the piston 3.2. The chamber on the front side of the piston 3.3 is connected to the pressure lines of the hydraulic pumps through lines in piston 3.2, the cylinder chamber 3.1, and the pressure manifold 3.11.

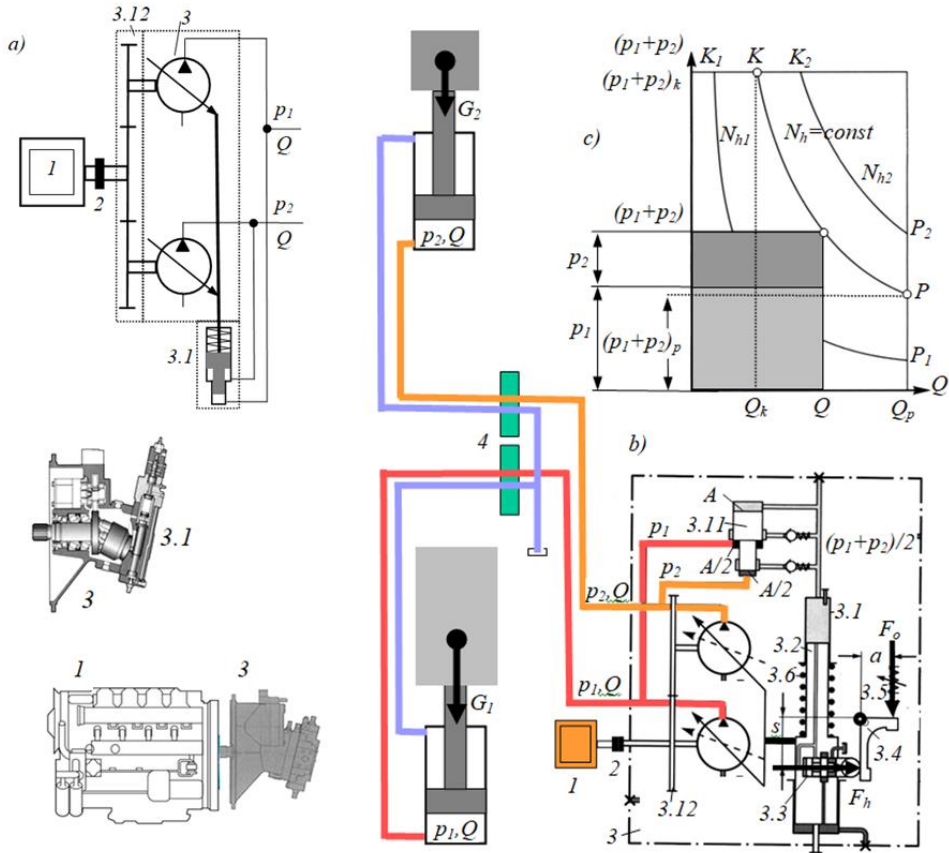


Fig. 2 Volumetric regulation of hydraulic pumps [22]: a) double hydraulic pumps with combined power regulation, b) the regulator, c) regulation with an ideal hyperbolic characteristic regulator

On one arm of the two-armed lever 3.4, one side is acted upon by the small piston 3.3 with the force created by the pressure in the pressure lines of the hydraulic pumps acting on the piston's front. On the other side, the same arm of the lever 3.4 is acted upon by the force of spring 3.5. The regulation signal is the sum of pressures $(p_1 + p_2)$ in the pressure lines of the hydraulic pumps, which is created in the pressure manifold 3.11, for which the balance condition applies:

$$p \cdot A = p_1 \frac{A}{2} + p_2 \frac{A}{2} \Rightarrow p = \frac{p_1 + p_2}{2} \quad (9)$$

On the front of piston 3.3, with a surface area A_k , the regulator of the hydraulic pump acts a pressure of $(p_1+p_2)/2$, creating a force.

$$F_h = \frac{p_1 + p_2}{2} A_k \tag{10}$$

so, according to the equilibrium condition of the lever 3.4, the displacement of the piston 3.2 of the regulator is equal to:

$$s = \frac{F_o \cdot a}{A_k} \cdot \frac{2}{p_1 + p_2} = \frac{k_r}{p_1 + p_2} = f_1(\alpha) = f_2(q_p) \tag{11}$$

The piston 3.2 is connected to a linkage that joins the blocks of the hydraulic pumps. Consequently, with the movement s of piston 3.2, the angle of rotation of the hydraulic pump blocks remains the same, ensuring that the specific flows q_p of the hydraulic pumps are identical.

Within the range of the hydraulic pump regulation, determined by the pressure $(p_1+p_2)_p$ at the start and $(p_1+p_2)_k$ at the end of regulation, the flow Q of the hydraulic pumps remains constant and changes hyperbolically with the change in the sum of the pressures (p_1+p_2) at a constant hydraulic power (Fig. 3c):

$$N_h = \frac{(p_1 + p_2)_p \cdot Q_{max}}{60 \cdot \eta_{pu}} = \frac{(p_1 + p_2) \cdot Q}{60 \cdot \eta_{pu}} = \frac{(p_1 + p_2)_k \cdot Q_{min}}{60 \cdot \eta_{pu}} = const \tag{12}$$

By changing the force in the spring 3.5 of the regulator, the initial pressure $p_p = (p_1 + p_2)_p$ of the regulation (points P1, P2) is altered, thereby changing the hydraulic power (N_{h1}, N_{h2}) encompassed by the regulation. At the same time, the pressure $p_k = (p_1 + p_2)_k$ at the end of regulation (points K1, K2) remains the same [25][26].

4. ANALYSIS

A comparative study of the hydraulic power parameters of the same model of excavator with dual fixed and variable displacement hydraulic pumps brought to light the significance of controlling the hydraulic pumps of the drive system of hydraulic excavators. The crawler excavator that was put through the test weighed 16,000 kg and included a three-part manipulator that included a boom, arm, and bucket with a 0,6 m³ capacity. The hydraulic power N_h of the hydraulic pumps, the number of rotations of the diesel engine, and the pressures p_1 , p_2 , and flow rate Q in the hydraulic pumps' pressure lines were all measured and calculated during the testing process while performing the following manipulation tasks: excavating, moving, unloading category III soil, and returning to the new digging position.

In excavators with dual fixed displacement hydraulic pumps (fig. 3a), the utilized power (fig. 3b) of the drive motor, i.e., the hydraulic power of the hydraulic pump, is proportional to the system pressure and the magnitude of the resistance. Full utilization of the drive motor power occurs only when both drive mechanisms are in motion.

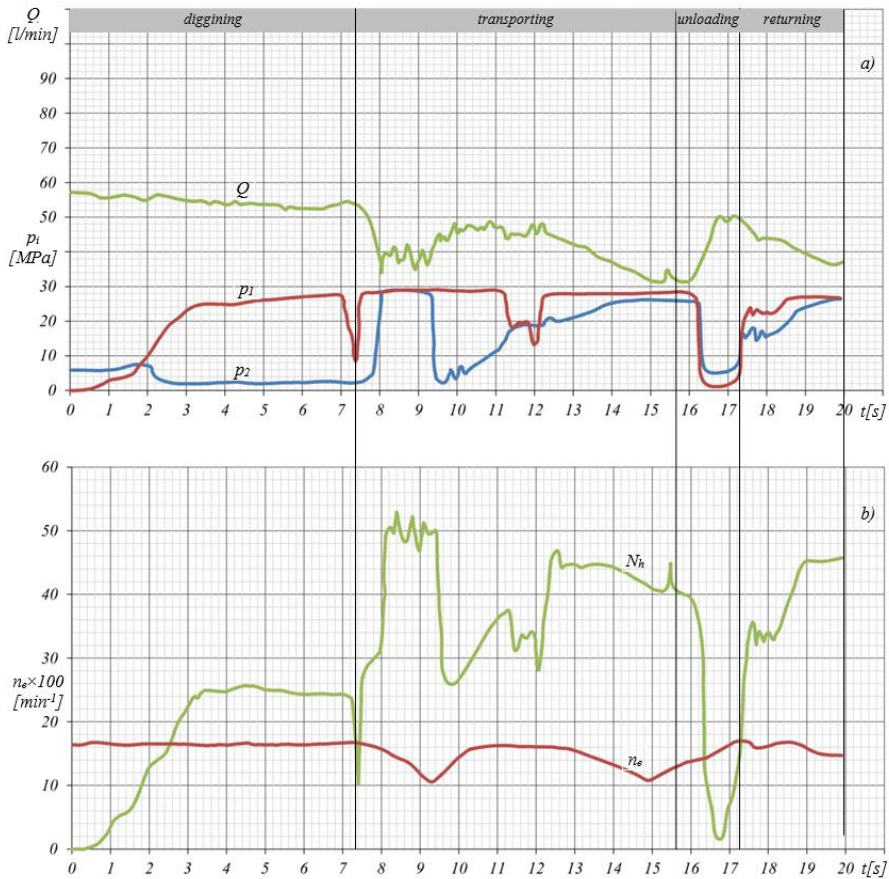


Fig. 3 Parameters of the drive system of a hydraulic excavator with fixed displacement hydraulic pumps: a) changes in pressures p_1 and p_2 , and the flow rate Q of the hydraulic pumps b) changes in hydraulic power N_h and the rotational speed n_{en} of the diesel engine

If the resistances cause maximum pressures in the system, it leads to overloading of the drive motor (drop in revolutions), making the operation of the excavator more complex, as the operator must monitor the engine's performance with their senses and select appropriate working movements to prevent motor overload. Since the resistances are variable and the system flow is approximately constant (fig. 3a), it is not always possible to fully utilize the motor power and synchronize the speeds of the drive mechanisms with such a drive system.

In the drive system of an excavator with a dual hydraulic pump with collective regulation based on the criterion of constant hydraulic power and an ideal hyperbolic characteristic regulator, there is a drop in flow at the beginning of the operational task when working pressures increase (fig. 4a). This leads to a corresponding increase in

engine power (fig. 4b). When one hydraulic pump is relieved, the engine power is sufficiently utilized at the maximum load of the other hydraulic pump [23].

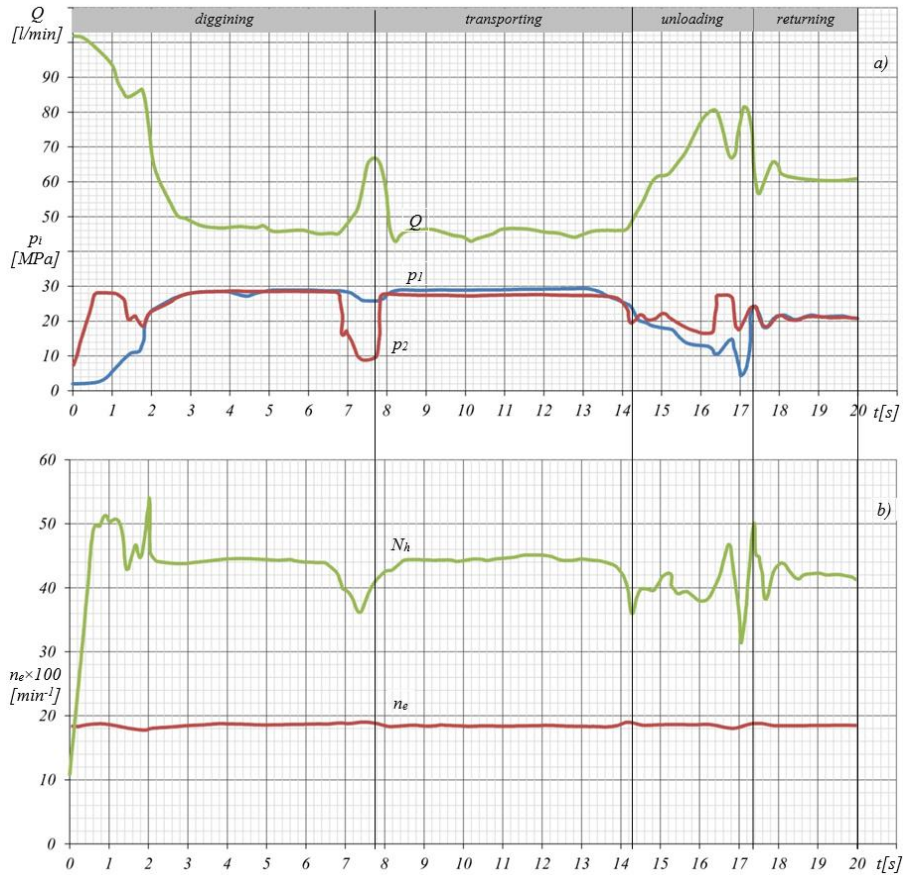


Fig. 4 Parameters of the drive system of a hydraulic excavator with hydraulic pumps of variable specific flow regulated by the criterion of constant hydraulic power
 a) changes in pressures p_1 and p_2 , and the flow rate Q of the hydraulic pumps
 b) changes in hydraulic power N_h and the rotational speed n_{en} of the diesel engine

An increase in flow rate, i.e., the speed of the drive mechanisms, occurs when the load is reduced within the regulation interval of the hydraulic pump, with pressure remaining constant. The principle of the hydraulic pump regulation becomes even more pronounced during multiple work movements, that is, while performing a complete operational task. The movement resistances are not such that they cause maximum pressure, but they fall within the regulation range of the hydraulic pumps. Since the flow rates of both hydraulic pumps are identical while the pressures p_1 and p_2 are generally different, the power received by each pump will vary. The engine does not become overloaded at any point during the operational task. The brief occurrence of a power surge above normal levels is due to the rapid change in load and the inability of the flow regulator to react to relatively fast signals.

5. CONCLUSION

The use of hydraulic pumps with integrated power regulation and an ideal hyperbolic characteristic regulator in a hydraulic crawler excavator's drive system is examined in this study. Pressure and flow in the hydraulic pump pressure lines, as well as other characteristics of the hydrostatic drive mechanism, were measured during tests on the excavator. The study shown that using a combined power regulator to regulate the hydraulic pump according to the constant hydraulic power criterion enables the maintenance of constant hydraulic power even under changing load conditions, thereby optimizing engine power usage. This rule guarantees that the excavator operates efficiently throughout all duties, including excavating, moving, unloading materials, and putting the rotating platform back in its starting cycle position. The engine overload is effectively prevented by the regulation mechanism. By effectively preventing the engine overload, the regulating system enables hydraulic excavators to adapt to a variety of operating situations. The occurrence of short-term power increases at certain moments is a result of rapid load changes, but it does not compromise the overall system performance. The conducted analysis highlights the importance of the proper hydropump regulation to achieve efficiency and machine longevity.

Acknowledgement: *This research was financially supported by the Ministry of Education, Science and Technological Development of the Republic of Serbia (Contract No. 451-03-9/2021-14/200109).*

REFERENCES

- [1] B. Xu, M. Cheng, "Motion control of multi-actuator hydraulic systems for mobile machineries: Recent advancements and future trends", *Front. Mech. Eng.*, 2018, vol. 13, no2, pp. 151–166, 2018, <https://doi.org/10.1007/s11465-018-0470-5>
- [2] Y. Wang, X. Liu, J. Chen, W. Chen, C. Li, D. Huo, "Design and control performance optimization of dual-mode hydraulic steering system for wheel loader", *Automation in Construction*, vol. 143, 2022, <https://doi.org/10.1016/j.autcon.2022.104539>
- [3] S. Li, Z. Zhang, H. Du, G. Zheng, X. Zhang, Z. Li, "Design and verification of a novel energy-efficient pump-valve primary-auxiliary electro-hydraulic steering system for multi-axle heavy vehicles", *Energy*, vol. 312, <https://doi.org/10.1016/j.energy.2024.133473>
- [4] S. Oshurbekov, V. Kazakbaev, V. Prakht, V. Dmitrievskii, "Increasing Service Life and System Efficiency of Parallel Pumps Using Combined Pump Regulation", *Water*, vol. 13, 2021, <https://doi.org/10.3390/w13131808>
- [5] B. Cao, X. Liu, W. Chen, P. Tan, P. Niu, "Intelligent operation of wheel loader based on electrohydraulic proportional control", *Math. Probl. Eng.* vol. 1, no.11, 2020, <https://doi.org/10.1155/2020/1730946>
- [6] G. Wu, J. Yang, J. Shang, D. Fang, "A rotary fluid power converter for improving energy efficiency of hydraulic system with variable load", *Energy*, vol. 195, 2020, <https://doi.org/10.1016/j.energy.2020.116957>.
- [7] X. Yan, S. Nie, B. Chen, F. Yin, H. Ji, Z. Ma, "Strategies to improve the energy efficiency of hydraulic power unit with flywheel energy storage system", *Journal of Energy Storage*, vol 59, 2023, <https://doi.org/10.1016/j.est.2022.106515>.
- [8] L. Ge, L. Quan, X. Zhang, B. Zhao, J. Yang, "Efficiency improvement and evaluation of electric hydraulic excavator with speed and displacement variable pump", *Energy Conversion and Management*, vol. 150, pp. 62-71, 2017, <https://doi.org/10.1016/j.enconman.2017.08.010>
- [9] M. Scherer, M. Geimer, B. Weiss, "Contribution on Control Strategies of Flow-On-Demand Hydraulic Circuits", *The 13th Scandinavian International Conference on Fluid Power, SICFP2013*, pp. 531-540 June 3-5, 2013, Linköping, Sweden
- [10] M. Axin, B. Eriksson, and P. Krus, "Flow versus pressure control of pumps in mobile hydraulic systems", *Proc. Inst. Mech. Eng. I, J. Syst. Control Eng.*, vol. 228, no. 4, pp. 245-256, 2014.

- [11] J. Zhou, C. Jing, W. Wu, "Energy efficiency modeling and validation of a novel swash plate-rotating type hydraulic transformer", *Energy*, vol. 193, 2020, <https://doi.org/10.1016/j.energy.2019.116652>
- [12] J. T. Jose, J. Das, S. Kr. Mishra, G. Wrata, "Early detection and classification of internal leakage in boom actuator of mobile hydraulic machines using SVM", *Engineering Applications of Artificial Intelligence*, vol. 106, 2021, <https://doi.org/10.1016/j.engappai.2021.104492>
- [13] P. Casoli and A. Anthony, "Gray box modeling of an excavator's variable displacement hydraulic pump for fast simulation of excavation cycles", *Control Eng. Pract.*, vol. 21, no. 4, pp. 483-494, 2013.
- [14] S. S. Nikolić, I. Kocić, D. Antić, D. Mitić, N. Danković, A. Milovanović, P. Đekić, "The winder dancer position control model using different PID control structures and micrologix PLC", *FACTA UNIVERSITATIS, Series: Automatic Control and Robotics*, vol. 21, no 2, 2022, pp. 77 – 93, 2022, <https://doi.org/10.22190/FUACR220409007N>
- [15] B.L. Wang, Y. Cai, J.C. Song, Q.K. Liang, "A singular perturbation theory-based composite control design for a pump-controlled hydraulic actuator with position tracking error constraint", *Actuators*, 2023, 12, 265. <https://doi.org/10.3390/act12070265>
- [16] D. Barchi, A. Macchelli, G. Bosi, L. Marconi, D. Foschi and M. Mezzetti, "Design of a Robust Adaptive Controller for a Hydraulic Press and Experimental Validation," *In IEEE Transactions on Control Systems Technology*, vol. 29, no. 5, pp. 2049-2064, Sept. 2021, doi: 10.1109/TCST.2020.3029359
- [17] K. Guo, Y. Xu1, J. Li, "A switched controller design for supply pressure tracking of variable displacement axial piston pumps", *in IEEE Access*, vol. 6, pp. 3932-3942, 2018, doi: 10.1109/ACCESS.2018.2796097
- [18] N. P. Mandal, R. Saha, S. Mookherjee, D. Sanyal, "Pressure compensator design for a swash plate axial piston pump", *ASME J. Dyn. Syst., Meas., Control*, vol. 136, no. 2, pp. 021001, 2013, <https://doi.org/10.1115/1.4025672>
- [19] M. R. Hansen, T. O. Andersen, and H. C. Pedersen, "Robust electric load sensing applied to an open circuit axial piston pump," *in Proc. ASME Int. Mech. Eng. Congr. Expo., Chicago, IL, USA*, pp. 1-8, Nov. 2006, <https://doi.org/10.1115/IMECE2006-13033>
- [20] P. T. Dean and R. C. Fales, "Modern control design for a variable displacement hydraulic pump," *in Proc. Amer. Control Conf., New York, NY, USA*, pp. 3535-3540, Jul. 2007, DOI: 10.1109/ACC.2007.4282826
- [21] V. Jovanović, A Contribution to the synthesis of the slewing platform drive mechanism of hydraulic excavators, doctoral dissertation, University of Niš, Faculty of Mechanical Engineering, Niš, 2008.
- [22] D. Janošević, Designing mobile machines, in Serbian, University of Niš, Faculty of Mechanical Engineering, Niš, 2006.
- [23] V. Jovanović, D. Janošević, J. Pavlović, N. Petrović, "Regulation of Hydraulic Pumps in the Drive System of Hydraulic Excavators", XVII International Conference on Systems, Automatic Control and Measurements, SAUM 2024, doi:10.46793/SAUM24.202J
- [24] D. Janošević, V. Jovanović, Synthesis of drive mechanisms of hydraulic excavators, in Serbian, University of Niš, Faculty of Mechanical Engineering, Niš, 2006.
- [25] International Mobile Hydraulics Conference, Mobile 2003, Ulm, Bosch Rexroth AG, Mobile hydraulics, Elchingen, 2003.
- [26] BoschRexrothAG, Produktkatalog Mobilhydraulik, Ulm, Elchingen, 2010.


A REVIEW OF DRILL STRING DYNAMICS AND MODELING TECHNIQUES

UDC ((621.95+534.232):602.1)

Nora Benmir

Applied Automation Laboratory, Faculty of Hydrocarbons and Chemistry,
M'Hamed Bougara University – Boumerdès, Algeria

ORCID iD: Nora Benmir

 <https://orcid.org/0009-0007-6856-1479>

Abstract. *The complex dynamics of drill strings under various vibration modes during drilling operations present significant challenges to the oil and gas industry due to the high costs associated with oil well drilling. This analytical study aims to provide a comprehensive overview of the most important and widely used mathematical modeling tools and techniques for describing the behaviors of drill strings under various conditions. The study highlights significant scientific contributions and research papers that have utilized or addressed these methods, including finite element, lumped mass, partial differential, wave equation, and Cosserat theory. This emphasis is meant to be partial but reflects the frequent use of these methods in drill string modeling. It also sheds light on the evolution and classification of different mathematical models used, divided into two main categories: static models and dynamics models, and how they have been involved with advancements in drilling technologies. Finally, this review underscores the potential for significant cost savings in the oil and gas industry by incorporating artificial intelligence and modern technologies into well drilling and drilling operations control, which is closely tied to improving the productivity and efficiency of oil and gas fields.*

Key words: *Drilling operation, vibration mode, finite element, mathematical models, modern technologies, static models.*

Received November 12, 2024 / Accepted December 16, 2024

Corresponding author: Nora Benmir

Applied Automation Laboratory, Department of Automation of Industrial Processes and Electrification, Faculty of Hydrocarbons and Chemistry, M'Hamed Bougara University, Boumerdès, Algeria

E-mail: n.benmir@univ-boumerdes.dz

1. INTRODUCTION

Drill string vibrations significantly influence the efficiency and performance of drilling operations, and understanding these dynamics is crucial for improving drilling processes. Various vibration forms, including torsional, axial, and lateral vibrations, lead to challenges such as stick-slip, bit-bounce, and wear-related issues[1].

This review aims to consolidate and synthesize insights from extensive scholarly investigations over the past two decades, focusing on modeling and describing the complex dynamics of drill strings under different vibration modes.

This work presents a novel and original tool for understanding the mathematical modeling of drill string behaviors under different environments and the main characteristics of these models. This scientific contribution analyzed many research papers from the last two decades.

The introductory section of this review delves into the harmful dynamic modes that emerge during well-drilling operations, presenting the biggest challenges for engineers and researchers to navigate in these research topics.

The second section exhaustively examines prior investigations concerning the modeling, quantification, and analytical understanding of drill string dynamics in the context of detrimental oscillations. We emphasize the procedural intricacies involved in modeling drill string behavior.

The third section offers a primary classification of existing modeling approaches used to describe BHA and discusses their development with advancements in drilling technologies.

Finally, the fourth section underscores the importance of integrating advanced technologies, such as edge computing and artificial intelligence, into drill string control operations. It provides a concise review of their applications.

2. DRILL STRING VIBRATIONS AND SHOCKS HARMFUL FORMS

The intricate dynamics of a drill string give rise to three distinct and severe vibratory modes, each with its own unique characteristics. These vibrational phenomena, aligned with harmful mechanical oscillations, have the potential to induce subtle perturbations that serve as early warning signs of wear and tear within the heterogeneous array of constituent elements. In the subsequent discourse, a comprehensive elucidation of these severe vibratory modes is presented, highlighting their mechanical attributes and the potential implications they carry [2].

2.1. Axial dynamic and Bit-Bounce vibration mode

This particular vibration mode, characterized by irregular movements of drilling components along their longitudinal axis, induces a phenomenon known as bit bounce.

This results in a rough and aggressive drilling behavior that can lead to excessive wear and damage to critical components. The drill bit, for instance, may suffer accelerated deterioration, and the Bottom Hole Assembly (BHA) can sustain damage, contributing to increased total drilling time. Additionally, downhole coupling mechanisms come into play, exacerbating the situation by exciting lateral displacements of the drill string. The complex motion patterns induced by this vibration mode are often observed when employing a roller-cone drill bit, also, referred to as a tricone bit due to its distinctive multiple-lobe structure. In this case, the erratic interaction of the bit with the well bottom can cause the bit to

momentarily lose contact with the rock formation, leading to an uneven and unpredictable drilling performance. These vibrations, including the bit bounce pattern, can propagate upwards and be detected at the surface, providing valuable insights into the drilling dynamics and underscoring the importance of comprehensive vibration analysis in drilling operations to mitigate detrimental effects on equipment and overall project timelines [3].

2.2. Torsional dynamic and Stick-Slip vibration mode

Downhole measurements reveal an intriguing phenomenon: the rotational motion of the drill bit does not always mirror the constant rotary speed applied at the surface. In fact, data show that during a significant portion of drilling time, the downhole torsional speed fluctuates wildly, deviating from a steady state. This self-excited rotational motion, known as stick-slip, arises from the nonlinear relationship between torque and angular velocity at the bit. The drilling assembly's torsional flexibility further amplifies these fluctuations, resulting in a nonuniform oscillatory behavior. Consequently, the drill bit can experience rotational speeds up to ten times higher than the nominal rotary table speed or, conversely, come to a complete standstill. These torsional vibrations inflict fatigue on drill collar connections, lead to drill bit damage, and slow down the drilling operation, thereby extending the overall drilling process [4].

2.3. Lateral dynamic and Whirling vibration mode

The detection of lateral vibrations is now possible due to the development of acceleration measurements at the bottom of the hole during drilling operations. According to research by Spanos et al. (2003), this type of vibration is caused by incorrect alignment of the drill string relative to the drill axis, its interaction with the drill walls, and weight variations on the tool. These vibrations cause drill pipe fatigue, failure, and premature tool wear. Repeated impacts between the drill string and the wellbore wall can lead to local enlargement of the hole, explaining the irregularity in the drill's whole diameter. It is important to note that the discovery of lateral vibrations is relatively recent compared to the understanding of axial and torsional vibrations. These lateral vibrations are quickly attenuated and do not propagate at the surface].

In the following table and figure, different harmful dynamics are presented with their severe forms cases [5].

Table 1 Harmful dynamic mode and sever forms

Vibration Mode	Severe Form	Direction of appearance	Main reason of appearance
Axial Mode	Bit-Bounce	Along axis of drill string	Component misalignment
Torsional Mode	Stick-Slip	Entire drill string	Elastic deformation and recovery of drill sting
Lateral Mode	Whirl, and Bit-Whirl	Perpendicular to drill string axis	Center eccentricity rod, Buckling

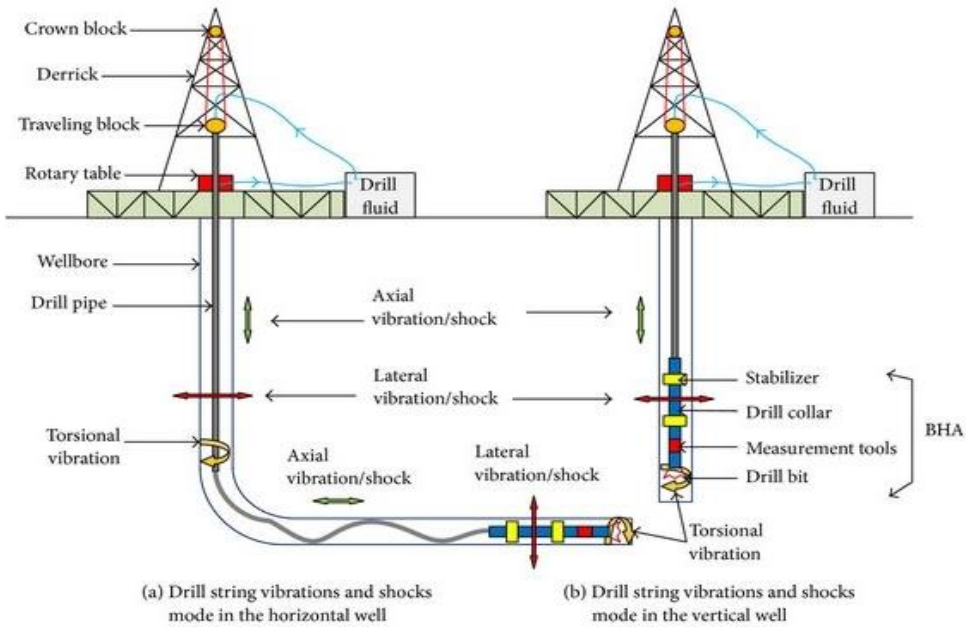


Fig. 1 Drill string vibrations and shocks in typical well

3. THE REVIEW STUDY

In this context, we propose a comprehensive review that unifies various research inquiries about the mathematical representation of drill string behavior. This review integrates several fundamental methodologies, including lumped theory, the finite element method, wave equations, partial differential equations, and the application of Cosserat modeling, to provide a holistic understanding of drill string dynamic. By analyzing these diverse approaches, we aim to offer a synthesis that contributes to a deeper insight into the complex behavior of drill strings during drilling operations.

3.1. Application of Finite Element (FEM) in Modeling

Finite Element Analysis (FEA) has revolutionized the understanding of drill string behavior within drilling systems, offering an invaluable and intricate lens into their complex dynamics. The versatility and sophistication of FEA have attracted researchers and investigators alike, providing a powerful tool to explore the diverse facets of drill string behavior. Over the years, many studies have employed FEA to unravel the mysteries of drill string interactions and phenomena during drilling operations. This analytical technique has proven indispensable in the quest to comprehend and optimize the performance of drilling systems, contributing significantly to advancements in both theoretical and practical aspects [6].

Trindade and Sampaio's 2005 investigation employed an advanced finite element model to explore axial-torsional coupled vibrations and their impact on drill string rotational

speed regulation. Their work shed light on the complex dynamics of the stick-slip phenomenon, a challenge in drilling operations [7].

In their paper [8], Y.A. Khulief and H. Al-Naser aimed to enhance the understanding and mitigation of drill string vibrations. They developed a dynamic model using the Lagrangian approach and the finite-element method to capture the complex vibrational behavior of drill strings. The model accounted for crucial factors such as gyroscopic effects, torsional-bending inertia coupling, and the influence of axial gravity.

In 2010 [9], Compton presented a proven approach to enhancing deep-water drilling efficiency. Their main objective was to optimize the combination of whole enlargement and drilling operations while mitigating damaging vibrations. They employed the advanced finite element dynamic formulation, to analyze the interactions between bottom hole assembly (BHA) components and identify the root causes of vibrations.

In 2015 [10], a novel experimental rig was designed to mimic various types of drill-string vibrations, including stick-slip oscillations and whirling. The nonlinear dynamics of the drill-string were described using the Finite Element Method (FEM), and the results verified experimentally.

Vromen et al. [11] Used a finite element method with eighteenth degree of freedom (DOF), to describe the structure of a jack-up drilling rig, to mitigate the Stick-Slip severe form of torsional vibration.

An evaluative investigation has determined the impact of two different formulations on the reliability and precision of the finite element method in large-diameter drilling operations. The updated Lagrangian formulation with dynamic re-meshing (UL-DR) in DEFORM 3D yielded the most accurate results. It provided the best predictions for drilling thrust force, torque, and chip thickness when compared to experimental data [12].

Mingjie Cai and colleagues in [13], developed a beam finite element (FE) model to analyze drill string dynamics in curved wells. They investigated the effects of various parameters on lateral vibration, including rotation speed, WOB, COF, and STB. While the model reproduced field data, it did not consider drill string-wellbore wall contact, a critical aspect of curved well drilling.

In the contribution in 2023 [14], the authors developed a rigid-flexible coupled model to analyze and optimize the vibration of a rock drilling arm. Their study showed that this model better describes the propelling beam's vibration, leading to reduced offset values and smaller vibration amplitudes at a steady state.

A finite element analysis coupled with The Taguchi method have used in the investigation conducted by A.L. Muthuveerappa et al. to determine the optimum drilling parameters with CNN drill material and specify cutting speeds and drill points angles recommended to minimize deformations and stress[15].

The work in [16] proposed two novel controller techniques relying on simple linear relations of measured signals to mitigate torsional vibrations. The proposed controllers were based on finite element theory with non-regularized dry friction, which proved their adaptation to these two novel techniques.

The study in [17] presented a significant advancement in understanding drill-string dynamics by employing a three-dimensional finite element model that considers dynamic friction and buckling effects. Validated by laboratory experiments, the model offers enhanced computational accuracy in predicting sliding force and vibration load transfer.

A key strength of the research lies in identifying the critical factors that control vibration propagation along the drill string. This leads to the establishment of a prediction

model for vibration propagation distance, providing a valuable tool for optimizing axial vibration parameters.

3.2. Application of Lumped Mass as a model

This section explores the use of lumped-parameter models as a powerful tool for analyzing and controlling various dynamic phenomena in drilling operations.

The application of lumped-parameter models offers a simplified and practical approach to studying the dynamic behavior of drill strings, providing a comprehensive framework for analyzing and addressing the challenges posed by various vibration modes and oscillations [18].

In 2010, authors undertook a semi-analytical investigation aimed at analyzing stick-slip oscillations within drilling operations. They employed a lumped mass methodology featuring singular inertia along the axial direction; the researchers successfully computed the precise limit cycle and optimized parameters hitherto unknown [19].

The research by Kamel and Yigit (2014), offered a comprehensive analysis of severe bit-bounce and stick-slip vibrations experienced by oil well drill strings with drag or PDC bits. Central to their work is introducing a meticulously crafted, two-degrees-of-freedom lumped parameter model, derived using the Lagrangian approach, which proves instrumental in deciphering the intricate nature of these vibrations [20].

The author's paper in, introduced a distributed-lumped modeling technique to simulate oil well drilling systems. The study aimed to mitigate vibrations at the BHA, focusing on drill string effective length. The distributed-lumped model found to be more precise than the lumped model, especially for long drill strings [21].

The paper published in 2020 focuses on the nonlinear dynamics of a drill string in a horizontal well. They introduced a novel and comprehensive six-degrees-of-freedom (6DoF) lumped mass model specifically designed for horizontal wells. The dynamic model accounts for the drill string's longitudinal, lateral, and torsional motions [22].

Idir Kessai et al. used a lumped mass model with multiple degrees of freedom to look at how drill bits change shape when there are large-amplitude stick-slip vibrations in rotary drilling systems. The results were validated using MWD data from real wells, providing insights into the dynamic behavior of drill bits during stick-slip phenomenon [23].

The thesis in [24] contributed to the development of advanced modeling and control systems for offshore drilling. Two new lumped-parameter models were proposed and analyzed for the stability of drill string dynamics. The first model was derived from Lagrangian mechanics and structures using the Bond Graph methodology, and the second one used Kane's methods based on the Newton-Euler formulations.

The 2022 study by Lelya A. Khajiyeva, focused on analyzing the nonlinear dynamics of drill strings using the lumped-parameter method (LPM). Their primary objective was to investigate lateral vibrations in a vertical drill string influenced by supersonic gas flow. LPM exhibited superior convergence and stability compared to its linear counterpart [25].

Laib et al.'s study proposed a hybrid interval type-2 fuzzy PID controller for a multi-DOF Lumped parameters oil well drill-string system. The system was modeled using a four-degree-of-freedom drill string model, incorporating nonlinear bit-rock interactions. The hybrid controller combined fuzzy logic (IT2FC) with conventional PID control, resulting in faster response times. Simulations and experimental testing validated the controller's performance, and proved its effectiveness compared to other controllers as sliding mode controllers [26].

To eliminate the stick-slip phenomenon Rian et al. designed an observer-based H_{∞} control, in collaboration with observer-based LQG controller using a lumped parameter model with ten degrees of freedom. This modeling approach has shown its adaptation with the control technique used in this investigation [27].

The main objective of the study in [28] was to develop a comprehensive drill string dynamics model based on the lumped parameter model (LPM). The developed model showed its capability to describe the fully coupled axial, torsional, and lateral vibrations of drill string.

The study in [29] explored lateral vibration in rotor-stator rubbing systems. Through experimental and numerical methods, authors investigated the effects of mass unbalance and radial clearance on system response. The study revealed significant impacts of these parameters on dynamic characteristics, including periodic and chaotic responses. A simple test rig and a two-degree-of-freedom lumped mass model were used, with numerical analysis employing the Runge-Kutta technique.

3.3. Application of Wave equations and PDE as models

Drill string vibrations can have significant negative consequences for the drilling industry, affecting efficiency and equipment integrity and compromising borehole stability. To address these concerns effectively, it is essential to utilize a wave equation model that accurately depicts the behavior of the drill string under various vibration modes. By adopting this modeling approach, engineers and researchers can gain valuable insights into the intricate dynamics of the drill string. The wave equation model considers the elastic nature of the drill string, the forces exerted on it, and the relevant boundary conditions [30].

Improving mud-pulse telemetry techniques to improve while-drilling data transmission was the aim of the study in 2000. The main objective was to develop a comprehensive model that accurately represents the complex behavior of wave propagation in drill strings, with the goal of improving data transmission speeds and mud-pulse telemetry [31].

Miroslav Krstic's 2013 study focused on developing an adaptive control strategy for anti-stable wave PDE systems, specifically for applications in oil drilling systems. The research proposed a tailored approach to address the challenges of wave equations, offering a stable and efficient control strategy for these complex systems [32].

The scholarly work presented by Boussaada et al, 2013 in [33] centers on investigating control strategies targeting the intricate interplay of axial and torsional vibrations encountered in drilling operations. The authors employ a neutral delay differential equations (NNDE) model, which stems from a systematic reduction of more complex partial differential equations (PDE) models. To address the control objectives, the study advocates the application of PID controllers and delayed feedback control mechanisms.

The authors in [34] adopt a coupled modeling framework that integrates wave and ordinary differential equations (ODE) to capture the system dynamics comprehensively.

The investigation conducted in [35], presents a novel observer-based boundary condition in which coupled ordinary differential equations (ODEs) and partial differential equations (PDEs) are used as a basic model, which proved its effectiveness in designing the controller and the novel observer.

He Zhang developed a high-dimensional coupled model of PDE (partial differential equation) and ODEs (ordinary differential equations) to analyze self-excited axial and torsional vibrations in rotary drilling systems. The model combines a multi-degrees-of-freedom representation with a rate-independent bit-rock interface law, capturing the

regenerative effect through a PDE and ODEs. The study includes a stability analysis and a parametric study to understand torsional stick-slip occurrences [36].

The contribution in [37] aimed to develop a more improved and comprehensive model for drill string dynamics. They used delay-differential equations to simulate the cutting process. The adopted equation avoided the delays and allowed for more continuous cutting during the drilling operations.

In their paper, Jean Auriol addressed a critical aspect of the drilling industry: improving the estimation of drill-string dynamics and rock properties during directional drilling. The drill-string dynamics was represented by a coupled dynamical model wave equations with an ordinary differential equation at the downhole boundary (bit-rock interaction) [38].

To design a hybrid full-state feedback controller and a state observer for a drilling system, the researchers combined the backstopping methodology and frequency analysis based on a linear 2 dimension hyperbolic PDE system coupled with proximal ODEs and distal Load ODEs [39].

Toumi's research delves into the complex dynamics of rotary drilling systems, proposing innovative control strategies. The study employs nonlinear models to identify critical factors contributing to drill string vibrations. Two distinct control approaches are introduced, using PDEs and ODEs as modeling tools, to mitigate these vibrations and ensure operational stability [40].

3.4. Application of Cosserat theory as a modeling technique

The Cosserat rod theory has attracted much interest lately as a solid and adaptable framework for simulating the complex behaviors of drill strings. These studies have presented and confirmed drill string dynamic models that are comprehensive and based on the Cosserat theory.

Marcos Silviers's paper presented an analysis of stick-slip oscillations in drill strings using a modified Cosserat rod element method. The integrated model captures the complex dynamical and geometrical behavior, including general deformations like flexure, extension, torsion, and shear. This approach offered computational advantages compared to Finite Element methods, enabling the simulation of stick-slip oscillations and drill-string-borehole wall contact [41].

To analyze the complex dynamics of the drill string, the authors in [42] employed a Cosserat rod theory, taking into account the slenderness of the structure and the geometrical aspects. This modeling approach gave rise to adaptations with the stochastic analysis technique used in the investigation.

The study conducted by Tucker and Wang in 2022 presents a novel approach to understanding the vibrational dynamics experienced by the functional components of a drilling assembly. The study focuses on creating a comprehensive mathematical framework based on the ideas of Cosserat's theory [43].

Fan Yu, Genlu Huang, and colleagues in 2023, present a comprehensive model for analyzing the lateral vibration of a bottom hole assembly (BHA) during drilling operations. The Cosserat theory, which treats the BHA as an elastic rod, was utilized to develop a more sophisticated drill string dynamics model. This model incorporates various factors encountered in practical drilling, such as wellbore constraints, deviation angle, friction, torque, centrifugal force, and material viscosity [44].

Hector Eduardo in his thesis developed a deterministic structural model using Cosserat rods to study the dynamics of drill strings in curved oil wells. The model considers drill pipes and the bottom hole assembly as a one-dimensional Cosserat structure, offering a strategy to address lateral contact in curvilinear well configurations [45].

To address the challenges in drilling complex oil and gas wells, Zambetti et al. developed a 3D geometrical dynamic model based on the Cosserat rod theory. The mathematical model demonstrated its advantages in simulating real-time scenarios [46].

In the study in [47], researchers developed a comprehensive continuous Cosserat rod model to study the dynamics of a drill-string in arbitrary well geometries. The model simulates 3D dynamics, including lateral, axial, and torsional motion, and incorporates lateral contact, offering a versatile tool for drill string's dynamics analysis.

3.5. Modelling techniques comparative study

The prior modeling approaches are summed up in the following table, which compares their benefits and drawbacks in explaining drill string dynamics.

Table 2 Comparison table of the most used mathematical techniques in drill string modelling

Year	Authors	Drill string model	Control strategy	Counting /considered parameters	Testing	Results
2000	J.M. Carcione et.al [31]	Wave equation model	/	MWD tool / Data transmutions speed	Simulation	Developed model proved its accurately represents the complex behavior of wave propagation in drill strings
2005	Trindade et.al [7]	Advanced finite element model	Active control strategy	Speed rotation	Simulation/ Experimental	Drill string vibration mitigation using finite element methodology modelling review
2005	Y.A. Khulief et.al [8]	Finite element analysis with 12DOF	/	Gyroscopic effect, Gravity factor Torsional/ bending inertia coupling	Simulation	The model accounts for the gyroscopic, as well as the bending/torsional inertia coupling. In addition, the axial gravitational filed effect on the drillstring
2010	Compton et.al [9]	Advanced finite element dynamic formulation	/	Drill bits / reamers drive systems/ MWD/LWD tools	Simulation / Experimental	A detail analysis of interactions between BHA components Identified root cause of vibrations
2013	Miroslav Krstic's [32]	Wave equations system	Adaptive control strategy	Rotary speed WOB Top Drive torque	Simulation	Modeling and control strategies were offered a stable and efficient understanding for the complex BHA dynamics

2013	Boussaada et al[33]	Neutral delay differential equations (NNDE) model	PID controllers Delayed feedback control mechanisms	Axial vibration trajectory	Simulation	The PID controller gain and the feedback gain are established the same to compare their regulations results
2013	Marcos Silviers et al[41]	Cosserat rod element method	/	Flexure deformation Torsion, Extension and shear deflections	Simulation	The proposed model captures the complex dynamics and geometrical behavior of drill string
2014	Kamel and Yigit [20]	Lumped parameter model	/	Rotary and translational motions of the drillstring Bit/rock formation interaction	Experimental	The model and the proper choice of operational parameters, may be possible to minimize the effects of stick-slip and bit-bounce and increase the ROP
2015	M. Kapitaniak et.al [10]	Finite element method	/	RPM/ WOB Friction factor	Experimental /numerical	Experimental rig to reproduce all modes of vibrations was investigated Great predictive capabilities of the developed model especially for stick-slip vibration
2016	B. Saldivar et al [34]	wave and ordinary differential equations (ODE)	Feedback controllers The soft-torque system Flatness-based control	Axial velocity Rotational velocity	Simulation	The proposed control systems could eliminate the stick-slip and the bit-bounce vibrations.
2017	H. Ibrahim Basturk et al [35]	Ordinary differential equations (ODEs) partial differential equations (PDEs)	Active control strategy	The angular velocity	Numerical Simulations.	The proposed control was effectively suppressed stick-slip oscillation.
2017	T. Vromen et al [11]	Finite element model	Robust control based on skewed- μ DK iteration	Top drive velocity Top drive torque Drill bit and well interaction	Simulation	The controller offered: only surface measurements are employed no need for down-hole measurements multimodal drill-string dynamics are dealt with it.

2020	P. Athanasius et.al [21]	Lumped parameter model Distributed Lumped modelling	/	Drill string effective length	Simulation	The D–L model was found to be more precise, particularly for long strings.
2020	D. Xie et.al [22]	6 DOF lump mass model	/	The friction and cutting effects	Simulation	The dynamic model established tested where the friction and cutting effects are gradually switched on. It analyzed the complex whirling of a horizontal drill-string.
2020	Idir Kessai et.al [23]	Several DOF mass-spring-damper model	/	Torque variation WOB / Drill bit radius	Simulation	hat the stick-slip vibrations are very damaging to the drill bit even if it is controlled by parametric variation because the delay between its appearance and the intervention.
2021	N. K. Tengesdal et al [24]	LPM based Lagrangian mechanics and Bond Graph LPM based used Kane's methods	Nonlinear predictive controller and Kalman filter Multivariable control PID controller	Rotational velocity The nonlinear frictional pressure forces	Simulation	The proposed advanced controllers proved effectiveness robust to mitigate vibrations in offshore drilling operations.
2021	J. Priest et al [12]	3D finite element model Update Lagrangian	/	Torque Chip thickness values	Simulation/ experimental	The update Lagrangian is not a computationally viable for large diameter drill string Combine the updated-Lagrangian with dynamic re-meshing methodology is the most suitable with large diameters.
2021	J. Auriol et.al [38]	Wave equations Ordinary differential equation	/	Rock proprieties	Simulation	The results was improving the estimation of drill string dynamics and rock properties during directional drilling.
2021	H. E. Goicoechea et al [42]	Cosserat model	/	The slenderness of the structure The geometrical proprieties	Simulation	The used modeling approach gave rise adaptations with the stochastic analysis technique of drill string dynamics

2022	L. A. Khajiyeva [25]	Lumped parameter method	/	Angular velocity Lateral displacements	Simulation / Numerical	The proposed model was effectively solve the nonlinear problems drill string dynamics
2022	H. Zhang and E. Detournay [36]	Partial differential equation ordinary differential equations	/	Rate of penetration Bit-rock interaction	Simulation	A stability analysis and parametric analysis of stick-slip and bit-bounce phenomenon
2022	Tucker and Wang et.al [43]	The Cosserat theory	/	The geometrical aspects of the structure	Simulation	The novel approach presented a high understanding level of BHA dynamics
2023	Neto et al [16]	Finite element method	Active control Based state feed back control (LQR) approach	Rotary velocity signals	Simulation	The proposed model can define which signals are relevant for state feedback for ensuring asymptotic stability.
2022	H. E. Goicoechea et al [37]	A delay-differential equations	/	The angular speed The bit-rock interaction	Simulation	The proposed equation could avoid the delays and allowed for more continuous cutting during the drilling operations.
2022	Fan Yu et.al [44]	The Cosserat theory	/	WOB / TOB / rotary speed	Simulation / Laboratory experiment	The Cosserat theory was used to develop more sophisticated drill string dynamics model
2023	Weili Liu et al [17]	3D FEM dynamic model	/	<u>Axial force friction model</u> Buckling effect	Laboratory experiment	The exciting force amplitude, drilling fluid density, axial force, friction coefficient, and drill-string dimension have significant effects on the friction reduction performance and effective
2023	A. L. Muthuveerappan et al [15]	Finite element analysis	/	Drilling bit cutting speed drill point angle	Simulation	Optimum drilling parameters for deformation were found for real value of rotational velocity
2023	J. Redaud et al [39]	2DOF hyperbolic PDE system Proximal ODEs	A hybrid full-state feedback Back-stepping strategy and frequency analysis	Rotational velocity	Simulation / Experimental	An adequate feedback control was designed in frequency domain and a robust tracking output stat observer was proposed.

2023	Zambetti et.al [46]	3D Cosserat rod theory in Euclidean strands	/	Contact points drill string-wellbore walls. The geometry of the rod	Simulation/experimental	The mathematical model demonstrated its advantages in simulating real-time scenarios
2023	Hector Eduardo [45]	Cosserat rods model	/	The geometrical rod proprieties	Simulation	The proposed model was offering a strategy to address lateral contact in curvilinear well configurations
2024	Y. Zhang et. al [28]	Lumped parameter model (LPM).	Oriented control	Angular velocity Top drive torque	Simulation	The developed model showed its capability to describe the fully coupled axial, torsional, and lateral vibrations
2024	S. Toumi and R. Mlayeh, [40]	Wave equation PDE coupled with ODEs	Feedback controller based on Lyapunov approach	The velocity at the bottom extremity The damping factor of BHA	Simulation	The proposed control effectively suppressed the harmful vibrations
2024	H. E. Goicoechea et.al [47]	3D Cosserat rod model	//	Lateral contact points Drill cutters-well contact	Simulation	The proposed modelling offered a versatile tool for drill string's dynamics analysis

Table 3 A summary of modelling strategies and theories to describe drill string dynamics.

Modelling technique	Description	Advantages	Drawbacks
Finite Element method	Numerical method, divide complex structures' behavior into smaller parts and solving mathematical equation	Using multiple approaches to analyse complex structures and systems	Need a powerful calculating process
The Lumped Mass Approach	This method simplifies complex structures by modelling them as masses and springs, aiding dynamic behaviours analysis.	It simplifies the complex structure to easier mathematical problems	Missing of important parts of systems , and ignore many structure's details
Wave Equation and PDE methods	The Wave Equation and Partial Differential Equations (PDEs) are essential tools in engineering. They describe wave propagation and changes in physical quantities.	Easy mathematical tools, They could adapt with many system's modelling	They represent analytical techniques can be away from the real process
The Cosserat Method	This technique in continuum mechanics considers microstructure and material rotations within deformable bodies	It is valuable for accurately modeling materials with micro scale deformations. Very precise method	It needs knowledge of the microscopic structure of systems which is not easy for many systems

4. STATIC AND DYNAMICS MODELS

The vibration phenomenon in drilling processes is complex due to the coupling of different modes and numerous parameters. Interactions between the drill string and the formation further complicate modeling efforts. Initially, static models focused on calculating stresses, deformations, and directional behavior. Dynamic models introduced, as a temporal and frequency approaches to predict stress evolution over time and identifying critical rotation speeds to prevent resonance. Both static and dynamic models are validated through site measurements or laboratory experiments, acknowledging the complexity of the complete mathematical problems [48].

4.1. Static models (Torque and Drag)

Static models are developed to calculate deformations, axial forces, and the twisting of models are called also Torque and drag models. They divide into two main categories: smooth models, which neglect the rigidity of the filling, and rigid models, which consider it [49].

In their pioneering work, Johancsik and Friesen set out to tackle the challenging issue of predicting torque and drag forces in directional wells. Their innovative computer model, developed in 1984, revolutionized the industry by providing a powerful tool to forecast these critical parameters accurately [50].

In their 1998 paper, M.S. Aston et al. addressed the growing importance of torque and drag minimization in drilling operations. They present a comprehensive review of the diverse techniques available in the industry to tackle these challenges [51].

In their 2003 work, D. Stuart introduced an innovative drilling technology to address torque and drag issues. By combining an extended-gauge bit design with a steerable motor or rotary steerable system, they achieved remarkable reductions in friction factors and wellbore cline [52].

The analysis in [53] aimed to enhance the accuracy and the practicality of torque and drag analysis in drilling operations through the application of the finite element method (FEM), leading to improved decision-making in well drilling operations.

In the context of offshore well operations, the torque and drag analysis using the 3D model to account for the friction forces was the object of the Master's thesis realized by Knut Tveitan, where the correspondence between the 3-dimensional friction model and field data was examined [54].

In the thesis of Mohammad Fazelizadeh delved into the critical aspects of torque and drag calculations in directional drilling. The thesis introduces novel torque and drag models, considering wellbore geometry and drill string interactions while accounting for drill string stiffness and partial wellbore contacts [55].

To improve Torque and Drag modeling using traditional and machine learning methods, Mayowa realized a full PhD research, using a soft-string model for torque and drag analysis. This involved addressing frictional losses, considering the well-path trajectory, and solving coupled differential equations [56].

Da Silva's study introduced real-time monitoring software, utilizing torque and drag models. This technology automatically diagnoses drilling problems, analyzing drill string loads and borehole contact. The model aims to optimize RAM actuation, minimizing risks [57].

Zou et al.'s research introduced a novel controllable hybrid steering drilling system CHSDS, aiming to minimize drag and torque challenges in extended-reach wells. Based on the stiff-string drag torque model combined with the friction-reducing performance of the CHSDS, the study revealed the system's efficacy, particularly in inclined sections, with rotary speed and fluid density enhancing friction reduction [58].

4.2. Dynamic models

The development of dynamic models linked to the evolution of surface and downhole measurements. There are two essential classes: temporal and frequency models. The first dynamic models appeared in the middle of the last decade [59].

The author in the paper in [60] presented a rigid-flexible multibody system approach to model drill string dynamics. The research modelled the drill string as a series of uniform flexible beams interconnected by linear viscous-elastic force elements. Showing a close match between theoretical and numerical results for static, buckling, and resonant frequency problems.

In 2013, the research paper discussed the development of the rigid-flexible multibody system for modeling drillstring dynamics and the influence of model parameters on simulation accuracy and calculation time [61].

To improve the dynamic friction model of drill strings under torsional-longitudinal coupling oscillation, researchers developed a model that considers friction forces and torsional vibration. The constructed dynamic friction model exhibited good agreement with experimental findings, confirming its accuracy in forecasting friction force changes owing to torsional vibration [62].

Using a multi-body system dynamics technique, Xiu-Quan Liu and colleagues performed a mechanical analysis of deep-water drilling riser systems. According to the study, tensioners efficiently reduce the riser system's deformation, resulting in lower static displacements. The researchers do point out that compared to simple dynamic models; the application of multi-body dynamic systems is more complicated [63].

In the scientific article [64], a nonlinear dynamic model with four-degree-of-freedom (4DOF) was established to characterize the behavior of the drill-string in a deviated well. The stick-slip phenomenon, the lateral and torsional deformations of the drill string, and the fluid-damping effects were also considered.

The scientific contribution in 2021 [65] implied the development of a nonlinear dynamic model using Galerkin's method coupled with a second-order differential equation, considering the effects of parameters such as forcing frequency, perturbation amplitude, mass ratio, and flow velocity.

In [66], a novel intelligent dynamic model was proposed to predict the drilling rate of penetration online. The proposed model showed its capacity for autonomous learning during the drilling process and it had a higher prediction accuracy than two online and five offline, well-known conventional methods.

In the same context of ROP online prediction, a multi-source information fusion-based dynamic drilling ROP model was proposed. This model takes into account the formation drillability and the time interval as updating conditions. Compared to well-known methods. This novel technique improved the effectiveness of ROP online prediction [67].

Based on two different techniques of modeling, the lumped mass method and the discrete element technique, a drill string dynamic model was proposed, taking into

account rock breaking as a crucial factor. The drilling simulation results conducted with the integrated model under different ground rotational speeds (GRSs) and weight-on-bits (WOBs) demonstrated that the developed model could be effectively used to investigate rock-breaking of drill bit and drill string motion simultaneously [68].

5. INCORPORATE ADVANCED AUTOMATION AND AI IN DRILLING CONTROL

Incorporating automation and cutting-edge technologies within the drilling operation can amplify the control over drilling parameters. Artificial Intelligence (AI) can scrutinize real-time rig activities, telemetry data, and Bottom Hole Assembly (BHA) particulars as an illustrative instance. It can thereby formulate astute suggestions for fine-tuning drilling processes toward optimization [69].

The figure below assesses technological advancements within the oil drilling industry over the past two decades (1999-2023).

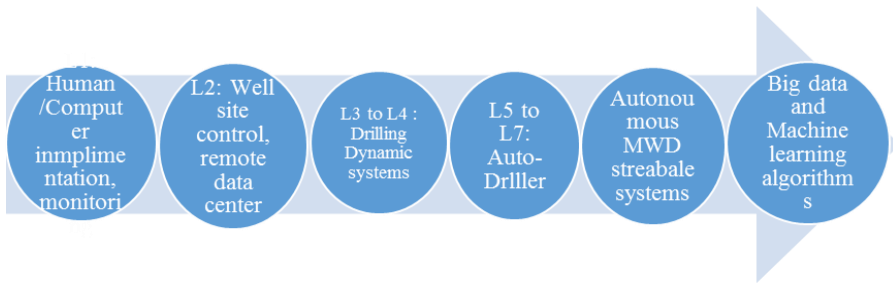


Fig. 2 Automations level in drilling operations

The objective of the investigation conducted by Kasiralvalad, 2014 in [70] is to comprehensively examine the using of nanomaterials in drilling and drilling fluids pertinent to petroleum development and production.

The review contribution conducted by Opeyemi. B et al. summarized the previous investigations that applied artificial intelligence in drilling operations optimization before 2015. They confirmed the importance of integrating these advanced tools in the control, analysis, and enhancing well drilling systems [69].

The investigation conducted in [71] showcases the efficacy of artificial neural networks (ANN) in estimating drill bit temperature and cutting force in drilling operations. The study applied artificial neural networks (ANN) to estimate the drill bit temperature and cutting force in the drilling process using coated carbide and uncoated drills. Also, the effects of the different network structures in the modeling of the drill bit temperature and cutting force were investigated.

In the work presented by Creegan and Jeffrey, an intelligent drilling optimization framework featuring an adaptive auto-driller mechanism is elucidated. This innovative approach integrates advanced artificial intelligence (AI) algorithms to enhance the efficacy of on-bottom drilling operations [72].

The study in [73] explored drilling vibration modes and penetration rate modeling in the Egyptian Western Desert. Utilizing Artificial Neural Networks and multiple linear

regression, the Authors developed an advanced model to predict penetration rate and vibration levels.

The study revealed that axial vibrations could be reduced by increasing the weight of the bit and rotary speed. Conversely, lateral and torsional vibrations were enhanced by increasing rotary speed and decreasing weight on the bit.

Ramy Saadeldin et al.'s study developed an Artificial Neural Network (ANN) model to predict drill string vibrations during horizontal drilling. The model utilized surface drilling data, including mud pumping pressure, rotating speed, and top drive torque. Validation was achieved through simulation and experimental data, with a separate dataset confirming the model's accuracy. The optimized model showed a high correlation between predicted and actual vibrations, indicating its effectiveness [74].

The study in [75] introduced the Well Control Space Out technology, an internet-of-things (IoT) solution that utilized deep learning to process real-time video images of the drill string. By automatically detecting and tracking key rig components, the system provides critical data for good control and improves decision-making in time-sensitive situations.

A study by Rouzgard and Shirazi, introduced an algorithmic approach for the autonomous steering of a drill bit during directional drilling activities. In manual control scenarios, challenges may arise due to operational imprecisions and human factors, resulting in deviations from the intended drilling trajectory [76].

Equinor et al. inaugurated the world's inaugural fully automated oil and gas platform, Oseberg Vestflanken H. This platform is a remarkable technological achievement, functioning autonomously without human intervention [77].

M. N. Al-Mudhaf discussed revolutionizing drilling efficiency with Neuro-autonomous solutions applied in the Kuwait oil and gas industry. The last adopted digital technologies, particularly AI and autonomous systems have revolutionized drilling operations. The oil companies have led the way with their implementation of Neuro Autonomous Solutions, including DrillOps Automate, DD Advisor, and Auto-Curve, coupled with Schlumberger's Well Construction Rig and Blue BHA. This integrated system enhances drilling efficiency, reduces costs, and improves safety by optimizing data processing and minimizing human error [78].

6. CONCLUSION

Previous theories and scientific contributions have focused on understanding, describing, and modeling drill string behaviors. The most used methods include the finite element method, which uses multiple techniques to analyze complex structures; the lumped masse technique, which simplifies complex systems but may miss many essential parts, wave equations, and PDE approaches, which provide analytical mathematical tools; and the Cosserat theory, which requires knowledge of microscopic structure details. Mathematical models used to describe drill strings can be classified into two main categories: static models, which calculate deflections, axial forces, and twisting of drill pipes, and dynamic models, which describe BHA behaviors under dynamic phenomena like stick-slip, bit-bounce, and bit-whirl. Incorporating automation and advanced technologies such as automated rigs and AI techniques to improve control of drill string vibrations and undesirable dynamics

was important to raise the level of efficiency and optimization in drilling operations in current gas and oil fields.

Acknowledgement: *This research is made possible by the collaborative environment created by the Applied Automation Laboratory (LAA) at the Faculty of Hydrocarbons and Chemistry at the University of M'Hamed BOUGARA Boumerdes (UMBB) in Algeria. The university's commitment to innovative research and academic excellence has been a constant source of inspiration throughout the review process.*

REFERENCES

- [1] I. Boussaada, H. Mounier, S.-I. Niculescu, and A. Cela, "Analysis of drilling vibrations: A time-delay system approach," in *2012 20th Mediterranean Conference on Control & Automation (MED)*, Barcelona, Spain: IEEE, Jul. 2012, pp. 610–614. doi: 10.1109/MED.2012.6265705.
- [2] A. Ghasemloonia, D. Geoff Rideout, and S. D. Butt, "A review of drillstring vibration modeling and suppression methods," *J. Pet. Sci. Eng.*, vol. 131, pp. 150–164, Jul. 2015, doi: 10.1016/j.petrol.2015.04.030.
- [3] W. R. Tucker and C. Wang, "An Integrated Model for Drill-String Dynamics," *J. Sound Vib.*, vol. 224, no. 1, pp. 123–165, Jul. 1999, doi: 10.1006/jsvi.1999.2169.
- [4] "The Genesis of Torsional Drillstring Vibrations | SPE Drilling & Completion | OnePetro." Accessed: May 29, 2024. [Online]. Available: <https://onepetro.org/DC/article-abstract/7/03/168/70661/The-Genesis-of-Torsional-Drillstring-Vibrations?redirectedFrom=fulltext>
- [5] D. Ezzeddine, "Modélisation du comportement dynamique d'un train de tiges de forage pétrolier: application aux vibrations latérales," phdthesis, Ecole Nationale Supérieure des Mines de Paris, 2013. Accessed: Jun. 02, 2024. [Online]. Available: <https://pastel.hal.science/tel-01511423>
- [6] E. Perrotet, "Bathe, K. J. Finite Element Procedures 1996 Prentice Hall", Accessed: Jun. 07, 2024. [Online]. Available: https://www.academia.edu/41727530/Bathe_K_J_Finite_Element_Procedures_1996_Prentice_Hall
- [7] M. A. Trindade and R. Sampaio, "Active Control of Coupled Axial and Torsional Drill-String Vibrations," 2005.
- [8] Y. A. Khulief and H. Al-Naser, "Finite element dynamic analysis of drillstrings," *Finite Elem. Anal. Des.*, vol. 41, no. 13, pp. 1270–1288, Jul. 2005, doi: 10.1016/j.finel.2005.02.003.
- [9] M. Compton, F. Verano, G. Nelson, S. X. Wu, and S. Bits, "Managing Downhole Vibrations for Hole-Enlargement-While-Drilling in Deepwater Environment: A Proven Approach Utilizing Drillstring Dynamics Model," in *All Days*, Lima, Peru: SPE, Dec. 2010, p. SPE-139234-MS. doi: 10.2118/139234-MS.
- [10] M. Kapitaniak, V. Vaziri Hamaneh, J. Páez Chávez, K. Nandakumar, and M. Wiercigroch, "Unveiling complexity of drill–string vibrations: Experiments and modelling," *Int. J. Mech. Sci.*, vol. 101–102, pp. 324–337, Oct. 2015, doi: 10.1016/j.ijmecsci.2015.07.008.
- [11] T. Vromen *et al.*, "Mitigation of Torsional Vibrations in Drilling Systems: A Robust Control Approach," *IEEE Trans. Control Syst. Technol.*, vol. PP, pp. 1–17, Nov. 2017, doi: 10.1109/TCST.2017.2762645.
- [12] J. Priest, H. Ghadbeigi, S. Avar-Soberanis, and S. Gerardis, "3D finite element modelling of drilling: The effect of modelling method," *CIRP J. Manuf. Sci. Technol.*, vol. 35, pp. 158–168, Nov. 2021, doi: 10.1016/j.cirpj.2021.06.001.
- [13] M. Cai, L. Mao, X. Xing, H. Zhang, and J. Li, "Analysis on the nonlinear lateral vibration of drillstring in curved wells with beam finite element," *Commun. Nonlinear Sci. Numer. Simul.*, vol. 104, p. 106065, Jan. 2022, doi: 10.1016/j.cnsns.2021.106065.
- [14] K. Yue, F. Liu, J. Liao, Y. Wang, J. Wu, and Y. Zhang, "Vibration Analysis and Optimization of Rock Drilling Arm," *SAE Int. J. Adv. Curr. Pract. Mobil.*, vol. 5, no. 1, Art. no. 2022-01–0290, Mar. 2022, doi: 10.4271/2022-01-0290.
- [15] A. L. Muthuveerappan and S. Sivarajan, "Finite element analysis of process parameters influences on deformation and von mises stress in drilling," *Mater. Today Proc.*, May 2023, doi: 10.1016/j.matpr.2023.05.113.
- [16] C. Neto and H. J. Da, "Active control of stick-slip oscillations in oil-well drilling systems," text, Universidade de São Paulo, 2023. doi: 10.11606/T.18.2023.tde-17042023-160638.

- [17] W. Liu, H. Ni, Y. Wang, Y. Guo, Y. Gao, and P. He, "Dynamic modeling and load transfer prediction of drill-string axial vibration in horizontal well drilling," *Tribol. Int.*, vol. 177, p. 107986, Jan. 2023, doi: 10.1016/j.triboint.2022.107986.
- [18] I. Kokalari, T. Karaja, and M. Guerrisi, "Review on lumped parameter method for modeling the blood flow in systemic arteries," vol. 2013, Jan. 2013, doi: 10.4236/jbise.2013.61012.
- [19] B. Besselink, N. Van De Wouw, and H. Nijmeijer, "A Semi-Analytical Study of Stick-Slip Oscillations in Drilling Systems," *J. Comput. Nonlinear Dyn.*, vol. 6, no. 2, p. 021006, Apr. 2011, doi: 10.1115/1.4002386.
- [20] J. M. Kamel and A. S. Yigit, "Modeling and analysis of stick-slip and bit bounce in oil well drillstrings equipped with drag bits," *J. Sound Vib.*, vol. 333, no. 25, pp. 6885–6899, Dec. 2014, doi: 10.1016/j.jsv.2014.08.001.
- [21] P. Athanasiou and Y. Hadi, "Simulation of Oil Well Drilling System Using Distributed–Lumped Modelling Technique," *Modelling*, vol. 1, no. 2, Art. no. 2, Dec. 2020, doi: 10.3390/modelling1020011.
- [22] D. Xie, Z. Huang, Y. Ma, V. Vaziri, M. Kapitanik, and M. Wiercigroch, "Nonlinear dynamics of lump mass model of drill-string in horizontal well," *Int. J. Mech. Sci.*, vol. 174, p. 105450, May 2020, doi: 10.1016/j.ijmecsci.2020.105450.
- [23] I. Kessai, S. Benammar, M. Z. Doghmane, and K. F. Tee, "Drill Bit Deformations in Rotary Drilling Systems under Large-Amplitude Stick-Slip Vibrations," *Appl. Sci.*, vol. 10, no. 18, Art. no. 18, Jan. 2020, doi: 10.3390/app10186523.
- [24] N. K. Tengedal, "Modelling and Simulation of Offshore Drilling Systems," Doctoral thesis, NTNU, 2021. Accessed: Aug. 06, 2024. [Online]. Available: <https://ntnuopen.ntnu.no/ntnu-xmlui/handle/11250/2788638>
- [25] L. A. Khajjiveya, I. V. Andrianov, Y. F. Sabirova, and A. K. Kudaibergenov, "Analysis of Drill-String Nonlinear Dynamics Using the Lumped-Parameter Method," *Symmetry*, vol. 14, no. 7, Art. no. 7, Jul. 2022, doi: 10.3390/sym14071495.
- [26] "(PDF) Hybrid Interval Type-2 Fuzzy PID+I Controller for a Multi-DOF Oilwell Drill-String System." Accessed: Oct. 25, 2024. [Online]. Available: https://www.researchgate.net/publication/361460627_Hybrid_Interval_Type-2_Fuzzy_PIDI_Controller_for_a_Multi-DOF_Oilwell_Drill-String_System
- [27] R. Riane, M. Z. Doghmane, M. Kidouche, K. F. Tee, and S. Djezzar, "Stick-Slip Vibration Suppression in Drill String Using Observer-Based LQG Controller," *Sensors*, vol. 22, no. 16, Aug. 2022, doi: 10.3390/s22165979.
- [28] Y. Zhang, P. Ashok, D. Chen, and E. van Oort, "A Control-Oriented Lumped Parameter Drillstring Dynamic Model for Real-Time Vibration Mitigation and Drilling Optimization," Accessed: Aug. 06, 2024. [Online]. Available: <https://dx.doi.org/10.2118/212453-MS>
- [29] "Experimental and numerical study of lateral vibration of a rotor–stator rubbing system | International Journal of Dynamics and Control." Accessed: Oct. 25, 2024. [Online]. Available: <https://link.springer.com/article/10.1007/s40435-024-01425-4>
- [30] M. D. Collins and W. L. Siegmund, *Parabolic Wave Equations with Applications*. Springer Nature, 2019.
- [31] J. M. Carcione and F. Poletto, "Simulation of stress waves in attenuating drill strings, including piezoelectric sources and sensors," *J. Acoust. Soc. Am.*, vol. 108, no. 1, pp. 53–64, Jul. 2000, doi: 10.1121/1.429443.
- [32] M. Krstic, "Adaptive Control of Anti-stable Wave PDE Systems: Theory and Applications in Oil Drilling," *IFAC Proc. Vol.*, vol. 46, no. 11, pp. 432–439, Jan. 2013, doi: 10.3182/20130703-3-FR-4038.00154.
- [33] I. Boussaada, A. Cela, H. Mounier, and S.-I. Niculescu, "Control of Drilling Vibrations: A Time-Delay System-Based Approach," *IFAC Proc. Vol.*, vol. 46, no. 3, pp. 226–231, 2013, doi: 10.3182/20130204-3-FR-4031.00162.
- [34] B. Saldivar, S. Mondié, and J. C. Ávila Vilchis, "The control of drilling vibrations: A coupled PDE-ODE modeling approach," *Int. J. Appl. Math. Comput. Sci.*, vol. 26, no. 2, pp. 335–349, Jun. 2016, doi: 10.1515/amcs-2016-0024.
- [35] H. Ibrahim Basturk, "Observer-Based Boundary Control Design for the Suppression of Stick-Slip Oscillations in Drilling Systems With Only Surface Measurements," *J. Dyn. Syst. Meas. Control*, vol. 139, no. 10, p. 104501, Oct. 2017, doi: 10.1115/1.4036549.
- [36] H. Zhang and E. Detournay, "A high-dimensional model to study the self-excited oscillations of rotary drilling systems," *Commun. Nonlinear Sci. Numer. Simul.*, vol. 112, p. 106549, Sep. 2022, doi: 10.1016/j.cnsns.2022.106549.
- [37] H. E. Goicoechea, R. Lima, F. S. Buezas, and R. Sampaio, "Drill-string with cutting dynamics: A mathematical assessment of two models," *J. Sound Vib.*, vol. 544, p. 117364, Feb. 2023, doi: 10.1016/j.jsv.2022.117364.

- [38] J. Auriol, N. Kazemi, and S.-I. Niculescu, "Sensing and computational frameworks for improving drill-string dynamics estimation," *Mech. Syst. Signal Process.*, vol. 160, p. 107836, Nov. 2021, doi: 10.1016/j.ymssp.2021.107836.
- [39] J. Redaud, F. Bribiesca-Argomedo, and J. Auriol, "Output regulation and tracking for linear ODE-hyperbolic PDE-ODE systems," *Automatica*, vol. 162, p. 111503, Apr. 2024, doi: 10.1016/j.automatica.2023.111503.
- [40] S. Toumi and R. Mlayeh, "Control strategies for mitigating torsional and axial vibrations in rotary oilwell drilling systems," *IMA J. Appl. Math.*, p. hxae030, Oct. 2024, doi: 10.1093/imamat/hxae030.
- [41] M. Silveira, C. Wang, and M. Wiercigroch, "Analysis of Stick-Slip Oscillations of Drill-String via Cosserat Rod Model," in *IUTAM Symposium on Nonlinear Dynamics for Advanced Technologies and Engineering Design*, M. Wiercigroch and G. Rega, Eds., Dordrecht: Springer Netherlands, 2013, pp. 337–345. doi: 10.1007/978-94-007-5742-4_26.
- [42] H. E. Goicoechea, R. Lima, R. Sampaio, M. B. Rosales, and F. S. Buezas, "A Stochastic Approach for a Cosserat Rod Drill-String Model with Stick-Slip Motion," in *Proceedings of the 5th International Symposium on Uncertainty Quantification and Stochastic Modelling*, J. E. S. De Cursi, Ed., Cham: Springer International Publishing, 2021, pp. 103–110. doi: 10.1007/978-3-030-53669-5_8.
- [43] R. W. Tucker and C. Wang, "A Simple Cosserat Model for the Dynamics of Drill-Strings," *Conference: The Seventh International Congress on Sound and Vibration, ICSV. International Institute of Acoustics and Vibration, Garmisch-Partenkirchen*.
- [44] F. Yu, N. Hongjian, H. Genlu, H. Bin, L. Wei, and L. Jing, "Lateral Vibration Simulation and Laboratory Experiment of Bottom Hole Assembly Based on Cosserat Theory," Sep. 11, 2022, *Rochester, NY*: 4215764. doi: 10.2139/ssrn.4215764.
- [45] H. Eduardo Goicoechea Manuel, "Cosserat Rods and their Application to Drill-String Dynamics," Doutor Em Engenharia Mecânica, Pontifícia Universidade Católica Do Rio De Janeiro, Rio de Janeiro, Brazil, 2023. doi: 10.17771/PUCRio.acad.62826.
- [46] R. Zambetti, "Modelling of a drill string in an oil well under dynamic and static conditions," Feb. 2024, Accessed: Aug. 06, 2024. [Online]. Available: <https://www.politesi.polimi.it/handle/10589/216614>
- [47] H. E. Goicoechea, R. Lima, F. S. Buezas, and R. Sampaio, "A comprehensive Cosserat rod drill-string model for arbitrary well geometry that includes the dynamics of the cutting and lateral contact," *J. Sound Vib.*, vol. 571, p. 118035, Feb. 2024, doi: 10.1016/j.jsv.2023.118035.
- [48] J. C. Roukema, "Mechanics and dynamics of drilling," University of British Columbia, 2006. doi: 10.14288/1.0080772.
- [49] "A Robust Torque and Drag Analysis Approach for Well Planning and Drillstring Design | SPE/IADC Drilling Conference and Exhibition | OnePetro." Accessed: Aug. 08, 2024. [Online]. Available: <https://onepetro.org/SPEDC/proceedings-abstract/98DC/All-98DC/190320>
- [50] C. A. Johancsik, D. B. Friesen, and R. Dawson, "Torque and Drag in Directional Wells-Prediction and Measurement," *J. Pet. Technol.*, vol. 36, no. 06, pp. 987–992, Jun. 1984, doi: 10.2118/11380-PA.
- [51] M. S. Aston, P. J. Hearn, and G. McGhee, "Techniques for Solving Torque and Drag Problems in Today's Drilling Environment," in *All Days*, New Orleans, Louisiana: SPE, Sep. 1998, p. SPE-48939-MS. doi: 10.2118/48939-MS.
- [52] D. Stuart, C. D. Hamer, C. Henderson, T. Gaynor, and D. C.-K. Chen, "New Drilling Technology Reduces Torque and Drag by Drilling a Smooth and Straight Wellbore".
- [53] A. Wu, G. Hareland, and M. Fazaelizadeh, "Torque & Drag Analysis Using Finite Element Method," *Mod. Appl. Sci.*, vol. 5, no. 6, p. p13, Nov. 2011, doi: 10.5539/mas.v5n6p13.
- [54] K. Tveitan, "Torque and drag analyses of North Sea wells using new 3D model," Master thesis, University of Stavanger, Norway, 2011. Accessed: Aug. 06, 2024. [Online]. Available: <https://uis.brage.unit.no/uis-xmlui/handle/11250/183305>
- [55] M. Fazaelizadeh, "Real Time Torque and Drag Analysis during Directional Drilling," 2013, *Graduate Studies*. doi: 10.11575/PRISM/27551.
- [56] M. O. Oyedere, "Improved torque and drag modeling using traditional and machine learning methods," Aug. 2020, Accessed: Aug. 06, 2024. [Online]. Available: <https://hdl.handle.net/2152/115839>
- [57] F. Rodrigues G. da Silva *et al.*, "Application of Torque and Drag Models to Prevent Real-Time Operational Problems," Accessed: Oct. 20, 2024. [Online]. Available: <https://dx.doi.org/10.2118/198952-MS>
- [58] J. Zou, P. Chen, T. Ma, Y. Liu, and X. Wang, "Drag-Reduction Performance Evaluation of Controllable Hybrid Steering Drilling System," *Shock Vib.*, vol. 2021, no. 1, p. 6688656, 2021, doi: 10.1155/2021/6688656.
- [59] M. C. Jensen, "The Modern Industrial Revolution, Exit, and the Failure of Internal Control Systems," *J. Finance*, vol. 48, no. 3, pp. 831–880, 1993, doi: 10.1111/j.1540-6261.1993.tb04022.x.
- [60] D. Pogorelov, G. Mikheev, N. Lysikov, L. Ring, R. Gandikota, and N. Abedrabbo, "A Multibody System Approach to Drill String Dynamics Modeling," in *Volume 4: Advanced Manufacturing Processes*;

- Biomedical Engineering; Multiscale Mechanics of Biological Tissues; Sciences, Engineering and Education; Multiphysics; Emerging Technologies for Inspection and Reverse Engineering; Advanced Materials and Tribology*, Nantes, France: American Society of Mechanical Engineers, Jul. 2012, pp. 53–62. doi: 10.1115/ESDA2012-82316.
- [61] Y. Liu and D. Gao, “A nonlinear dynamic model for characterizing downhole motions of drill-string in a deviated well,” *J. Nat. Gas Sci. Eng.*, vol. 38, pp. 466–474, Feb. 2017, doi: 10.1016/j.jngse.2017.01.006.
- [62] “Modeling Friction Performance of Drill String Torsional Oscillation Using Dynamic Friction Model - Wang - 2017 - Shock and Vibration - Wiley Online Library.” Accessed: Aug. 06, 2024. [Online]. Available: <https://onlinelibrary.wiley.com/doi/full/10.1155/2017/4051541>
- [63] X.-Q. Liu *et al.*, “Mechanical analysis of deepwater drilling riser system based on multibody system dynamics,” *Pet. Sci.*, vol. 18, no. 2, pp. 603–617, Apr. 2021, doi: 10.1007/s12182-020-00506-1.
- [64] R. Wang, X. Liu, G. Song, and S. Zhou, “Non-Linear Dynamic Analysis of Drill String System with Fluid-Structure Interaction,” *Appl. Sci.*, vol. 11, no. 19, Art. no. 19, Jan. 2021, doi: 10.3390/app11199047.
- [65] G. C. Downton, “Challenges of Modeling Drilling Systems For the Purposes of Automation and Control,” *IFAC Proc. Vol.*, vol. 45, no. 8, pp. 201–210, 2012, doi: 10.3182/20120531-2-NO-4020.00054.
- [66] C. Gan, W.-H. Cao, K.-Z. Liu, and M. Wu, “A novel dynamic model for the online prediction of rate of penetration and its industrial application to a drilling process,” *J. Process Control*, vol. 109, pp. 83–92, Jan. 2022, doi: 10.1016/j.jprocont.2021.12.002.
- [67] C. Gan *et al.*, “Multi-source information fusion-based dynamic model for online prediction of rate of penetration (ROP) in drilling process,” *Geoenergy Sci. Eng.*, vol. 230, p. 212187, Nov. 2023, doi: 10.1016/j.geoen.2023.212187.
- [68] B. Huang, H. Ni, Y. Jin, and Y. Lu, “The integrated drill string dynamic model based on the lumped mass method and discrete element method,” *Mech. Syst. Signal Process.*, vol. 221, p. 111723, Dec. 2024, doi: 10.1016/j.ymsp.2024.111723.
- [69] O. Bello, J. Holzmann, T. Yaqoob, and C. Teodoru, “Application Of Artificial Intelligence Methods In Drilling System Design And Operations: A Review Of The State Of The Art,” *J. Artif. Intell. Soft Comput. Res.*, vol. 5, no. 2, pp. 121–139, Apr. 2015, doi: 10.1515/jaiscr-2015-0024.
- [70] E. Kasiralvalad, “The great potential of nanomaterials in drilling & drilling fluid applications,” 2014.
- [71] R. Çakıroğlu, S. Yağmur, A. Acir, and U. Şeker, “Modelling of Drill Bit Temperature and Cutting Force in Drilling Process Using Artificial Neural Networks,” vol. 20, pp. 333–340, Jan. 2017.
- [72] A. Bani Mustafa, A. K. Abbas, M. Alsaba, and M. Alameen, “Improving drilling performance through optimizing controllable drilling parameters,” *J. Pet. Explor. Prod. Technol.*, vol. 11, no. 3, pp. 1223–1232, Mar. 2021, doi: 10.1007/s13202-021-01116-2.
- [73] S. A. Ezz, M. S. Farahat, S. Kamel, and A. Z. Nouh, “Drilling Vibration Modes and Penetration Rate Modeling using Artificial Neural Network and Multiple Linear Regression Analysis in Khoman Formation at the Egyptian Western Desert,” Apr. 21, 2021. doi: 10.21203/rs.3.rs-337955/v1.
- [74] “Intelligent Model for Predicting Downhole Vibrations Using Surface Drilling Data During Horizontal Drilling | J. Energy Resour. Technol. | ASME Digital Collection.” Accessed: Oct. 25, 2024. [Online]. Available: <https://asmedigitalcollection.asme.org/energyresources/article-abstract/144/8/083002/1122632/Intelligent-Model-for-Predicting-Downhole?redirectedFrom=fulltext>
- [75] “Well Control Space Out: A Deep-Learning Approach for the Optimization of Drilling Safety Operations | IEEE Journals & Magazine | IEEE Xplore.” Accessed: Aug. 08, 2024. [Online]. Available: <https://ieeexplore.ieee.org/abstract/document/9438629>
- [76] A. Rouzgard and K. Heidari Shirazi, “Automatic Path tracking control in directional drilling equipped with MWD systems,” Nov. 2023.
- [77] “World first: Profiling Equinor’s fully automated oil and gas platform.” Accessed: Jul. 23, 2023. [Online]. Available: <https://www.nsenergybusiness.com/features/first-automated-oil-gas-platform/>
- [78] M. N. Al-Mudhaf *et al.*, “Revolutionizing Drilling Efficiency With Neuro Autonomous Solutions: DrillOps Automate, DD Advisor, And Auto Curve Coupled With SLB Well Construction Rig & Blue BHA,” Accessed: Oct. 18, 2024. [Online]. Available: <https://dx.doi.org/10.2118/216690-MS>

A COMPREHENSIVE REVIEW OF ORTHOGONAL POLYNOMIALS AND FUNCTIONS WITH APPLICATION IN FILTER DESIGN

UDC (517.587:621.372.834.1)

**Nikola Danković¹, Saša S. Nikolić¹, Dragan Antić¹,
Miodrag Spasić¹, Petar Đekić²**

¹University of Niš, Faculty of Electronic Engineering, Department of Control Systems,
Republic of Serbia

²The Academy of Applied Technical and Preschool Studies-Niš, Republic of Serbia

ORCID iDs: Nikola Danković

 <https://orcid.org/0000-0003-0986-5695>

Saša S. Nikolić

 <https://orcid.org/0000-0003-2745-3862>

Dragan Antić

 <https://orcid.org/0000-0002-5880-5173>

Miodrag Spasić

 <https://orcid.org/0000-0002-3061-6872>

Petar Đekić

 <https://orcid.org/0000-0001-9506-7301>

Abstract. *This paper presents some of the results and contributions to the theory of orthogonal polynomials, orthogonal functions and corresponding filters, achieved in the last fifteen years. This theory is based on new definitions and specific generalisations of orthogonal functions and polynomials derived directly in the complex domain. The main objective of this paper is to enable some new applications of orthogonal polynomials in the identification, modelling, signal processing and control of dynamical systems. Accordingly, the paper is divided into seven sections. All central chapters, which describe specific classes of orthogonal polynomials and functions, begin with a brief mathematical background and proposed forms for filter design. In this paper, we give some main results for classical, almost, improved almost, quasi-, generalised and their applications in filter design.*

Key words: *Almost orthogonal polynomials, quasi-orthogonal polynomials, generalised orthogonal polynomials, Legendre type polynomials, orthogonal filters, bilinear transformation.*

Received November 28, 2024 / Accepted December 18, 2024

Corresponding author: Nikola Danković

University of Niš, Faculty of Electronic Engineering, Department of Control Systems, Aleksandra Medvedeva 4,
18104 Niš, Republic of Serbia

E-mail: nikola.dankovic@elfak.ni.ac.rs

I. INTRODUCTION

In this century, great progress has been made in the field of orthogonal rational functions, orthogonal algebraic and trigonometric polynomials, and orthogonal systems in general. In particular, there are a large number of papers dealing with the application of orthogonal systems in electronics, circuit theory, digital signal processing and telecommunications. One of the most important applications of orthogonal functions is the design of orthogonal filters, which can be successfully used for design of orthogonal signal generators, for the modelling and identification of dynamical systems, and for the practical implementation of optimal and adaptive systems.

Legendre polynomials and their orthogonal properties were intensively researched at the end of the eighteenth century to determine the attraction between the celestial bodies during their orbits [1]. Hermite polynomials were invented as a result of solving differential equations on infinite and semi-infinite intervals, and development of arbitrary functions on these intervals [1]. The theory of continuous fractals gave a strong impetus to the later study of orthogonal polynomials by Szegő, and thus the mathematicians of the mid-nineteenth century laid the foundation for Laguerre polynomials [2]. All the mentioned types of polynomials which are orthogonal on the real axis with respect to the defined weight function have been effectively used for the numerical evaluation of the integral value using the quadrature formulas since the Gaussian era. In 1807, while solving partial differential equations related to the heat conduction, Fourier noticed that the solution can be represented as a series of sine functions with exponential weights. He later transferred the same idea to the representation of arbitrary function as the final sum of sine and cosine functions. In his researches, Chebyshev established that of all the approximation polynomials of an arbitrary function over the interval $[-1, 1]$, the best minimization of the maximum error can be achieved with a linear combination of certain polynomials, which today are referred to as Chebyshev. Somewhat later, Jacobi and Gegenbauer polynomials were developed. A certain class of orthogonal functions, the so-called part by part constant basis functions, founded application in the identification of dynamical systems. These families of functions include Haar and Walsh functions [3]. In the first half of the twentieth century, generalised orthonormal rational basis functions were studied in separate papers by Takenaka [4] and Malmquist. The applications of these functions to the approximation of functions defined on the unit circle (analysis of discrete systems) and the semi-plane (continuous systems) were developed by Walsh in the middle of the last century. During this period, we can also recognize significant research of Szegő and Geronimus [5], [6] on the analysis of polynomials orthogonal in the different domains [7], [8], as well as work of Djrbashian on orthogonal rational functions on the unit circle with fixed poles [7]. Due to certain special properties, the works on orthogonality on the real axis and the unit circle are most numerous [8].

Authors of this paper have paid significant attention in recent years to investigating new types of orthogonal polynomials and their possible applications in control systems and other applications. The main contributions of these researches are new types of orthogonal functions and polynomials with the use of several different types of transfer functions for their generating [9]-[20]. Based on these functions we obtained new classes of improved almost and quasi-orthogonal polynomials as well as practically implemented orthogonal filters in the form of printed circuit boards [11], [12]. As some possible application of the newly derived almost orthogonal filters can be found in [12], [21]. It should be mentioned that in [11], new types of filters based on orthogonal Legendre and Malmquist quasi-orthogonal polynomials

have been proposed. For these polynomials, we derived a complete mathematical apparatus in terms of the definition of the inner products, calculating the appropriate norms, as well as the deriving significant relations (Christoffel and Rodrigues formula). In [16], a new class of orthogonal Legendre type filters with complex poles and zeroes were designed with application in the modelling of a real industrial system.

Most of the polynomials and functions mentioned in this paper were used to design filters that were practically realised and later used in modelling, identification and control of systems. Sometimes it was necessary to adapt the obtained transfer functions to a specific filter design.

The rest of this paper is organised as follows. In Sections 2-5, classes of orthogonal polynomials are presented (shifted, almost orthogonal, quasi-orthogonal and finally orthogonal polynomials based on symmetric transformations). Appropriate orthogonal filters practically designed from these polynomials and functions are described in Section 6. Concluding remarks and further work can be found in Section 7.

2. SHIFTED ORTHOGONAL POLYNOMIALS

Considered polynomials are orthogonal over certain interval. To allow an analysis over arbitrary intervals, we can introduce shifted polynomials [12], [14], [22] which are suitable for describing the signal over any considered interval.

All orthogonal polynomials over a finite range (Legendre, Chebyshev of first and second type, Jacobi and Gegenbauer) are defined over the interval $[-1, 1]$. For the purpose of analysing and processing real signals which can have values over arbitrary intervals, classical polynomials can be redefined, i.e. shifted to the desired interval $[\tau_a, \tau_b]$. Shifted orthogonal polynomials $\{\psi_k(\tau)\}$ are defined over an arbitrary interval $[\tau_a, \tau_b]$ and can be obtained from regular (unshifted) $\{\phi_k(x)\}$ by substitution $x = \tau^*$, where:

$$\tau^* = \frac{2(\tau - \tau_a)}{\tau_b - \tau_a} - 1 = A\tau + B. \tag{1}$$

$A = \frac{2}{\tau_b - \tau_a}$ and $B = -\frac{(\tau_b + \tau_a)}{(\tau_b - \tau_a)}$, with the condition that the interval of orthogonality is finite. Then, the definition of orthogonality is also changed:

$$(\psi_n, \psi_k) = \int_{\tau_a}^{\tau_b} \psi_n(\tau)\psi_k(\tau)\omega(\tau)d\tau = \begin{cases} 0, & k \neq n, \\ \|\psi_k\|^2 = \|\phi_k\|^2 / A, & k = n, \end{cases} \tag{2}$$

where $\omega(\tau) = w(\tau^*)$ and $\phi_k(\tau) = \psi_k(\tau^*)$, and norms $\|\phi_k\|$ can be found in [7] for different types of polynomials.

Classical Laguerre polynomials are orthogonal over the interval $[0, +\infty]$ with the weight function $w(x) = e^{-x}$, and Hermite over $[-\infty, +\infty]$ with $w(x) = e^{-x^2}$. It can be noticed that in both cases the following relations are valid: $w(0) = 1$ and $w(x \rightarrow \infty) \rightarrow 0$. That means that these weight functions differently sample large and small values of x . So, in order to better represent the function $f(x)$, $x \in [\tau_a, \tau_b]$, we have to move (shift) the centre ($x = 0$) into τ_a by substituting $x = \tau - \tau_a$, so that the new weight function becomes 1 in both cases

for $\tau = \tau_a$. Obtained polynomials are also shifted, but we have to emphasize that described shifting of Laguerre and Hermite polynomials has completely different meaning than shifting polynomials orthogonal over the finite interval [23].

3. ALMOST ORTHOGONAL POLYNOMIALS AND FUNCTIONS

For simplicity, we now introduce the concept of generalised orthogonal functions using the well-known Legendre polynomials for the sake of simplicity (the same concept can be used for other classical orthogonal polynomials as well) [13], [15]. Our design is based on shifted Legendre polynomials that are orthogonal over the interval (0, 1). On the other hand, technical systems operate in real time, so we need the corresponding approximation over the interval (0, ∞). The solution is to use the substitution $x = e^{-t}$. In this way, the polynomial sequence orthogonal over (0, 1), becomes an exponential polynomial sequence orthogonal over the interval (0, ∞).

Let us consider the orthogonal Legendre polynomials in their explicit form [12]:

$$P_n(x) = \sum_{i=0}^n A_{n,i} x^i, \quad (3)$$

where:

$$A_{n,i} = \frac{1}{n!} (-1)^{n-i} \binom{n}{i} \frac{(n+i)!}{i!}. \quad (4)$$

These polynomials are orthogonal over the interval (0, 1), with the weight function $w(x) = 1$, and the following definition of orthogonality based on the inner product:

$$\int_0^1 P_m(x) P_n(x) dx = \begin{cases} 0, & m \neq n \\ N_i, & m = n, \end{cases} \quad (5)$$

and they can be successively used for modelling, and control of dynamical systems as well as for identification of specific systems parameters.

Corresponding almost orthogonal polynomials $P_n^{(\varepsilon)}(x)$ can be defined as [13], [24]:

$$\int_0^1 P_m^{(\varepsilon)}(x) P_n^{(\varepsilon)}(x) dx = \begin{cases} \varepsilon, & m \neq n \\ N_n^{(\varepsilon)}, & m = n, \end{cases} \quad (6)$$

where ε represent a very small positive constant ($0 < \varepsilon \ll 1$). The connection between classical orthogonal and almost orthogonal polynomials is proved in [12] with the following relation:

$$P_n^{(\varepsilon)}(x) = P_n(x) + \sum_{k=1}^{n-1} \frac{b_k}{\|P_k\|^2} P_k(x), \quad (7)$$

where $\|P_k\|^2$ represents the square of the norm and b_k are polynomials dependent on ε . Obviously, for $\varepsilon=0$ almost orthogonal polynomials become strictly orthogonal, i.e. $\lim_{\varepsilon \rightarrow 0} P_n^{(\varepsilon)}(x) = P_n(x)$. For design of almost orthogonal filters, it is very convenient to use the following three term recurrent relation, derived in [12], [14]:

$$W_{n+1}^{(\varepsilon)}(s) = W_n^{(\varepsilon)}(s) + W_{n+1}(s) + W_n(s)k_n, \tag{8}$$

where: $k_n = \frac{b_n(\varepsilon)}{\|P_n\|^2} - 1$, $k_0 = \varepsilon$. The first few members of the almost orthogonal polynomials

$\{P_n^{(\varepsilon)}(x)\}$ over the interval (0, 1) with the weight function $w(x)=1$ sequence are:

$$\begin{aligned} P_0^{(\varepsilon)}(x) &= 1, \\ P_1^{(\varepsilon)}(x) &= 2x - (1 - 2\varepsilon), \\ P_2^{(\varepsilon)}(x) &= 6x^2 - 6(1 - 12\varepsilon + 12\varepsilon^2)x + (1 - 30\varepsilon + 36\varepsilon^2), \\ &\vdots \end{aligned} \tag{9}$$

In [13], we defined almost orthogonality in a different manner in order to accomplish further simplifications and improvements in filters design. First, we defined almost orthogonal Legendre polynomials $P_n^{(\delta)}(x)$:

$$P_n^{(\delta)}(x) = \sum_{i=0}^n A_{n,i}^{\delta} x^i, \tag{10}$$

where $A_{n,i}^{\delta}$ represents coefficients defined by:

$$A_{n,i}^{\delta} = (-1)^{n+i} \frac{\Gamma(n\delta + i + 1)}{\Gamma(n\delta + 1) i!(n-i)!}, \tag{11}$$

δ is a constant near to one: $\delta=1+\varepsilon \approx 1$ and Γ is a symbol for the gamma function [5], [7]. Parameter δ is an uncertain quantity, which describes the imperfection of the system. Variations of δ contain cumulative impacts of all imperfect elements, model uncertainties, and measurement noise on the system output. The range of variations can be determined by conducting several experiments. Hence, it is expected that responses obtained from different experiments are mutually different. The responses are in certain boundaries, which depend on parameter δ i.e., on the real system components quality, or the noise level present in signal.

After applying the substitution $x = e^{-t}$ to (10) and Laplace transform, we obtain a transfer function suitable for designing almost orthogonal filters:

$$W_n^{(\delta)}(s) = \frac{\prod_{i=1}^n (s - i\delta)}{\prod_{i=0}^n (s + i)} = \frac{(s - \delta)(s - 2\delta) \cdots (s - n\delta)}{s(s + 1)(s + 2) \cdots (s + n)}. \tag{12}$$

As a mapping function use the transformation $\bar{s} + s = 0$, i.e., $\bar{s} = -s$. In this case, the left semi plane of the complex plane s is being transformed into the right semi plane [21], [25]. Almost orthogonality can be analysed from the following inner product:

$$N_{mm} = \oint_C W_n^{(\delta)}(s) \bar{W}_m^{(\delta)}(s) w(s) ds, \tag{13}$$

with weight $w(s) = 1, m > n$. Now, applying the Cauchy theorem, we obtain:

$$N_{nm} = 2\pi j \sum_{k=1}^m \text{Res} \left[W_n^{(\delta)}(s) \bar{W}_m^{(\delta)}(s) \right]. \tag{14}$$

$$N_{nm} = 2\pi j \sum_{k=1}^m \frac{(-1)^{n+1} \prod_{i=1}^n (k+i\delta) \prod_{i=1}^m (k-i\delta)}{k^2 \prod_{i=1}^n (k-i) \prod_{i=1}^m (k+i)}. \tag{15}$$

The first few members of the improved almost orthogonal polynomials $\{P_i^{(\delta)}(x)\}$ over the interval $(0, 1)$ with weight function $w(x)=1$ sequence are:

$$\begin{aligned} P_0^{(\delta)}(x) &= 1, \\ P_1^{(\delta)}(x) &= (\delta + 1)x - \delta, \\ P_2^{(\delta)}(x) &= (\delta + 1)(\delta + 2)x^2 - (\delta + 1)(2\delta + 1)x + \delta^2, \\ &\vdots \end{aligned} \tag{16}$$

4. QUASI-ORTHOGONAL POLYNOMIALS AND FUNCTIONS

The final generalisation of the concept of orthogonality can be introduced by the following definition of quasi-orthogonality for the polynomial set $P_n(x)$ [11], [18], [21]:

$$(P_n^k(x), P_m^k(x)) = \int_a^b w(x) P_n^k(x) P_m^k(x) dx = \begin{cases} 0, & 0 \leq m \leq n - k - 1, \\ N_{n,m}^k \neq 0, & n - k \leq m \leq n, \end{cases} \tag{17}$$

where k represents the order of quasi-orthogonality, a and b are the limits of quasi-orthogonality interval, and $w(x)$ is the weight function. In our case of Legendre quasi-orthogonal polynomials of the first order [11]:

$$\int_0^1 P_n^k(x) P_m^k(x) x dx = \begin{cases} = 0, & 0 \leq m \leq n - k - 1 \\ \neq N_{n,m}^k, & n \geq k + 1, \end{cases} \tag{18}$$

$$P_n^k(x) = \sum_{i=0}^n A_{n,i}^k x^i = x \sum_{i=0}^n A_{n,i}^k x^{i-1}, \tag{19}$$

$$A_{n,i}^k = \frac{(-1)^{n-k+i} (n+i-k-1)!}{i!(i-1)!(n-i)!}. \tag{20}$$

In the similar way as in the case of almost orthogonal polynomials we obtain orthogonal functions (poles are integer) [11], [21]:

$$W_n^k(s) = \frac{(s-1)(s-2) \cdots [s-(n-k-1)]}{(s+1)(s+2) \cdots (s+n)}, \tag{21}$$

or in the following form (shifted and more suitable for filter design):

$$W_n^k(s) = \frac{1}{s(s+1)\cdots(s+k)} \cdot \frac{(s-2)}{(s+k+1)} \cdot \frac{(s-i)}{(s+k+(i+1))} \cdots \frac{(s-(n-k))}{(s+n-1)}. \quad (22)$$

The first few members of quasi-orthogonal polynomials of the order $k=1$, $P_n^1(x)$ over the interval $(0, 1)$ with the weight function $w(x)=x$ sequence are:

$$\begin{aligned} P_1^1(x) &= -x + 1, \\ P_2^1(x) &= -2x^2 + 3x - 1, \\ P_3^1(x) &= -5x^3 + 10x^2 - 6x + 1, \\ &\vdots \end{aligned} \quad (23)$$

and a few second order ($k=2$) quasi-orthogonal polynomials:

$$\begin{aligned} P_2^2(x) &= \frac{1}{2}x^2 - x + \frac{1}{2}, \\ P_3^2(x) &= \frac{5}{6}x^3 - 2x^2 + \frac{3}{2}x - \frac{1}{3}, \\ P_4^2(x) &= \frac{7}{4}x^4 - 5x^3 + 5x^2 - 2x + \frac{1}{4}, \\ &\vdots \end{aligned} \quad (24)$$

If we apply the definition of quasi-orthogonality on almost orthogonal polynomials given by the following relation [11], [16]:

$$P_n^{(\delta)}(x) = \sum_{i=0}^n A_{n,i}^{\delta} x^i, \quad (25)$$

$$A_{n,i}^{\delta} = (-1)^{n+i} \frac{\Gamma(n\delta + i + 1)}{\Gamma(n\delta + 1)i!(n-i)!}, \quad (26)$$

and Γ is a symbol for the gamma function, we obtain quasi-almost orthogonal Legendre type, polynomials over the interval $(0, 1)$ with the weight function $w(x) = 1$:

$$P_n^{(k,\delta)}(x) = \sum_{i=0}^n A_{n,i}^{k,\delta} x^i, \quad (27)$$

$$A_{n,i}^{k,\delta} = (-1)^{n+i+k} \frac{\prod_{j=1}^{n-k} (i + j\delta)}{i!(n-i)!}. \quad (28)$$

In the previous relation, k is the order of quasi-orthogonality, and δ is a constant, defined as $\delta = 1 + \varepsilon \approx 1$ [11], [13], [16]. The range of the parameter δ can be determined by conducting several experiments based on the designers' experience. Polynomials defined via (25) and (26) represent generalised quasi-orthogonal polynomials.

Now, let us define the quasi-orthogonality over the interval $(0, 1)$ with the weight function $w(x) = 1$ via the inner product in the following manner:

$$\left(P_n^{(k,\delta)}(x), P_m^{(k,\delta)}(x) \right) = \int_a^b P_n^{(k,\delta)}(x) P_m^{(k,\delta)}(x) w(x) dx = \begin{cases} Q_k(\delta), & m \neq n, \\ N_n^{(k,\delta)}, & m = n, \end{cases} \quad (29)$$

$$Q_k(\delta) = q_0 + q_1\delta + q_2\delta^2 + \dots + q_k\delta^k. \quad (30)$$

In the similar way as in the previous classes of orthogonal polynomials we obtain appropriate orthogonal functions:

$$W_n^{(k,\delta)}(s) = \frac{\prod_{i=1}^{n-k} (s-i\delta)}{\prod_{i=0}^n (s+i)} = \frac{(s-\delta)(s-2\delta)\dots(s-(n-k)\delta)}{s(s+1)(s+2)\dots(s+n)}, \quad (31)$$

or in the form adjusted for the filter design:

$$W_n^{(k,\delta)}(s) = \frac{1}{s(s+1)\dots(s+k)} \cdot \frac{s-\delta}{s+k+1} \dots \frac{s-(i-1)\delta}{s+k+(i-1)} \dots \frac{s-(n-k)\delta}{s+n}. \quad (32)$$

A few first order ($k=1$) generalised quasi-orthogonal polynomials of this sequence are:

$$\begin{aligned} P_1^{(1,\delta)}(x) &= -x+1, \\ P_2^{(1,\delta)}(x) &= -\frac{(\delta+2)}{2}x^2 + (\delta+1)x - \frac{\delta}{2}, \\ P_3^{(1,\delta)}(x) &= -\frac{(\delta+3)(2\delta+3)}{6}x^3 + (\delta+1)(\delta+2)x^2 - \frac{(\delta+1)(2\delta+1)}{2}x + \frac{\delta^2}{3}, \\ &\vdots \end{aligned} \quad (33)$$

and a few second order ($k=2$) generalised quasi-orthogonal polynomials:

$$\begin{aligned} P_2^{(2,\delta)}(x) &= \frac{1}{2}x^2 - x + \frac{1}{2}, \\ P_3^{(2,\delta)}(x) &= \frac{(\delta+3)}{6}x^3 - \frac{(\delta+2)}{2}x^2 + \frac{(\delta+1)}{2}x - \frac{\delta}{6}, \\ P_4^{(2,\delta)}(x) &= \frac{(\delta+2)(\delta+4)}{12}x^4 - \frac{(\delta+3)(2\delta+3)}{6}x^3 + \\ &+ \frac{(\delta+1)(\delta+2)}{2}x^2 - \frac{(\delta+1)(2\delta+1)}{6}x + \frac{\delta^2}{12}, \\ &\vdots \end{aligned} \quad (34)$$

5. ORTHOGONAL POLYNOMIALS AND FUNCTIONS
 BASED ON SYMMETRIC TRANSFORMATIONS

By using Legendre orthogonal functions:

$$W_n(x) = \prod_{j=0}^{n-1} \frac{s + \alpha_j + 1}{s - \alpha_j} \frac{1}{s - \alpha_n}. \tag{35}$$

Müntz-Legendre polynomials [18], [26], which are orthogonal on the interval (0, 1), were obtained by [26], [27]:

$$P_n(x) = \frac{1}{2\pi i} \oint_{\Gamma} \prod_{j=0}^{n-1} \frac{s + \alpha_j + 1}{s - \alpha_j} \frac{x^s}{s - \alpha_n} ds, \tag{36}$$

where the contour Γ surrounds all the poles of the integrand. Functions $W_n(x)$ are used for designing orthogonal Legendre filters. Müntz-Legendre polynomials are used for obtaining outputs from these filters. Let us notice that in these filters the zeroes are obtained by linear transformation of the poles. Orthogonal Laguerre functions where the zeroes have reciprocal values of the poles:

$$W_n(s) = \frac{\sqrt{1 - \alpha^2}}{1 - \alpha} \left(\frac{1 - \alpha s}{s - \alpha} \right)^{n-1}, \tag{37}$$

are used for design of orthogonal Laguerre filters [7]. The Takenaka-Malmquist rational function system [28]-[30]:

$$W_n(s) = \frac{\sqrt{1 - \alpha_n^2}}{1 - \alpha_n s} \prod_{k=0}^{n-1} \frac{(\alpha_k - s)}{(1 - \alpha_k s)}, \quad n = 0, 1, 2, \dots \tag{38}$$

is used for designing appropriate orthogonal filters (Takenaka-Malmquist filters), [7], [21]. Let us notice that the zeroes of $W_n(s)$ have reciprocal values of the poles. The generalisation of Malmquist functions was performed in [31] by using the mapping $s \rightarrow b/s$:

$$W_n(s) = \frac{\prod_{k=0}^{n-1} (s + \alpha_k^*)}{\prod_{k=0}^n (s + \alpha_k)} = \frac{1}{s + \alpha_0} \prod_{k=1}^n \frac{s + \alpha_{k-1}^*}{s + \alpha_k}, \quad \alpha_k^* = \frac{b}{\alpha_k}, \quad \alpha_k \in R, \quad \alpha_k \geq 0. \tag{39}$$

By using these functions and the following relation:

$$P_n(x) = \frac{1}{2\pi i} \oint_{\Gamma} W_n(s) x^s ds, \tag{40}$$

a class of orthogonal Müntz polynomials which are orthogonal with respect to the special inner product was derived. In this way, generalised Takenaka-Malmquist filters are designed. Outputs of these filters are obtained using (40). A new class of Müntz polynomials derived from a sequence of orthogonal Malmquist functions, is introduced by [22]. These Müntz polynomials are orthogonal with respect to the special inner product. In [31] we have

applied them for design of a new class of filters based on reciprocal transformation (generalised Malmquist type) (39) which are orthogonal with respect to a new special inner product.

In this paper, the focus is on a more general class of orthogonal rational functions and filters, to which the above belong. Namely, the zeroes in the all above mentioned rational orthogonal basis functions are obtained either by the linear transformation $s \rightarrow as + b$ or the reciprocal transformation $s \rightarrow b/cs$ of the poles. The transfer functions of the orthogonal filters are $W_n(s)$, and the outputs are obtained using Müntz polynomials derived by (38). A class of orthogonal cascade filters which represents a generalisation of all the mentioned filters obtained by using linear and reciprocal mapping poles to zeroes is realised by using the symmetric bilinear transformation:

$$s \rightarrow \frac{as+b}{cs-a}, \quad (a^2+bc > 0), \quad (a, b, c \in \mathbb{R}). \quad (41)$$

By using this transformation for mapping poles α_k to zeroes α_k^* we obtain:

$$\alpha_k^* = \frac{\overline{a\alpha_k + b}}{c\alpha_k - a}. \quad (42)$$

For design of orthogonal cascade filters with real poles, with taking into account that the bilinear transformation is symmetric, we have:

$$\alpha_k^* = \frac{a\alpha_k + b}{c\alpha_k - a}, \quad \alpha_k = \frac{a\alpha_k^* + b}{c\alpha_k^* - a}. \quad (43)$$

The sequence of the appropriate rational functions has the following form now:

$$W_n(s) = \frac{\prod_{k=0}^{n-1} \left(s - \frac{a\alpha_k + b}{c\alpha_k - a} \right)}{\prod_{k=0}^n (s - \alpha_k)}. \quad (44)$$

If we apply the transformation (41) onto $W_n(s)$ we obtain:

$$W_n^*(s) = \frac{\prod_{k=0}^{n-1} (s - \alpha_k)}{\prod_{k=0}^n \left(s - \frac{a\alpha_k + b}{c\alpha_k - a} \right)}. \quad (45)$$

Let us consider the inner product:

$$(W_n, W_m) = \frac{1}{2\pi i} \oint_{\Gamma} W_n(s) W_m^*(s) ds, \quad (46)$$

where the contour Γ surrounds all the poles of $W_n(s)$. If $m \neq n$ due to the symmetry of the bilinear transformation, all the poles of the integrand (46) that lie inside the contour Γ are

annulled with appropriate zeroes of $W_m^*(s)$, so the contour integral (46) is equal to zero. In the case of $m = n$, there exists one first-order pole inside the contour Γ . After applying the Cauchy theorem, we can obtain the following expression: $(W_n(s), W_m(s)) = N_n^2 \neq 0$. Finally, all the expressions stated above imply:

$$(W_n, W_m) = N_n^2 \delta_{n,m}, \tag{47}$$

where $\delta_{n,m}$ represents Kronecker symbol, and poles α_k lie inside the contour Γ , while all the zeroes α_k^* (43) lie outside the contour Γ . Thus, the sequence of the rational functions $W_n(s)$ is orthogonal in the complex domain bordered by the contour Γ with respect to the inner product (43).

Using the sequence $W_n(s)$ we can obtain a class of orthogonal Müntz polynomials based on (40) in the following way [32], [33]:

$$P_n(x) = \frac{1}{2\pi i} \oint_{\Gamma} \frac{\prod_{k=0}^{n-1} \left(s - \frac{a\bar{\alpha}_k + b}{c\bar{\alpha}_k - a} \right)}{\prod_{k=0}^n (s - \alpha_k)} ds. \tag{48}$$

These polynomials can be written as:

$$P_n(x) = \sum_{k=0}^n A_{n,k} x^{\alpha_k}, \tag{49}$$

$$A_{n,k} = \frac{\prod_{j=0}^{n-1} \left(\alpha_k - \frac{a\bar{\alpha}_j + b}{c\bar{\alpha}_j - a} \right)}{\prod_{j=0, j \neq k}^n (\alpha_k - \alpha_j)}, \quad k = 0, 1, 2, \dots, n. \tag{50}$$

It is shown that these Müntz polynomials are orthogonal with respect to an inner product which is defined below. First, the operation \otimes on monoms x^α and x^β is defined in the following way [33]:

$$x^\alpha \otimes x^\beta = x^{c\alpha\beta - a(\alpha + \beta) - b}. \tag{51}$$

Using this operation, the product of two Müntz polynomials, $P_n(x) = \sum_{k=0}^n p_k x^{\alpha_k}$ and

$P_m(x) = \sum_{j=0}^m q_j x^{\alpha_j}$ can be defined in the following manner:

$$P_n(x) \otimes Q_m(x) = \sum_{k=0}^n \sum_{j=0}^m p_k q_j x^{c\alpha_k \alpha_j - a(\alpha_k + \alpha_j) - b}. \tag{52}$$

Using this product of Müntz polynomials, a new inner product can be defined as:

$$(P_n(x), P_m(x))_{\otimes} = \int_0^1 P_n(x) \otimes \overline{P_m(x)} \frac{dx}{x^2}. \tag{53}$$

Finally, by using (41) and (48) we obtain [33]:

$$(P_n(x), P_m(x))_{\otimes} = \frac{(a^2 + bc)^n}{\prod_{k=0}^{n-1} |c\alpha_k - a|^2} \frac{\delta_{n,m}}{c|\alpha_n|^2 - 2a \operatorname{Re} \alpha_n - b} = N_n^2 \delta_{n,m}. \tag{54}$$

Hence, Müntz polynomials (40) derived from orthogonal rational functions $W_n(s)$ are orthogonal on the interval $(0, 1)$ with respect to the inner product (18). If rational functions $W_n(s)$ have real poles, then Müntz polynomials $P_n(x)$ are with real exponents. In that case, substituting $x = e^{-t}$ into $P_n(x)$, we obtain exponential functions:

$$\varphi_n(t) = P_n(e^{-t}) = \sum_{k=0}^n A_{n,k} e^{-\alpha_k t}. \tag{55}$$

Using (47), (51), (52), and (55) we obtain:

$$(\varphi_n(t), \varphi_m(t))_{\otimes} = \int_0^{\infty} \varphi_n(t) \otimes \varphi_m(t) e^{-t} dt = N_n^2 \delta_{n,m}, \tag{56}$$

$$\varphi_n(t) \otimes \varphi_m(t) = \sum_{k=0}^n A_{n,k} e^{-\alpha_k t} \otimes \sum_{j=0}^m A_{m,j} e^{-\alpha_j t} = \sum_{k=0}^n \sum_{j=0}^m A_{n,k} A_{m,j} e^{-[c\alpha_k \alpha_j - a(\alpha_k + \alpha_j) - b]t}. \tag{57}$$

The functions (44) can be written in the form more suitable for a practical filter design:

$$W_n(s) = \frac{1}{s + \alpha_0} \prod_{k=1}^n \frac{s + \frac{a\alpha_{k-1} + b}{c\alpha_{k-1} - a}}{s + \alpha_k}, \quad \alpha_k \in R, \quad \alpha_k \geq 0. \tag{58}$$

As we have already said, this is a generalisation of a filter based on a simple reciprocal transformation $a = 0, c = 1$, but also of most existing filters by choosing specific values for parameters a, b , and c . Hence, filters based on a bilinear transformation are adaptive and by adjusting the parameters we can achieve better performances.

Remark: There are also corresponding classes of digital filters where the basis for the realisation are the corresponding transfer functions in the z -domain, but the focus of this paper is on the functions in continuous s -domain with real poles and analogue filters.

This is a new generalised inner product based on the bilinear transformation of poles to zeroes. For illustrative purposes, a sequence of polynomials of the first few polynomials for the following values of poles $\alpha_0 = -2, \alpha_1 = -3, \alpha_2 = -4, \alpha_3 = -5, \alpha_4 = -6$ and parameters of bilinear transformation $a = 1, b = 1, c = 1$ are:

$$\begin{aligned} P_0(x) &= x^2, \\ P_1(x) &= \frac{10}{3}x^3 - \frac{7}{3}x^2, \\ P_2(x) &= \frac{39}{4}x^4 - \frac{35}{3}x^3 + \frac{35}{12}x^2, \\ P_3(x) &= \frac{1232}{45}x^5 - \frac{897}{20}x^4 + 21x^3 - \frac{91}{36}x^2, \\ &\vdots \end{aligned} \tag{59}$$

6. ORTHOGONAL FILTERS DESIGN AND PRACTICAL REALISATIONS

One of the most important applications of orthogonal functions is the design of orthogonal filters [11]-[17]. These filters can be used for signal approximation [14], for the design of orthogonal signal generators [12], for modelling and system identification [13], [21], [22], [37], [39] as well as for the practical implementation of optimal and adaptive systems [36] and control methods [25]. The theory of classical orthogonal filters has been well studied and described in numerous papers [7], [11]-[21], [40]. In [25], the design procedures for classical, almost quasi-orthogonal filters of Legendre and Müntz-Legendre type are described [21]. To successfully design and implement certain types of filters, we need to start from the rational functions given in the form (7) and (12) for almost orthogonal, (19) and (20) for quasi-orthogonal, (23) for generalisation quasi-orthogonal and, (34) and (39) for orthogonal cascade filters based on symmetric transformations.

Figure 1 shows an almost orthogonal filter of the Legendre type [13], [14] with six sections, which was realised in the analogue technique. The transfer function of this filter corresponds to the expression (8) in which the poles and zeroes have integer values ($i = 1, 2, \dots, 6, n = 5$). The following components were used for the realisation of this filter: 15 operational amplifiers ($\mu\text{A} 741\text{CN}$), 60 resistors, 12 potentiometers and 6 electrolytic capacitors.

Figure 2 presents the realised printed circuit board of the improved almost orthogonal filters [13]. The following components were used for the realisation of this filter: 8 operational amplifiers (LM 324N), 48 resistors, 9 potentiometers and 8 electrolytic capacitors.

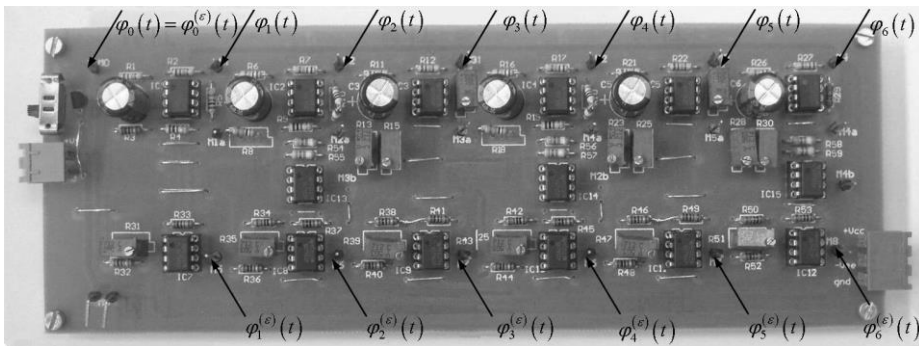


Fig. 1 Almost orthogonal Legendre type filter - printed circuit board

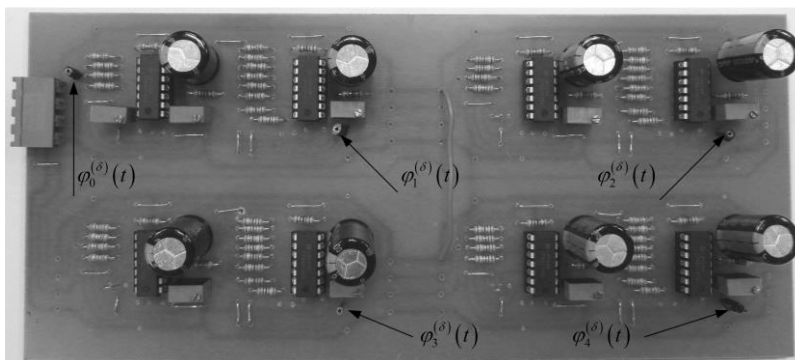


Fig. 2 Improved almost orthogonal Legendre type filter - printed circuit board

A laboratory setup for testing our quasi-orthogonal filter is given in Fig. 3 [11], [21]. The setup consists of a printed circuit board with the realised first order Legendre quasi-orthogonal filter, microprocessor unit and power supply. A practically realised experimental printed circuit board for a generalised quasi-orthogonal first-order filter with four sections ($n=4$) is given in Fig. 4 [21]. The following components were used for the realisation of this filter: 7 operational amplifiers (LM 324N), 55 resistors, 9 potentiometers and 7 electrolytic capacitors.

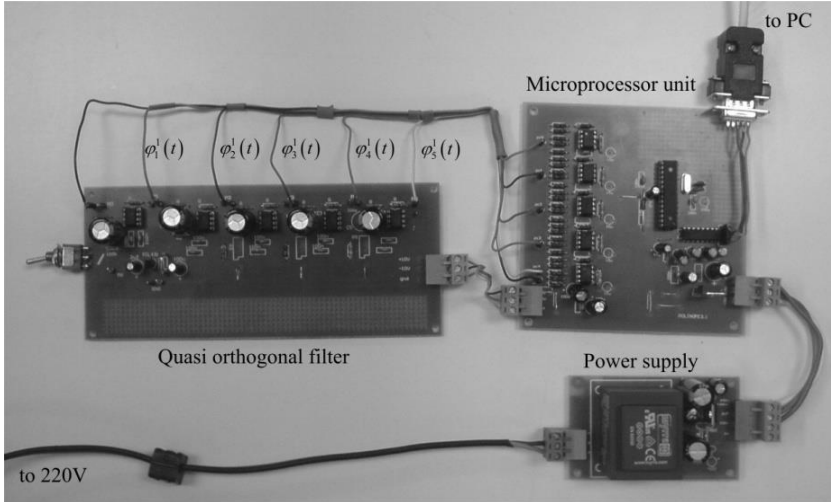


Fig. 3 Laboratory setup for a first-order Legendre quasi-orthogonal filter

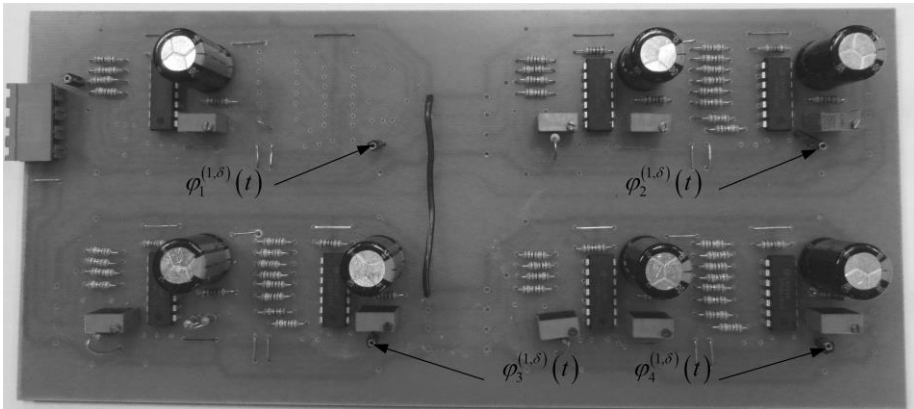


Fig. 4 Generalised Legendre first-order quasi-orthogonal filter - printed circuit board

Relations (34) and (39) represent transfer functions of the new orthogonal cascade filter based on symmetric transformations, and it is a base for its practical realisation (Fig. 5). The designed filter in Fig. 5 is based on the bilinear transformation which is a generalisation of the reciprocal one so the printed circuit board is for both.

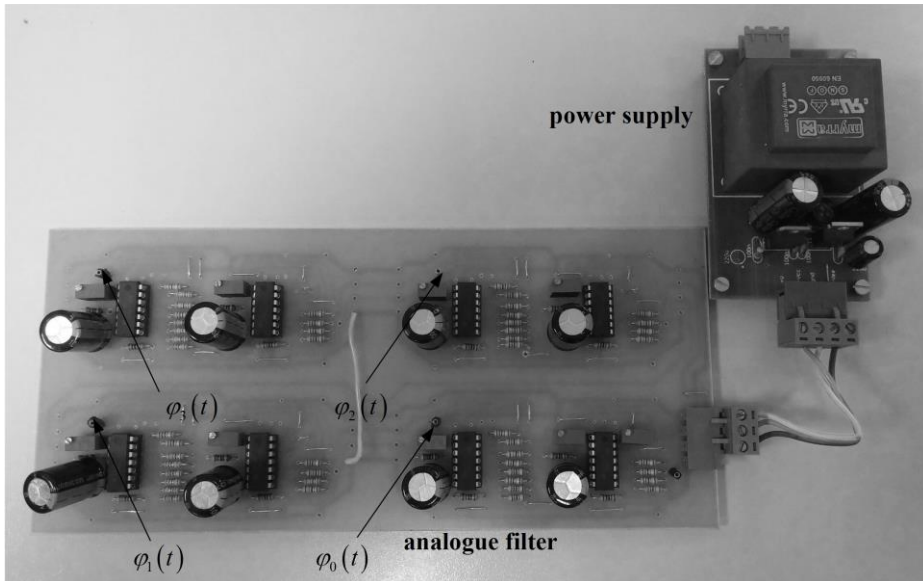


Fig. 5 An orthogonal filter based on bilinear transformation, a printed circuit board

7. CONCLUSION AND FUTURE WORK

In this paper we have made a survey study of new classes of orthogonal polynomials (almost, improved almost, quasi-, generalised quasi-, and polynomials obtained by symmetric transformations) derived in recent years. These polynomials and functions can have a wide range of applications in various scientific and engineering fields (modelling [9], [14], [19], [31], identification [21], [39], sensitivity analysis [15], [38], model predictive control [41]-[43], control systems theory [18], [21], [34], neural networks [17], [18], [35], [37], [38], fuzzy systems [21], ANFIS [21], [36], DPCM system [20], [31] etc.) [19], [20]. Some of the systems and devices where these orthogonal functions and filters have found application are modular DC servo drive [14], [36], [42], [43], magnetic levitation system [17], two rotor aero-dynamical system (TRAS) [37], tower crane [38], multi tank system [15], [39], [41], protector cooling system [9], [19], [31], anti-lock braking system (ABS) [18], differential pulse-code modulation (DPCM) system [20], [31].

The aim is to synthesize all these polynomials and functions that are important to us in some way and compare them using certain measures of quality evaluation. Of course, the further development and generalisation of already existing functions and filters, especially the discrete ones, which have been talked about the least here, and the continuation of their application in various fields is also planned.

Acknowledgement: *This work was supported by the Ministry of Science, Technological Development and Innovation of the Republic of Serbia [grant number 451-03-66/2024-03/200102].*

REFERENCES

- [1] M. Kline, *Mathematical Thought from Ancient to Modern Times*, Oxford University Press, New York, 1972.
- [2] E. T. Bell, *The Development of Mathematics*, McGraw-Hill, New York, 1945.
- [3] J. L. Walsh, *Interpolation and Approximation by Rational Functions in the Complex Domain*, vol. 20, American Mathematical Society Colloquium Publications, American Mathematical Society, Providence, Rhode Island, USA, 1975.
- [4] S. Takenaka, "On some properties of orthogonal functions", in *Proceedings of the Japan Academy, Series A*, vol. 2, no. 3, pp. 106-108, 1926.
- [5] G. Szegő, *Orthogonal Polynomials*, Providence, American Mathematical Society, Colloquium Publications, 1975.
- [6] Ya. L. Geronimus, *Polynomials Orthogonal on a Circle and Interval*, Fiz. Mat. Lit., Moscow, 1958.
- [7] P. V. Hof Heuberger, B. Wahlberg, *Modelling and identification with rational orthogonal basis functions*. London: Springer-Verlag, 2005.
- [8] P. S. Heuberger and T.J. de Hoog, "Approximation and Realization Using Generalized Orthonormal Base", in *Proceedings of the 1999 European Control Conference*, Karlsruhe, Germany, 1999.
- [9] D. Antić, Z. Jovanović, V. Nikolić, M. Milojković, S. Nikolić, and N. Danković, "Modeling of cascade-connected systems using quasi-orthogonal functions", *Elektronika ir Elektrotehnika*, vol. 18, no. 10, pp. 3-8, 2012. doi: 10.5755/j01.eee.18.10.3051
- [10] M. Alfaro and L. Moral, "Quasi-orthogonality on the unit circle and semi-classical forms", *Port. Mathematica*, vol. 51, pp. 47-62, 1991.
- [11] M. T. Milojković, D. S. Antić, S. S. Nikolić, Z. D. Jovanović, and S. Lj. Perić, "On a new class of quasi-orthogonal filters", *International Journal of Electronics*, vol. 100, no. 10, pp. 1361-1372, 2013. doi: 10.1080/00207217.2012.743087
- [12] B. Danković, S. Nikolić, M. Milojković, and Z. Jovanović, "A class of almost orthogonal filters", *Journal of Circuits, Systems, and Computers*, vol. 18, no. 5, pp. 923-931, 2009. doi: 10.1142/S0218126609005447
- [13] D. Antić, B. Danković, S. Nikolić, M. Milojković, and Z. Jovanović, "Approximation based on orthogonal and almost orthogonal functions", *Journal of the Franklin Institute*, vol. 349, no. 1, pp. 323-336, 2012. doi: 10.1016/j.jfranklin.2011.11.006
- [14] M. Milojković, S. Nikolić, B. Danković, D. Antić, and Z. Jovanović, "Modelling of dynamical systems based on almost orthogonal polynomials", *Mathematical and Computer Modelling of Dynamical Systems*, vol. 16, no. 2, pp. 133-144, 2010. doi: 10.1080/13873951003740082
- [15] D. Antić, S. Nikolić, M. Milojković, N. Danković, Z. Jovanović, and S. Perić, "Sensitivity analysis of imperfect systems using almost orthogonal filters", *Acta Polytechnica Hungarica*, vol. 8, no. 6, pp. 79-94, 2011.
- [16] S. S. Nikolić, D. S. Antić, S. Lj. Perić, N. B. Danković, and M. T. Milojković, "Design of generalised orthogonal filters: Application to the modelling of dynamical systems", *International Journal of Electronics*, vol. 103, no. 2, pp. 269-280, 2016. doi: 10.1080/00207217.2015.1036367
- [17] S. S. Nikolić, D. S. Antić, M. T. Milojković, M. B. Milovanović, S. Lj. Perić, and D. B. Mitić, "Application of neural networks with orthogonal activation functions in control of dynamical systems", *International Journal of Electronics*, vol. 103, no. 4, pp. 667-685, 2016. doi: 10.1080/00207217.2015.1036811
- [18] S. Lj. Perić, D. S. Antić, M. B. Milovanović, D. B. Mitić, M. T. Milojković, and S. S. Nikolić, "Quasi-sliding mode control with orthogonal endocrine neural network-based estimator applied in anti-lock braking system", *IEEE/ASME Transactions on Mechatronics*, vol. 21, no. 2, pp. 754-764, 2016. doi: 10.1109/TMECH.2015.2492682
- [19] N. Danković, D. Antić, S. Nikolić, S. Perić, and M. Spasić, "Generalized cascade orthogonal filters based on symmetric bilinear transformation with application to modeling of dynamic systems", *FILOMAT*, vol. 32, no. 12, pp. 4275-4284, 2018. doi: 10.2298/FIL1812275D
- [20] N. Danković, D. Antić, S. Nikolić, M. Milojković, and S. Perić, "New class of digital Malmquist-type orthogonal filters based on generalized inner product; application to modeling DPCM system", *FACTA UNIVERSITATIS Series: Mechanical Engineering*, vol. 17, no. 3, pp. 385-396, 2019.
- [21] M. Milojković, S. Nikolić, and Staniša Perić, *Applications of Orthogonal Functions in Modelling and Control of Dynamical Systems*, University of Niš, Serbia, 2022.
- [22] S. S. Nikolić, D. Antić, N. Danković, M. Milojković, and S. Perić, "New classes of the orthogonal filters - An overview", in *Proceedings of the 8th Small Systems Simulation Symposium-SSSS 2020*, Niš, Serbia, February 12.-14., 2020., pp. 117-122.
- [23] M. Riesz, "Sur le probleme des moments", *Troisième Note, Arkiv för Matematik, Astronomi och Fysik*, vol. 17, no. 16, pp. 1-52, 1923.

- [24] J. S. Dehesa, F. Marcellan, and A. Ronveaux, "On orthogonal polynomials with perturbed recurrence relations", *Journal of Computational and Applied Mathematics*, vol. 30, pp. 203–212, 1990. doi: 10.1016/0377-0427(90)90028-X
- [25] S. Nikolić, D. Antić, B. Danković, M. Milojković, Z. Jovanović, and S. Perić, "Orthogonal functions applied in antenna positioning", *Advances in Electrical and Computer Engineering*, vol. 10, no. 4, pp. 35–42, 2010. doi: 10.4316/AECE.2010.04006
- [26] A. K. Taslakyán, "Some properties of Legendre quasi-polynomials with respect to a Müntz system", *Mathematics* vol. 2, pp. 179–189, 1984.
- [27] P. B. Borwein, T. Erdelyi, and J. Zhang, "Müntz systems and orthogonal Müntz-Legendre polynomials", *Transactions of the American Mathematical Society*, vol. 342, no. 2, pp. 523–542, 1994. doi: 10.1090/S0002-9947-1994-1227091-4
- [28] M. M. Djrbashian, "Orthogonal systems of rational functions on the circle with given set of poles", *Dokl. Akad. Nauk SSSR*, vol. 147, pp. 1278–1281, 1962.
- [29] M. M. Djrbashian, "A survey on the theory of orthogonal systems and some open problems", in P. Nevai (ed.) *Orthogonal polynomials*, Springer, Netherlands, pp. 135–146, 1990.
- [30] G. V. Badalyan, "Generalisation of Legendre polynomials and some of their applications" *Akad. Nauk Armyan. SSR Izv. Ser. Fiz.-Mat. Estest. Tekhn. Nauk*, vol. 8, no. 5, pp. 1–28, 1955.
- [31] N. B. Danković, D. S. Antić, S. S., Nikolić, S. Lj., Perić, and M. T. Milojković, "A new class of cascade orthogonal filters based on a special inner product with application in modeling of dynamical systems", *Acta Polytechnica Hungarica*, vol. 13, no. 7, pp. 63–82, 2016. doi: 10.12700/APH.13.7.2016.7.4
- [32] B. Danković, G. V. Milovanović, S. Rančić, "Malmquist and Müntz Orthogonal Systems and Applications", in Rassias TM (ed.), *Inner product spaces and applications*, Harlow: Addison-Wesley Longman, pp. 22–41, 1997.
- [33] S. B. Marinković B. Danković, M. S. Stanković, and P. M. Rajković, "Orthogonality of some sequences of the rational functions and the Müntz polynomials", *Journal of Computational and Applied Mathematics*, vol. 163, no. 2, pp. 419–427, 2004. doi: 10.1016/j.cam.2003.08.037
- [34] M. B. Milovanović, D. S. Antić, M. T. Milojković, S. S. Nikolić, S. Lj. Perić, and M. D. Spasić, "Adaptive PID control based on orthogonal endocrine neural networks", *Neural Networks*, vol. 84, pp. 80–90, 2016. doi: 10.1016/j.neunet.2016.08.012
- [35] M. Milovanović, A. Oarcea, S. Nikolić, A. Đorđević, and M. Spasić, "An approach to networking a new type of artificial orthogonal glands within orthogonal endocrine neural networks", *Applied Sciences*, vol. 12, iss. 11, 5372, 2022. doi: 10.3390/app12115372
- [36] M. Milojković, D. Antić, M. Milovanović, S. S. Nikolić, S. Perić, and M. Almalawwe, "Modeling of dynamic systems using orthogonal endocrine adaptive neuro-fuzzy inference systems", *Journal of Dynamic Systems, Measurement, and Control*, vol. 137, no. 9, pp. 091013-1+091013-6, DS-15-1098, 2015. doi: 10.1115/1.4030758
- [37] M. Milojković, M. Milovanović, S. S. Nikolić, M. Spasić, and A. Antić, "Designing optimal models of nonlinear MIMO systems based on orthogonal polynomial neural networks", *Mathematical and Computer Modelling of Dynamical Systems*, vol. 27, no. 1, pp. 242–262, 2021. doi: 10.1080/13873954.2021.1909069
- [38] S. S. Nikolić, D. S. Antić, N. B. Danković, A. A. Milovanović, D. B. Mitić, M. B. Milovanović, and P. S. Djekić, "Generalized quasi-orthogonal functional networks applied in parameter sensitivity analysis of complex dynamical systems", *Elektronika ir Elektrotehnika*, vol. 28, no. 4, pp. 19–26, 2022. doi: 10.5755/j02.eie.31110
- [39] S. S. Nikolić, M. B. Milovanović, N. B. Danković, D. B. Mitić, S. Lj. Perić, A. D. Djordjević, and P. S. Djekić, "Identification of nonlinear systems using the Hammerstein-Wiener model with improved orthogonal functions", *Elektronika ir Elektrotehnika*, vol. 29, no. 2, pp. 4–11, 2023. doi: 10.5755/j02.eie.33838
- [40] N. Danković, S. S. Nikolić, D. Antić, M. Spasić, and P. Djekić, "Orthogonal polynomials – Development and design", *Proceedings of the XVII International Conference on Systems, Automatic Control and Measurements, SAUM 2024*, Niš, Serbia, November 14.-15., 2024., pp. 104–111. doi: 10.46793/SAUM24.104D
- [41] M. Spasić, D. Antić, N. Danković, S. Perić, and S. S. Nikolić, "Digital model predictive control of the three tank system based on Laguerre functions", *FACTA UNIVERSITATIS Series: Automatic Control and Robotics*, vol. 17, no. 3, pp. 153–164, 2018. doi: 10.22190/FUACR1803153S
- [42] M. Spasić, D. Mitić, S. S. Nikolić, M. Milojković, M. Milovanović, and A. Đorđević, "Malmquist orthogonal functions based tube model predictive control with sliding mode for DC servo system", *Proceedings of the Romanian Academy*, vol. 25, no. 3, pp. 241–251, 2024. doi: 10.59277/PRA-SER.A.25.3.09
- [43] M. Spasić, D. Mitić, D. Antić, N. Danković, and S. S. Nikolić, "Generalized Malmquist orthogonal functions based model predictive control", *Measurement and Control*, doi: 10.1177/00202940241302672

**FACTA UNIVERSITATIS, Series: Automatic Control and Robotics
would like to acknowledge the expertise of the following reviewers,
which has helped to set the standard of the journal in 2024**

Blaža Stojanović/Dr./University of Kragujevac, Faculty of Engineering,
Republic of Serbia/Full professor

Dragomir El Mezeni/Dr./University of Belgrade, School of Electrical Engineering,
Republic of Serbia/Assistant professor

Goran Marković/Dr./ University of Kragujevac, Faculty of Mechanical and Civil
Engineering in Kraljevo, Republic of Serbia/Assistant professor

Gordana Ostojić/Dr./University of Novi Sad, Faculty of Technical Sciences,
Republic of Serbia/Full professor

Igor Jovančević/Dr./University of Montenegro, Faculty of Science and Mathematics,
Montenegro/Assistant professor

Ivan Ćirić/Dr./University of Niš, Faculty of Mechanical Engineering,
Republic of Serbia/Associate professor

Ivan Krstić/Dr./University of Kragujevac, Faculty of Engineering,
Republic of Serbia/Assistant professor

Ivana Radonjić Mitić/Dr./University of Niš, Faculty of Sciences and Mathematics,
Republic of Serbia/Research associate

Jelena Radić/Dr./University of Novi Sad, Faculty of Technical Sciences,
Republic of Serbia/Associate professor

Juliana Javorova/Dr./University of Chemical Technology and Metallurgy,
Department of Applied Mechanics, Bulgaria/Associate professor

Leposava Ristić/Dr./University of Belgrade, School of Electrical Engineering,
Republic of Serbia/Associate professor

Martin Čalasan/Dr./University of Montenegro, Faculty of Electrical Engineering,
Montenegro/Associate professor

Milan Bebić/Dr./University of Belgrade, School of Electrical Engineering,
Republic of Serbia/Associate professor

Milan Gocić/Dr./University of Niš, Faculty of Civil Engineering and Architecture,
Republic of Serbia/Associate professor

Milica Ćirić/Dr./University of Niš, Faculty of Civil Engineering and Architecture,
Republic of Serbia/Teaching assistant

Miodrag Spasić/Dr./University of Niš, Faculty of Electronic Engineering,
Republic of Serbia/Assistant professor

Mirko Raković/Dr./University of Novi Sad, Faculty of Technical Sciences,
Republic of Serbia/Associate professor

Mladen Tomić/Dr./University of Novi Sad, Faculty of Technical Sciences,
Republic of Serbia/Associate professor

Nebojša Mitrović/Dr./University of Kragujevac, Faculty of Technical Sciences Čačak,
Republic of Serbia/Full professor

Nikola Danković/Dr./University of Niš, Faculty of Electronic Engineering,
Republic of Serbia/Assistant professor

Petar Đekić/Dr./Academy of Technical and Teaching Vocational Studies,
Republic of Serbia/Professor of vocational studies

Radomir Đokić/Dr./University of Novi Sad, Faculty of Technical Sciences,
Republic of Serbia/Associate professor

Radu-Emil Precup/Dr./ Politehnica University of Timisoara,
Department of Automation and Applied Informatics, Romania/Full professor

Srdan Đorđević/Dr./University of Niš, Faculty of Electronic Engineering,
Republic of Serbia/Assistant professor

Sreten Stojanović/Dr./University of Niš, Faculty of Technology,
Republic of Serbia/Full professor

Žarko Čojbašić/Dr./University of Niš, Faculty of Mechanical Engineering,
Republic of Serbia/Full professor

CIP - Каталогизacija y publikaciji
Народна библиотека Србије, Београд

62

FACTA Universitatis. Series, Automatic Control and Robotics / editor-in-chief Staniša Lj. Perić. - Vol. 7, no. 1 (2008)- . - Niš : University of Niš, 2008- (Niš : Atlantis). - 24 cm

Polugodišnje. - Delimično je nastavak: Facta Universitatis. Series: Mechanics, Automatic Control and Robotics = ISSN 0354-2009 . - Drugo izdanje na drugom medijumu: Facta Universitatis. Series: Automatic Control and Robotics (Online) = ISSN 1820-6425
ISSN 1820-6417 = Facta Universitatis. Series:Automatic Control and Robotics
COBISS.SR-ID 158108940

